PROGRESS REPORT
UPDATED EVALUATION OF THE DEEP BEDROCK AQUIFERS IN AND AROUND THE MIDDLE RIO GRANDE BASIN NEW MEXICO

prepared by

Michael A. Jones, M.S.
Erwin A. Melis, Ph.D.
Jake Baggerman
JOHN SHOMAKER & ASSOCIATES, INC.
Water-Resource and Environmental Consultants
2611 Broadbent Parkway NE
Albuquerque, New Mexico 87107
505-345-3407
www.shomaker.com

prepared for

New Mexico
Interstate Stream Commission
Santa Fe, New Mexico

June 2013

PROGRESS REPORT
UPDATED EVALUATION OF THE DEEP BEDROCK AQUIFERS IN AND AROUND THE MIDDLE RIO GRANDE BASIN NEW MEXICO

by

Michael A. Jones, M.S.

Erwin A. Melis, Ph.D.

Jake Baggerman

JOHN SHOMAKER & ASSOCIATES, INC.
Water-Resource and Environmental Consultants
2611 Broadbent Parkway NE
Albuquerque, New Mexico 87107

505-345-3407
www.shomaker.com

prepared for

New Mexico Interstate Stream Commission
Santa Fe, New Mexico

June 2013

PROGRESS REPORT
UPDATED EVALUATION OF THE DEEP BEDROCK AQUIFERS IN AND AROUND THE MIDDLE RIO GRANDE BASIN, NEW MEXICO

EXECUTIVE SUMMARY

A numerical groundwater-flow model of the Middle Rio Grande Basin, the underlying bedrock units, and the upland extensions of these units west of the Middle Rio Grande Basin, has been further developed and calibrated. The calibration database has been expanded to include measured water levels over time in 122 monitored wells. An historical transient simulation has been established and calibrated.

The updated and recalibrated model was used to simulate potential withdrawal from the deep bedrock aquifers, and project resulting groundwater drawdown and surface discharge effects, for three levels of potential deep aquifer pumping.

Results indicate reduction in discharge to the Rio Grande growing after 40 years to about 7.1 percent of the total pumping rate for the lowest level of development and 4.6 percent for the highest level. Reduced discharge to the Rio San Jose – Rio Puerco system after 40 years would range from 4.6 percent of pumping rate in the low-development case, to 9.5 percent in the high development case. Maximum aquifer drawdown would range from about 1,900 ft in the low-development scenario to about 3,000 ft in the high-development scenario.

The updated model, with the historical transient simulation, is a platform for assimilating and evaluating more water-level and pumping data as they become available, and for incorporating further geologic information. The model can be periodically updated and calibrated as further information is developed.

The model may be used to project the results of other deep-aquifer pumping scenarios as required.

CONTENTS

page

TABLES

page

ILLUSTRATIONS

page

ILLUSTRATIONS

page

ILLUSTRATIONS

page

ILLUSTRATIONS

page

PROGRESS REPORT
UPDATED EVALUATION OF THE DEEP BEDROCK AQUIFERS IN AND AROUND THE MIDDLE RIO GRANDE BASIN, NEW MEXICO

1.0 INTRODUCTION

An updated numerical groundwater-flow model of the deep aquifers underlying the Santa Fe Group (SFG) aquifer of the Middle Rio Grande Basin (MRGB) has been prepared. The outline of the model domain is shown on Figure 1.1 and includes the SFG aquifer of the MRGB, the deep aquifer units below, and the extension of these units in the upland areas west of the MRGB.

The model was updated to include calibration to historical water levels measured in 122 wells. The updated and recalibrated model was then used to evaluate the effects of developing selected deep-aquifer water-supply scenarios, and to evaluate the quantities of water available.

This report presents the geologic and hydrogeologic settings and the hydrogeologic conceptual model of the study area. Next, the numerical model is presented including structure, input parameters, and calibration results. Finally, results are presented for model simulations of a selection of potential deep aquifer development scenarios.

1.1 History of Study

The study was motivated by the potential for development of water supplies from the deep, saline aquifers in the bedrock units beneath the margins of the MRGB. The model was previously developed as an extension of the U.S. Geological Survey (USGS) numerical model of the MRGB (McAda and Barroll, 2002), modified to represent the underlying and adjacent bedrock aquifers.

The bedrock aquifer study began in September of 2008, and was described in three early progress reports (Melis, 2008; Melis, 2009, Melis and McCoy, 2010). A preliminary model was constructed in 2009, and was expanded and developed in 2011 (JSAI, 2011). The model was developed based on new geological research and structural mapping, a survey of study area springs and water chemistry, and evaluation of measured Rio Puerco flows.

The model was calibrated to a database of measured bedrock-aquifer water levels and the results of a 2008 deep-well aquifer test by Sandoval County (INTERA, 2008). The resulting model was used to estimate the effects of proposed deep-aquifer groundwater pumping on flows in the Rio Grande stream system as well as on flows in the Rio San Jose – Rio Puerco stream system.

The 2013 model update has included gathering available water-level data and developing hydrographs for 122 wells throughout the study area. A historical transient model simulation has been developed and calibrated to the hydrographs. The updated model is now a platform for incorporating additional information as it becomes available, including measured water levels, pumping rates, well depths, and completion data.

1.2 Study Area

The study area of approximately 11,384 mi^2 in central New Mexico (Fig. 1.1) includes the MRGB and tributary basins west to the Continental Divide. The bedrock units beneath the Santa Fe Group aquifer of the MRGB extend to the west and form aquifers in the western part of the study area.

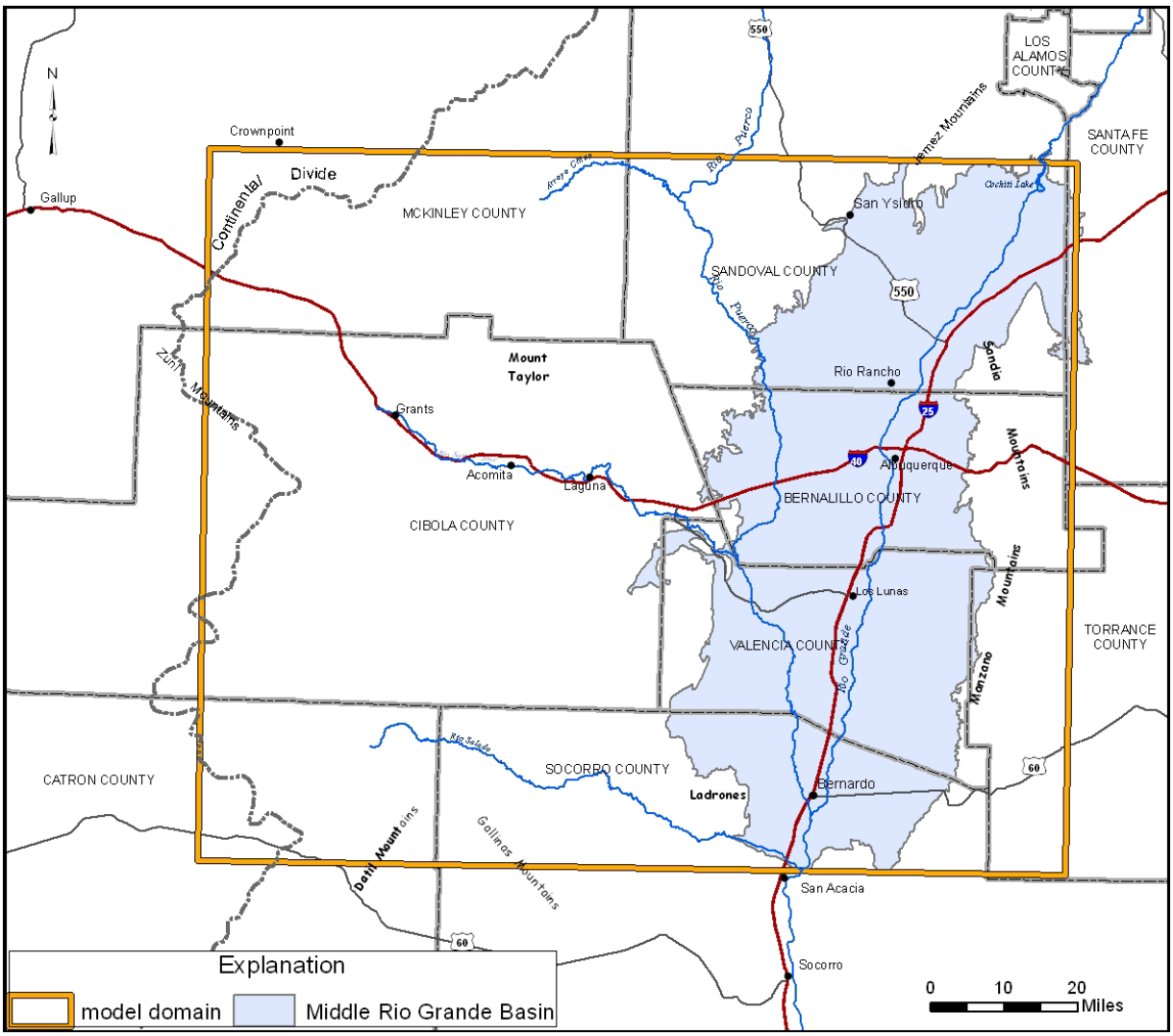

Figure 1.1. Study area.

2.0 GEOLOGIC SETTING

Major geologic features are shown on Figure 2.1. The study area encompasses the Albuquerque structural basin and the southeastern part of the San Juan structural basin. The Albuquerque Basin was formed by rifting, and filled by Santa Fe Group sediments that form the MRGB, the major aquifer of the Albuquerque Basin.

West of the Albuquerque Basin is the topographically elevated Colorado Plateau that lies within the southeastern San Juan Basin, containing a 12,000-ft-thick sequence of Paleozoic- and Mesozoic-age sedimentary rocks. The same sequence extends beneath the Santa Fe Group sediments of the Albuquerque Basin.

The sedimentary sequence generally dips away from the Zuni Uplift, the Lucero Uplift and the Nacimiento Uplift, disappearing beneath basin-fill deposits of the Albuquerque Basin. The uplifts expose older, crystalline basement rock that, away from the uplifts, lies beneath the sedimentary sequence.

Between the Albuquerque Basin and the San Juan Basin is a transition zone, the Rio Puerco fault zone, defined by numerous faults, some springs, and rapid uplift and channel-incision rates (Wright, 1946). The area east of the Rio Puerco fault zone within the Albuquerque Basin is called the Laguna Bench, a zone of relatively thin Santa Fe Group deposits. West of the fault zone is the Acoma Embayment, an entrant of the San Juan Basin between the Zuni and Lucero Uplifts.

Between the Zuni and Nacimiento Uplifts is the Jemez lineament, a northeast-oriented zone of Neogene volcanism (Hallett et al., 1997) including Mount Taylor and the surrounding mountains and mesas. The volcanic features cover a large area of the surface, but the associated dikes and necks occupy only a small proportion of the subsurface and do not constitute a regional barrier to groundwater flow at depth.

2.1 Geologic Units

A geologic map of the study area is shown on Figure 2.2. Characteristics of individual units are described below, from youngest to oldest.

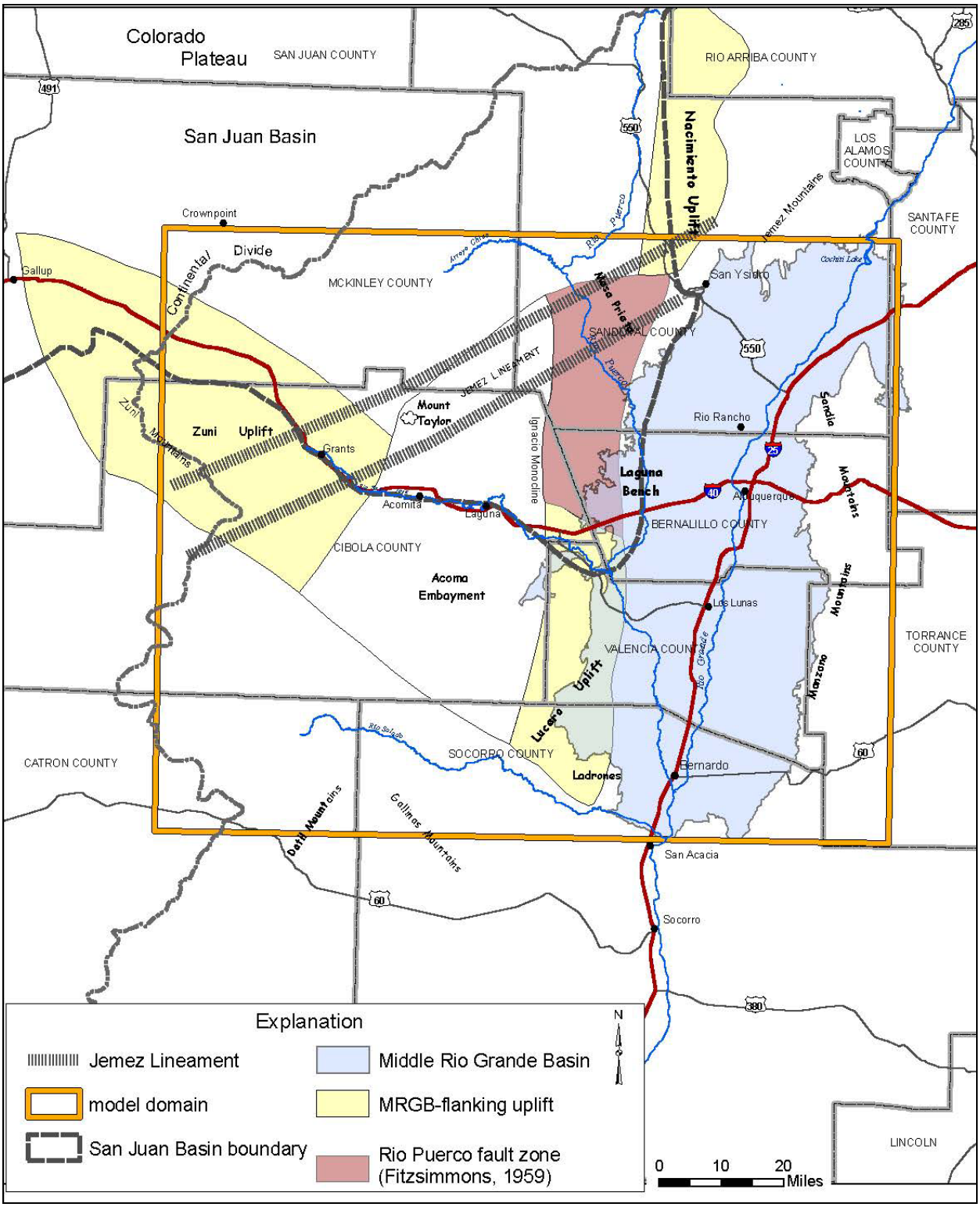

Figure 2.1. Structural geologic features.

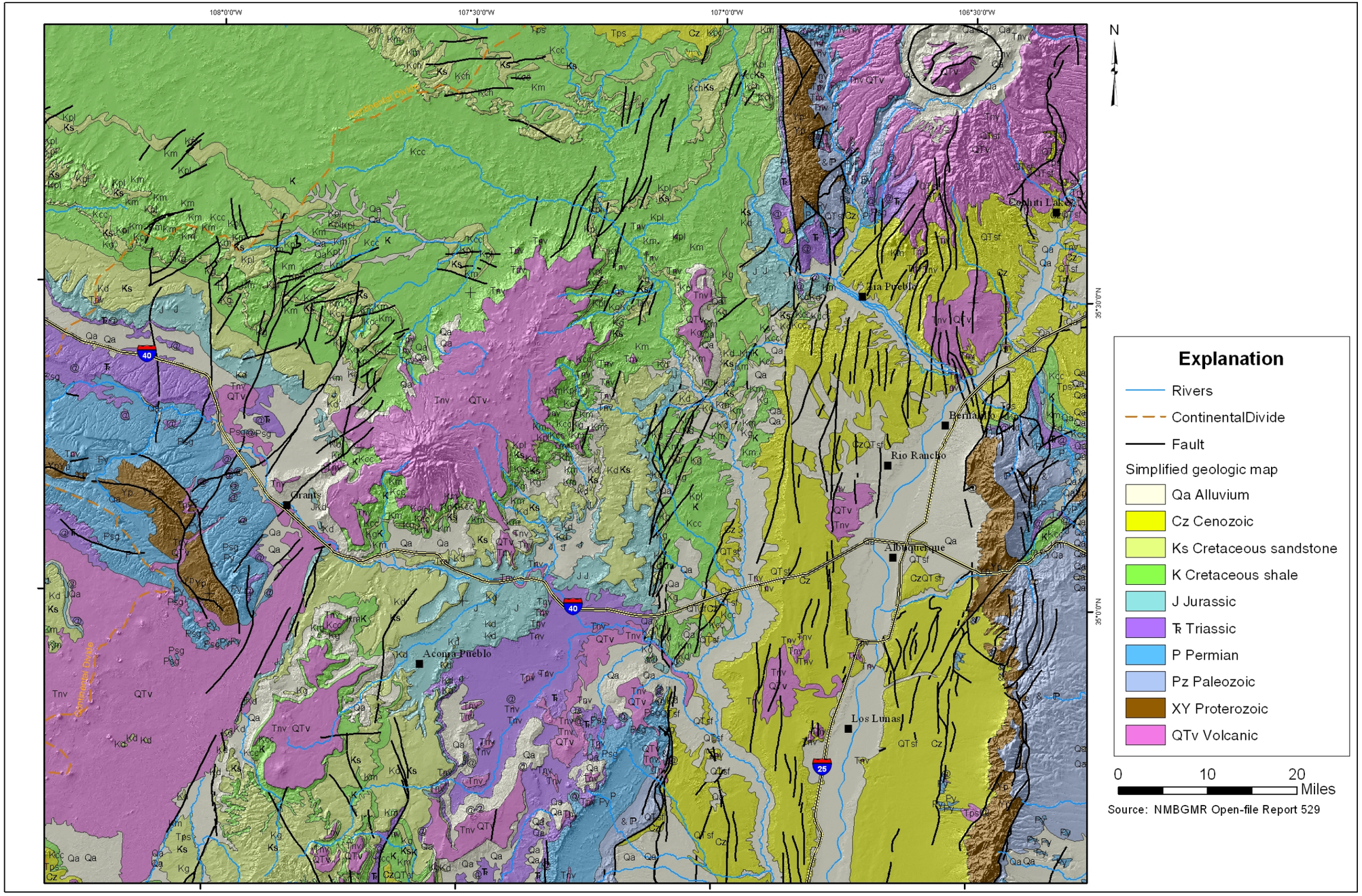

Figure 2.2. Map showing regional geology.

2.1.1 Cenozoic-Age Unconsolidated Units

Alluvium: Quaternary-age alluvium occurs in valleys and arroyo channels throughout the study area. The alluvium serves as a conduit for recharge to deeper aquifers, and forms the shallowest part of the valley-fill aquifer in the Albuquerque Basin, mostly along active fluvial channels.

Santa Fe Group: The Santa Fe Group, in places up to 14,000 to 17,000 ft thick, is the collective name of the unconsolidated and partly consolidated sedimentary fill within the Albuquerque Basin. In terms of its hydrogeologic properties it can be divided into lower, middle, and upper parts (see, e.g., Hawley and Haase, 1992).

The lower Santa Fe Group, as much as 3,500 ft thick, contains basin-floor playa, alluvial fan, and eolian deposits characteristic of closed basin deposition. Grain-size variation tends to be large, and hydraulic conductivities are generally low.

The middle Santa Fe Group is similar to the lower Santa Fe Group but additionally contains fluvial and lacustrine deposits, with an overall thickness of up to 9,000 ft (Hawley and Haase, 1992).

The upper part of the Santa Fe Group is thinnest (about 1,500 ft thick), has the highest sediment maturity, and is characteristic of the development of the ancestral Rio Grande, a through-flowing river system. It contains the coarsest sediments and has the highest local conductivities (McAda and Barroll, 2002).

Thicknesses of the Santa Fe Group in the MRGB were obtained from oil and gas tests, and modeling of Albuquerque Basin geophysical data, resulting in a contour map of the base of the Santa Fe Group (Connell, 2011), presented as Figure 2.3.

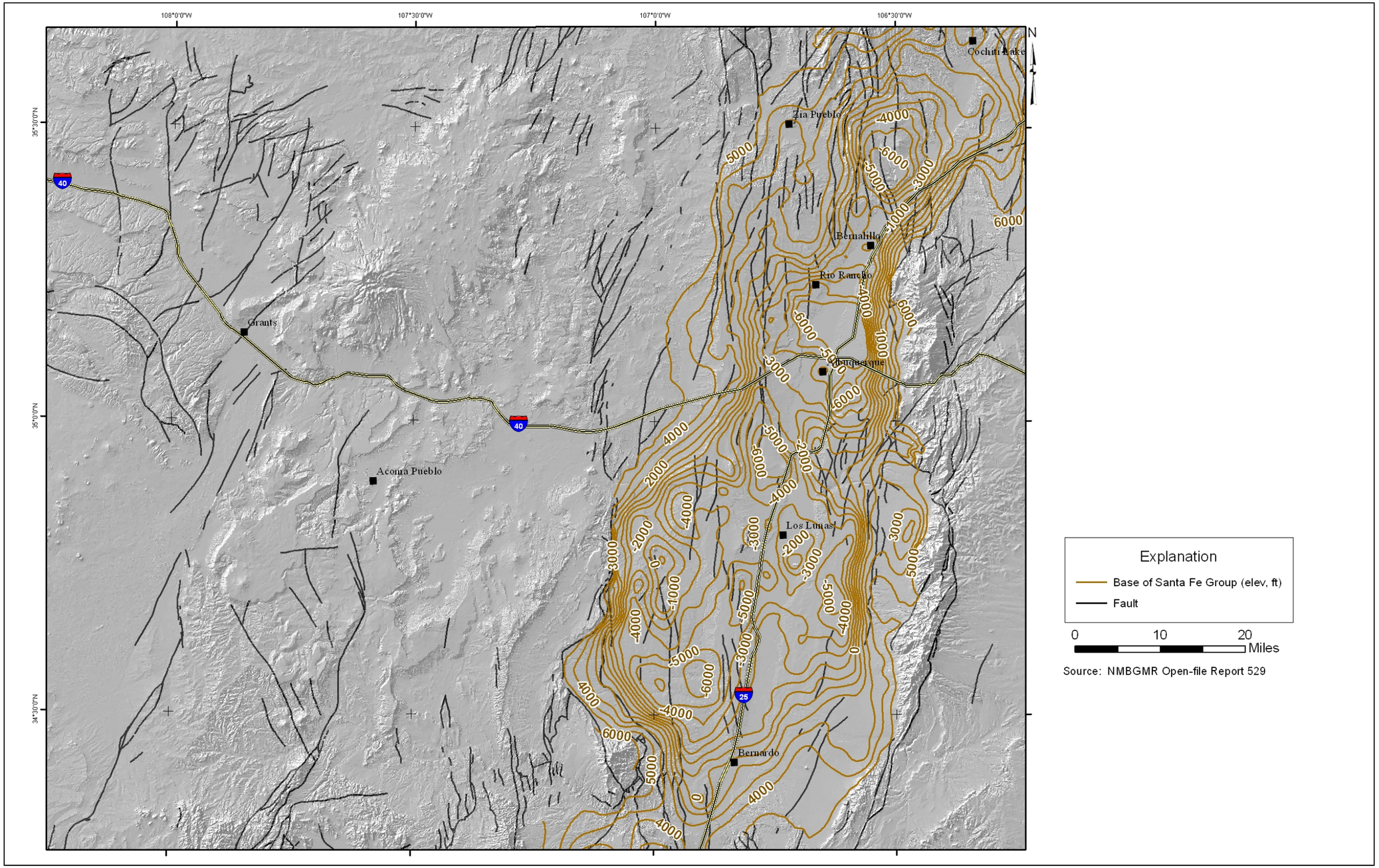

Figure 2.3. Elevation of the base of the Santa Fe Group.

2.1.2 Mesozoic- and Paleozoic-Age Sedimentary Units

West of the MRGB, and beneath the basin fill in the MRGB, is the sedimentary bedrock sequence, summarized on Table 2.1. The units of the sequence are discussed below from youngest to oldest.

Table 2.1. Typical thickness of Paleozoic- and Mesozoic-age sedimentary rock units of the Albuquerque Basin and the southeastern San Juan Basin

era	system	series	lithologic unit		average thickness (JSAI, 2011, appendix A), ft
MESOZOIC	Cretaceous	Upper Cretaceous	Mesaverde Fm., Crevasse Canyon Fm., Gallup Sandstone		1,946
			Mancos Shale		
		Upper Cretaceous	Dakota Sandstone		1,363
	Jurassic	Upper Jurassic	Morrison Formation		
			Todilto Limestone		
			Entrada Sandstone		
	Triassic	Upper Triassic	Chinle Group		1,418
PALEOZOIC	Permian		San Andres Limestone		323
			Glorieta Sandstone		
			Yeso Formation		798
			Abo Formation		935
	Pennsylvanian		Magdalena Group	Madera Limestone	1,103
				Sandia Formation	216
	Mississippian	Upper Mississippian	Arroyo Peñasco Formation		-

Mesaverde Formation: The Cliff House Sandstone, the Menefee Formation, and the Point Lookout Sandstone form part of the Cretaceous-age Mesaverde Group (Beaumont, 1961). The Cliff House Sandstone consists of several hundred feet of thick-bedded, well-cemented sandstone. The Menefee Formation beneath it is a sequence of interbedded and lenticular sandstone, siltstone, shale, and coal beds, thickening to a maximum of about 2,000 ft in the southern San Juan Basin. The Point Lookout Sandstone is similar in character to the Cliff House, with thickness ranging from 40 to 415 ft (Stone et al., 1983).

Crevasse Canyon Formation and Gallup Sandstone: The Cretaceous-age Crevasse Canyon Formation consists of three members, the Dilco Coal, the Dalton Sandstone and the Gibson Coal, and overlies the Gallup Sandstone. The coal members are made up of lenticular sandstone, siltstone, shale, and coal beds; the Dalton and Gallup are predominantly thick-bedded sandstone. The combined thickness of the Crevasse Canyon and Gallup averages 809 ft in the study area (JSAI, 2011). Stone et al., 1983 list a thickness from 513 to 1,400 ft.

Note that the Cretaceous-age units above the lower Mancos Shale are not a series of widespread beds with consistent characteristics, but an interfingering assemblage of laterally equivalent and lithologically complex strata representing an oscillating shoreline with migrating depositional environments (Shomaker et al., 1971, p. 16).

Lower Mancos Shale: The lower Mancos is a thick marine shale, with thin sandstone interbeds at the top and bottom. In the study area, reported thickness ranges from 69 to 1,460 ft (JSAI, 2011).

Dakota-Morrison-Entrada Sequence: A number of distinct units are encompassed in this sequence, designated as a single aquifer for this report. The uppermost unit is the Cretaceous-age Dakota Sandstone, which consists of buff, tan, or brown sandstone beds, with gray and dark-gray carbonaceous or coaly shales. Thickness encountered in the study area ranges from 105 to 396 ft (JSAI, 2011). The interpreted contour map of the base of the Dakota (Connell, 2011) is presented as Figure 2.4.

Beneath the Dakota is the Jurassic-age Morrison Formation, within which the Westwater Canyon Member, the most prominent aquifer, is a yellowish-gray or tan sandstone, interbedded with mudstone. The Westwater Canyon Member is 100 to 300 ft thick, while the entire Morrison Formation in the study area ranges from 312 to 1,082 ft thick, (JSAI, 2011; Stone et al., 1983). About 50 percent of the entire sequence is well-cemented sandstone, and 50 percent is shale and siltstone (Baldwin and Anderholm, 1992, p. 24). Below the Morrison Formation is a limestone and gypsum unit: the Todilto Limestone, on average 76 ft thick (JSAI, 2011, appendix A).

The Jurassic-age Entrada Sandstone, conformably underlying the Morrison Formation, is an arkosic sandstone and siltstone, with an average thickness of 208 ft (JSAI, 2011). Both the Morrison Formation and the Entrada Sandstone thin to the south of Interstate 40, merging into the Zuni Sandstone in the southernmost study area. Both units were eroded prior to renewed deposition during the Cretaceous (Baldwin and Anderholm, 1992).

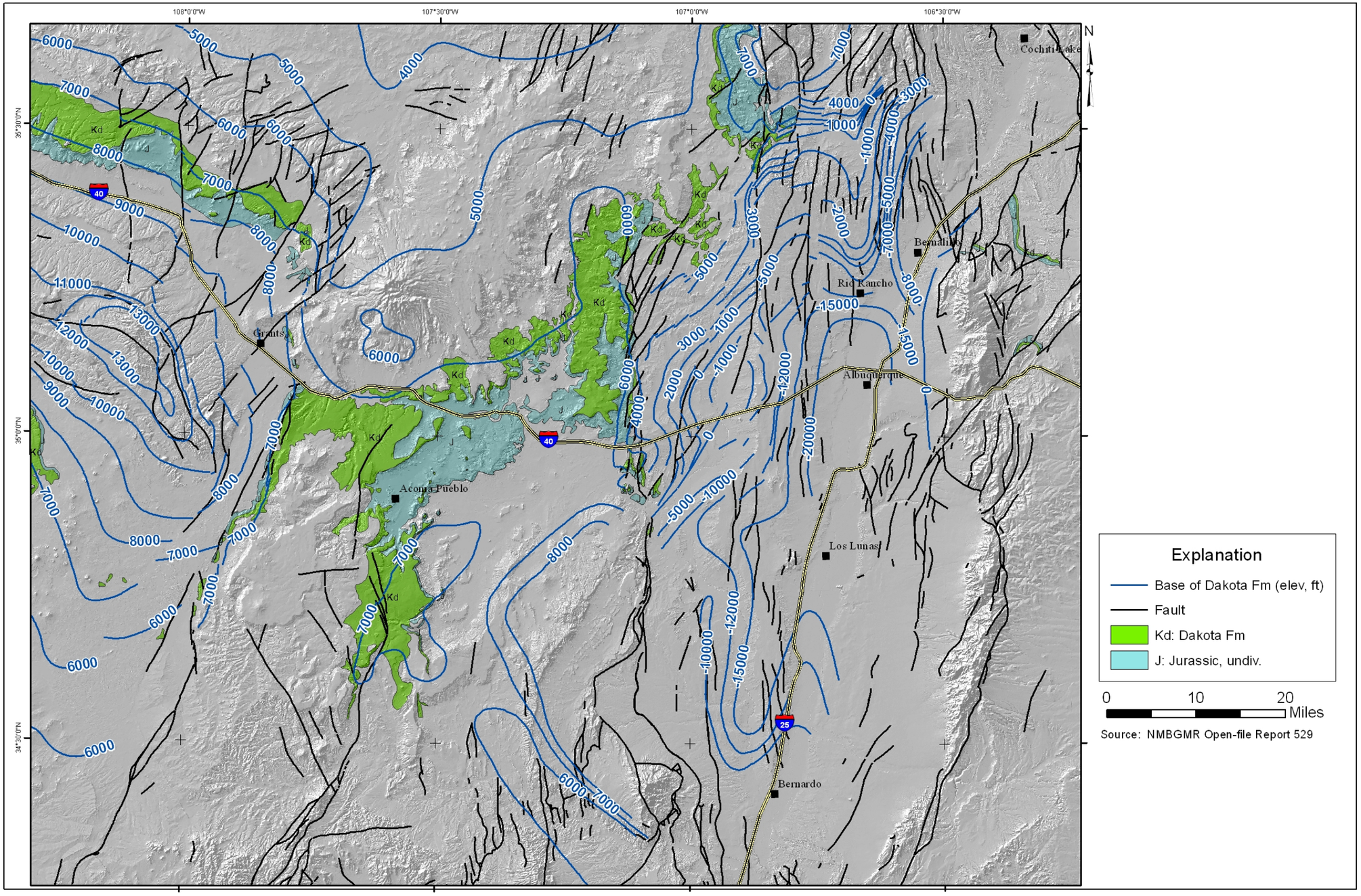

Figure 2.4. Elevation of the base of the Dakota Sandstone.

Chinle Formation: The Triassic-age Chinle Formation is an aquitard, and is composed of reddish-brown siltstone and mudstone, grayish-purple mudstone, and minor sandstone and limestone. Some local sandstone beds of limited extent within the Chinle are known to produce water, but the overall great thickness and low permeability of the unit make it a barrier to regional groundwater flow. Thickness of the Chinle Formation ranges from 1,011 to 1,678 ft and averages 1,418 ft (JSAI, 2011).

San Andres-Glorieta Sequence: The top of the Permian-age section is defined by the San Andres Limestone, which interfingers with the Glorieta Sandstone, with total thickness ranging from 123 to 660 ft (Baldwin and Anderholm, 1992) and averages 323 ft (JSAI, 2011). The aquifer thins from south to northeast, from the Lucero Uplift to the northern part of the study area (Baars, 1962). Local solution channels, where limestone has been dissolved by groundwater, greatly enhance the permeability of the unit, in particular west of Grants, New Mexico (Frenzel, 1992). The unit is continuous from the Zuni Uplift to the Albuquerque Basin (e.g., Frenzel, 1992; Baldwin and Anderholm, 1992).

The Yeso Formation: The Yeso Formation consists of the upper gypsiferous San Ysidro shale and siltstone member and the lower Mesita Blanca sandstone member. It ranges in thickness from 315 to 1,345 ft (JSAI, 2011).

Abo Formation: The Abo Formation is composed of reddish-brown siltstone, sandstone and shale with ubiquitous mud-crack and ripple impressions. It forms a conformable contact with the underlying Madera Formation; usually the first appearance of a significant limestone ledge marks the boundary between the Madera and the Abo (Kelley and Northrop, 1975). In the western part of the study area near the Zuni Uplift, the underlying Pennsylvanian units are absent and the Abo Formation was deposited directly on Precambrian-age basement (Foster, 1957; Baldwin and Anderholm, 1992). Thickness in the study area ranges from 506 to 1,372 ft (JSAI, 2011).

Madera Group and Sandia Formation: The Pennsylvanian-age Madera Group and the underlying Sandia Formation are lithologically similar as they consist predominantly of limestone and minor sandstone. Siltstone, conglomeratic sandstone, and mudstone are locally present in the Madera Group. Thickness of the Madera Group is a maximum of 1,600 to 1,900 ft in the area of the Lucero Uplift, with a typical additional Sandia Formation thickness of 400 ft (Baldwin and Anderholm, 1992). The average reported thickness of each unit in the study area is 1,103 ft and 216 ft, respectively, but the maximum combined thickness locally exceeds 2,600 ft (JSAI, 2011). Both units thin to the west and the northwest, and disappear southwest of the Zuni Uplift over roughly the entire southwestern part of the study area. The Pennsylvanian-age units are of low permeability (Stone et al., 1983) and are thought to be only locally a significant source for groundwater.

2.1.3 Precambrian-Age Crystalline Rocks

Precambrian-age igneous rock and metamorphic rocks are exposed in the Zuni Uplift, the Lucero Uplift, the Nacimiento Uplift, the Sandia Mountains, the Manzano Mountains, and the Ladrones (Fig. 2.1). The rocks consist mostly of granite with some gneiss, metavolcanic rocks, gabbros and metasedimentary rocks among more mafic amphibolites (Brown et al., 1999; Strickland et al., 2003).

The elevation of the Precambrian basement falls away from the above-mentioned uplifts, and underneath the Albuquerque Basin to depths in excess of 25,000 ft. A contour map of the top of the Precambrian is presented on Figure 2.5.

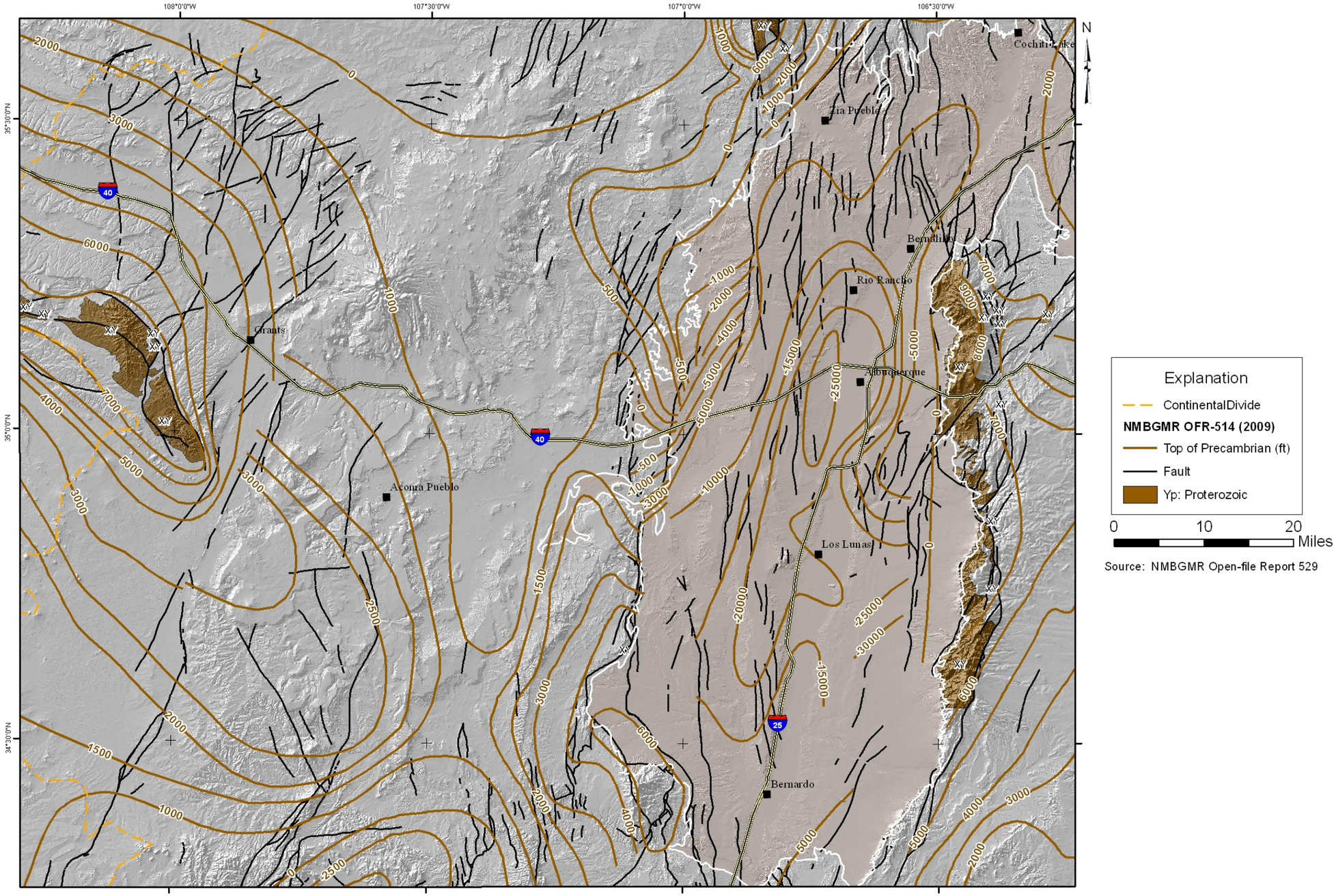

Figure 2.5. Elevation of the top of the Precambrian basement.

3.0 HYDROGEOLOGY

The bedrock aquifers of the study area are recharged in the outcrop areas around the Zuni, Nacimiento and Lucero Uplifts, and around Mount Taylor (Fig. 2.1). Water discharges as spring flow to surface channels, or as groundwater flow to the San Juan Basin and to the MRGB.

Recharge enters the Dakota-Morrison-Entrada aquifer particularly in the outcrop areas around Mount Taylor, flowing northwest to the San Juan Basin and southeast to the MRGB. Recharge enters the San Andres-Glorieta aquifer particularly along the northeastern perimeter of the Zuni Mountains, flowing generally north to the San Juan Basin and east toward the MRGB.

Water discharging as springs from the bedrock aquifers may be consumptively used, or may re-infiltrate to local groundwater systems. Water discharging as springs along the Rio Puerco fault zone may re-infiltrate from Rio Puerco flows to the Santa Fe Group aquifer of the MRGB.

3.1 Aquifers and Confining Zones

The main aquifer units of the MRGB are alluvium and Santa Fe Group basin-fill deposits. Outside the MRGB, the bedrock geologic units described above are grouped hydrogeologically into principal aquifers and confining zones as follows:

- The Upper Cretaceous aquifer composed of the Mesaverde Formation, Crevasse Canyon Formation, and Gallup Sandstone;
- The confining zone represented by the Mancos Shale;
- The Cretaceous and Upper Jurassic aquifer made up of the Dakota Sandstone, Morrison Formation, and Entrada Sandstone;
- The confining zone formed by the mudstones of the Triassic-age Chinle Group; and
- The aquifer consisting of the Permian-age San Andres Limestone, Glorieta Sandstone, and Yeso Formation.

Upper Cretaceous Aquifer: The Mesaverde Group, Crevasse Canyon Formation and the Gallup Sandstone form local aquifer units above the lower Mancos Shale.

Mancos Shale: The Mancos Shale is a confining layer above the Dakota Sandstone. In the study area, the Mancos is interfingered with sandstones that locally can be a source of groundwater, but the limited extent of the sandstones and the thick shale surrounding them make the Mancos a regional aquiclude with limited vertical leakance to aquifers below and above it.

Dakota – Morrison Entrada Aquifer: The interpreted potentiometric-surface contours of the Morrison Formation and the overlying Dakota Sandstone are presented on Figure 3.1 indicating groundwater flow toward the northeast into the San Juan Basin and southeast toward the Rio Puerco fault zone from a potentiometric high around Mount Taylor where the Morrison Formation outcrops. The unit thins to the north and is absent southwest of the Zuni Uplift.

Chinle Formation and Associated Units: The Chinle Group is the confining layer of the San Andres – Glorieta aquifer, overlying it with a total thickness in excess of 1,000 ft (Table 2.1). According to Baldwin and Anderholm (1992), fracturing and faulting probably have little significance in creating upward flow paths as the clay-rich unit tends to be self-healing.

San Andres-Glorieta-Yeso Aquifer: These combined units are a significant regional aquifer characterized by local high-transmissivity solution channel (karst) features (Baldwin and Anderholm, 1992).

Interpreted potentiometric surface contours for the San Andres-Glorieta aquifer are presented on Figure 3.2. The contours show groundwater flow to the south and east, from the Zuni and Nacimiento Uplifts toward the confluence of Rio Puerco and Rio San Jose at the north end of the Lucero Uplift. Hydraulic gradients steepen below Bluewater Lake and again across the Rio Puerco fault zone.

Most groundwater moves in the networks of solution channels. Within such channels, apparent transmissivities are high (Baldwin and Anderholm, 1992). Away from the channels, overall transmissivities are lower (Baldwin and Anderholm, 1992; Frenzel, 1992).

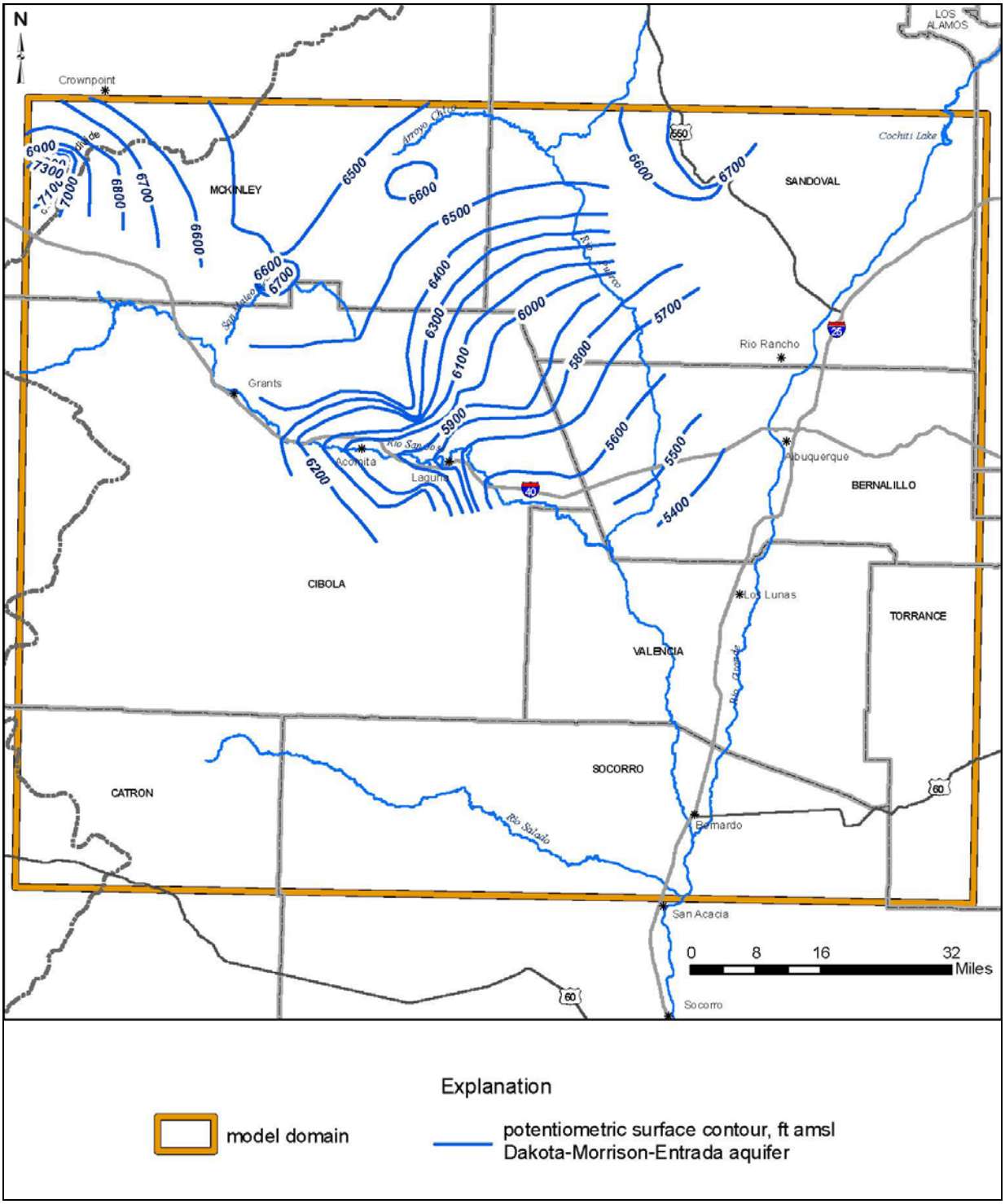

Figure 3.1. Potentiometric surface elevation for the Dakota -Morrison-Entrada aquifer.

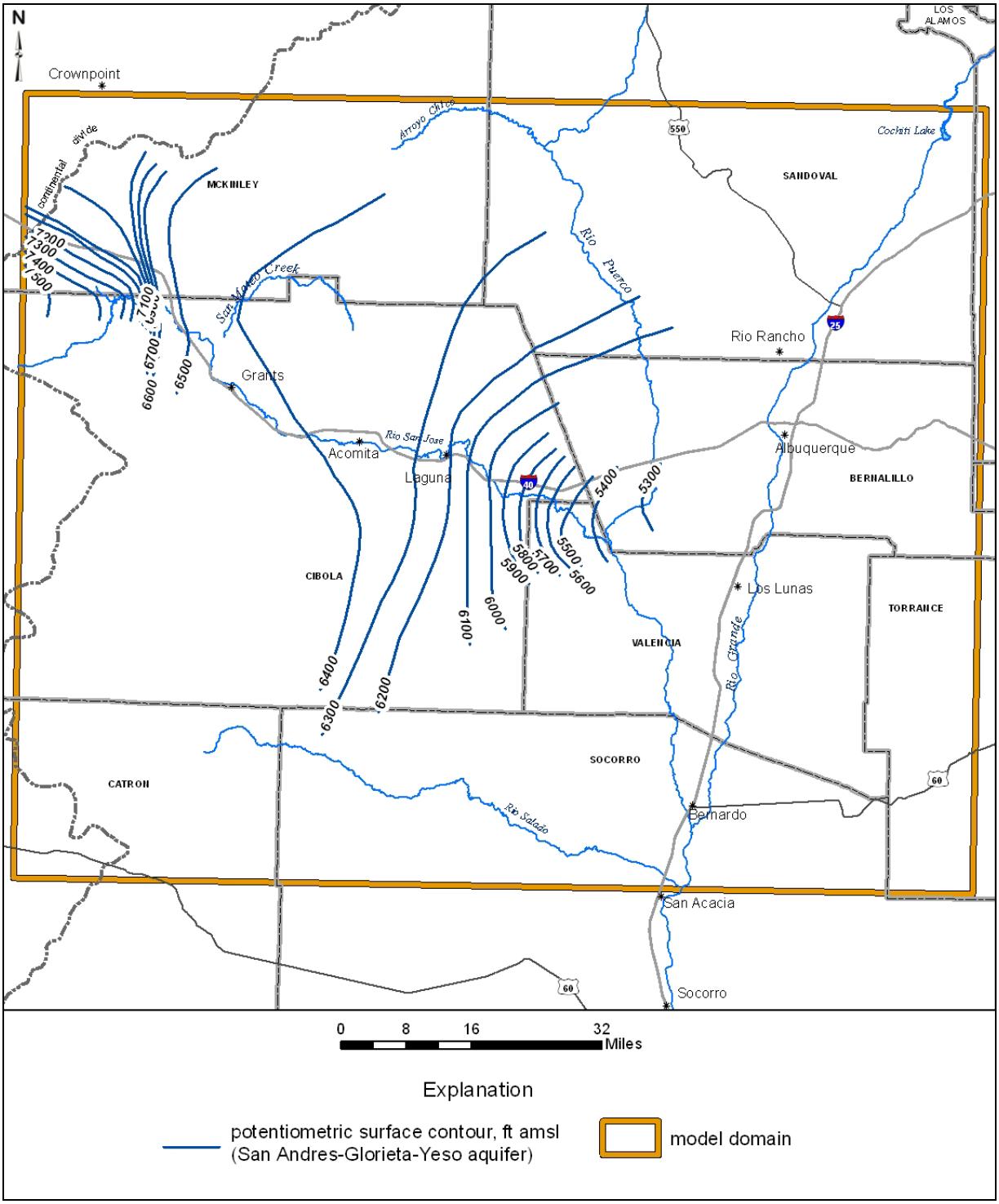

Figure 3.2. Potentiometric surface elevation for the San Andres-Glorieta-Yeso aquifer.

3.2 Aquifer Properties

The spatial distribution of aquifer parameters was estimated based on the distributions presented in previous studies (Frenzel, 1992; McAda and Barroll, 2002; Kernodle, 1996), and on results of the pumping test of Sandoval County Well 6 (Shomaker, 2008). Other information was obtained from bedrock-aquifer wells in the study area (JSAI, 2011).

The basin-fill (alluvium plus Santa Fe Group) aquifer of the MRGB is generally more transmissive than the bedrock aquifers. McAda and Barroll (2002) indicate hydraulic conductivities of Santa Fe Group ranging from 4 to 150 ft/day. Ranges of transmissivity and hydraulic conductivity valves for bedrock units are summarized in Table 3.1.

Table 3.1. Estimates of aquifer transmissivity/hydraulic conductivity

geologic unit	transmissivity, ft^2/day	hydraulic conductivity, ft/day	range of layer thickness,[1] ft	reference
Mancos Shale	-	0.0005 - 0.05005	1,204 – 2,440	Shomaker and Petronis, unpublished
Dakota Ss., Morrison Fm., Entrada Ss.	1 - 749	0.1 - 8.3	65 - 2,502	Shomaker and Petronis, unpublished
Chinle Fm.	-	0.1 - 0.0000001	1,036 - 1,815	Frenzel, 1992
Agua Zarca Ss., San Andres Ls., Glorieta Ss.	10 - 450,000	0.003 - 20	25 - 730	Frenzel, 1992
		0.25 - 0.36		Shomaker, 2008
Yeso Fm.	0.5 - 1,000	0.1 - 2	315 - 1,345	Frenzel, 1992
Abo Fm.	0.5 - 1,000	0.03 - 2	506 - 1,372	Frenzel, 1992

[1] layer thicknesses from appendix A (Connell, 2011)
Fm. - Formation
Lm. - Limestone
Ss. – Sandstone

3.3 Recharge

Recharge from precipitation was estimated (Frenzel, 1992) for the San Andres-Glorieta aquifer; recharge occurs in the outcrops around the Zuni Uplift, through the basalt and alluvium near Grants and through infiltration of runoff from the Bluewater-upper Rio San Jose stream system.

McAda and Barroll (2002) estimate mountain front recharge along the eastern side of the MRGB and the eastern side of the Lucero Uplift, and stream-channel recharge from Rio Puerco and Rio Salado to the MRGB. Shomaker and Petronis (unpublished) estimate recharge in the San Juan Basin and around Mount Taylor. Recharge estimates for the study area are summarized on Table 3.2 and Figure 3.3.

Table 3.2. Estimates of recharge to the study area

area	affected flow area and direction	recharge, ac-ft/yr	reference
Sandia – Manzano Uplift	flow into the MRGB	10,936	Anderholm, 2001; McAda and Barroll, 2002
Jemez Mountains	flow to the MRGB	2,040	Sanford et al., 2004
Sierra Nacimiento	flow to the MRGB	1,000	McAda and Barroll, 2002
Mount Taylor area	flow into the MRGB and the San Juan Basin	>32,950	Shomaker and Petronis, unpublished
Zuni Uplift	northeast and east flow	3,660	Frenzel, 1992
Acoma Embayment	northward flow to the Rio San Jose	3,650	Shomaker and Petronis, unpublished
Lucero Uplift	flow to the MRGB	1,530	Sanford et al., 2004
Sierra Ladrones (southern Lucero Uplift)	flow to the MRGB	808	McAda and Barroll, 2002
Rio Puerco (within MRGB)	inflow to MRGB	960	McAda and Barroll, 2002

ac-ft/yr - acre-feet per year MRGB - Middle Rio Grande Basin

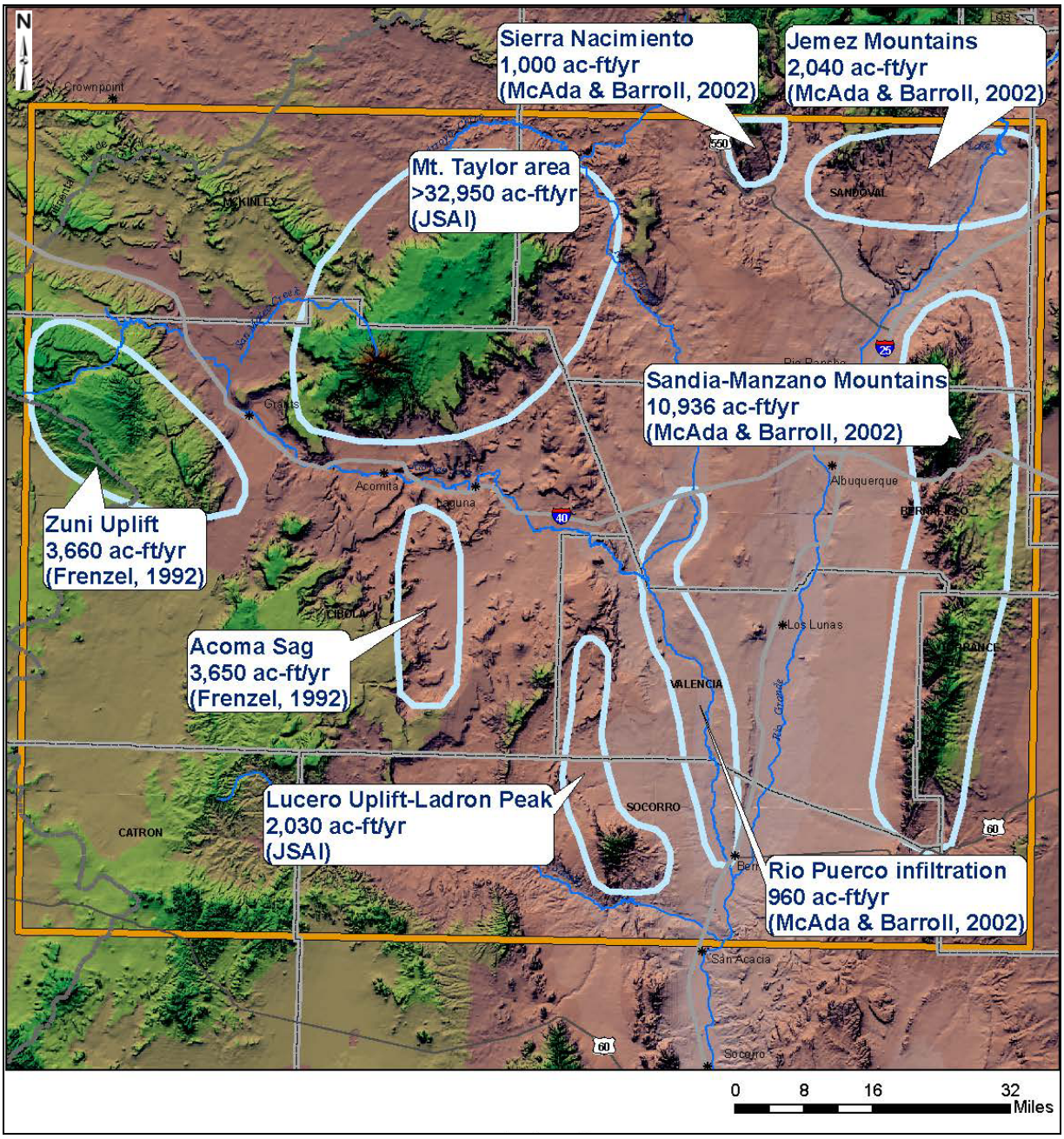

Figure 3.3. Groundwater recharge estimates for study area.

3.4 Spring Discharge

Groundwater flow discharges from the bedrock aquifers at springs within the study area, shown on Figure 3.4. A survey of springs was conducted (JSAI, 2011, appendix B) as well as an analysis of spring and groundwater chemistry to estimate sources of spring discharge (JSAI, 2011, appendix C). An analysis of surface-flow data on Rio Puerco was also conducted to further inform estimates of spring discharge and stream-channel recharge (JSAI, 2011, appendix D).

Ojo de Gallo discharges from the San Andres-Glorieta aquifer across the San Rafael Fault that juxtaposes the San Andres-Glorieta with the Chinle Group aquitard. Discharge rate, estimated at 3,000 gallons per minute (4,800 acre-feet per year; ac-ft/yr) (White and Kues, 1992), has declined over time due to groundwater pumping (Baldwin and Anderholm, 1992).

Horace Springs discharges below Grants from the McCarty basalt, at a rate estimated (White and Kues, 1992) at 2,000 gallons per minute (3,200 ac-ft/yr). Discharge has declined over time due to groundwater pumping (Baldwin and Anderholm, 1992).

Spring discharge along the Lucero Uplift is estimated at 1,739 ac-ft/yr, plus about 165 ac-ft/yr of gain at the northern end of the Rio Puerco fault zone (Melis and McCoy, 2010) in the Rio Salado across the southern edge of the uplift.

Springs discharge across the Rio Puerco fault zone. The Rio San Jose is estimated to gain about 2,200 ac-ft/yr across the fault zone and other, minor springs contribute an estimated 7 ac-ft/yr. Spring flow discharging across the fault zone may infiltrate from Rio Puerco into the MRGB Santa Fe Group aquifer. An estimated 1,500 to 7,000 ac-ft/yr could flow from the San Juan Basin to the MRGB across the fault zone (e.g., Sanford et al., 2004) according to a calibration of the McAda and Barroll (2002) MRGB model using the geochemical data of Plummer et al. (2004a).

3.5 Groundwater Discharge

Water from the bedrock aquifers, not discharging to springs, flows as groundwater to the MRGB and to the San Juan Basin. Upward leakage into the Santa Fe Group aquifer of the MRGB is thought to be small, except along the Rio Puerco fault zone where poor water quality (JSAI, 2011, appendix C) indicates substantial upward leakage. Plummer et al. (2003) suggest that up to 7 percent of fault-zone water comes from the San Juan Basin.

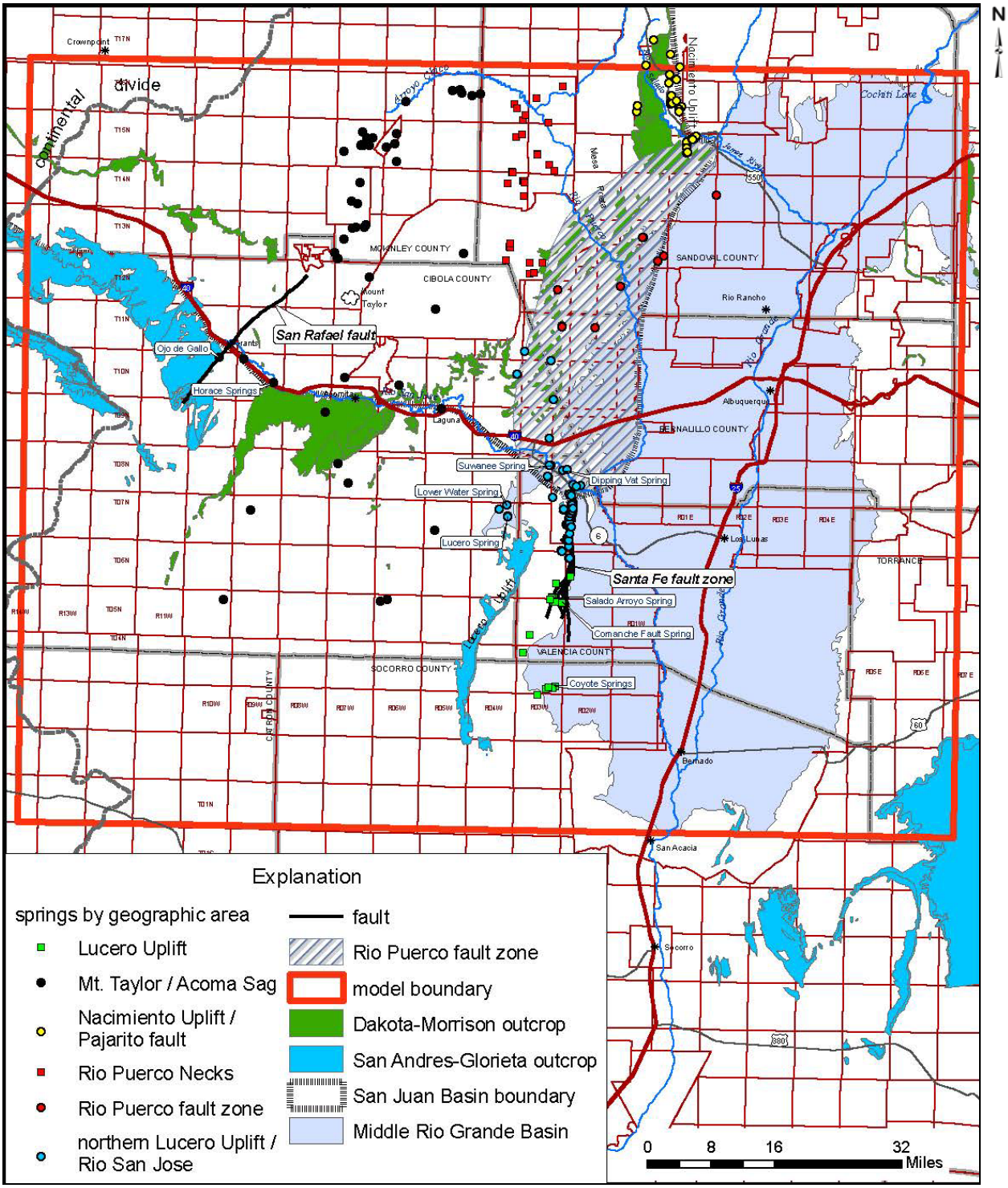

Figure 3.4. Springs and seeps in the study area.

4.0 GROUNDWATER-FLOW MODEL

The numerical groundwater-flow model represents the MRGB, the underlying bedrock units and the extension of these units to the west (Fig. 1.1). The western part of the model domain coincides approximately with the topographic watershed of the Rio San Jose.

The model was built from an existing MRGB model (McAda and Barroll, 2002), extending the model domain deeper and to the west. The model domain includes most of the area represented by a previous model of the Bluewater Basin (Frenzel, 1992).

The model electronic files will be included in the final document.

4.1 Previous Work

Multiple models of the MRGB have been developed, which represent historical groundwater withdrawals in the basin, and the effects on groundwater levels and surface discharges (e.g., Kernodle and Scott, 1986; Kernodle et al., 1995; Barroll, 2001; McAda and Barroll, 2002; Sanford et al., 2004). Differences among the models include a range of recharge rates and hydrogeologic properties.

Models of the Rio San Jose system include a two-dimensional numerical model of the alluvial groundwater system (Risser and Lyford, 1983) that provides detailed estimates of seepage rates along the river. A model of the Permian-age bedrock aquifer in the southeastern San Juan Basin and Western Rio San Jose (Frenzel, 1992) estimates recharge in the Zuni Uplift and simulates groundwater pumping along the middle reaches of the Rio San Jose from Grants to Laguna.

Studies of the San Juan Basin (Gordon, 1961; Cooper and John, 1968; Stone et al., 1983) provide information on the northwestern part of the study area. Regional groundwater models of the Cretaceous- and Jurassic-age San Juan Basin aquifers (Hearne, 1977; Guyton, 1978; Lyford and Frenzel and Lyford, 1982; Lyford, 1979; Lyford et al., 1980) began in connection with past and proposed withdrawals from the Morrison Formation. Larger-scale models (Shomaker, 1995; Kernodle, 1996; Carpenter and Shomaker, 1998) simulate groundwater flow in the San Juan Basin. Shomaker and Petronis (unpublished) re-evaluated the models of the San Juan Basin aquifers and estimated recharge around Mount Taylor.

4.2 Computer Code

The computer program used for the model is a modified version of MODFLOW-2000 (Harbaugh et al., 2000). The original USGS code was modified by the following:

1. The addition of modules OUT1 and ZON1 (JSAI, 2010), used to manage output from large and complex models.
2. The addition of module RIV2 (JSAI, 2010, modified from Miller, 1988), used to represent streamflow routing in the Rio Puerco system and in the Rio Salado. The San Andres-Glorieta model (Frenzel, 1992) utilized RIV2 in a version of MODFLOW-1988 (McDonald and Harbaugh, 1988) to represent the Bluewater - Rio San Jose system tributary to Rio Puerco.
3. The modification of module WEL (McDonald and Harbaugh, 1988) to automatically transfer specified pumping from a dry cell to the underlying cell. This modification to MODFLOW-2000 was employed in the USGS MRGB model (McAda and Barroll, 2002).
4. The addition of module LAK2 (Jones, 2011), used to simulate water levels in pumping wells. The simulation of pumping water levels is employed in the calibration to pumping test results and used to constrain future simulated pumping rates to realistic minimum pumping water levels.

4.3 Model Grid

The model domain, shown on Figure 4.1, is divided into a matrix of 9 layers, 156 rows, and 189 columns, with uniform horizontal cell-dimensions of 1 km by 1 km, following the origin and gridding of McAda and Barroll (2002).

Model layering in the Rio Grande Basin is modified from McAda and Barroll (2002) by (1) activating previously inactive cells, corresponding to bedrock units, in the lower model layers at the margins of the basin, (2) thickening Layers 6 and 7, and (3) using Layers 8 and 9 to represent bedrock units beneath the basin fill, rather than basin fill as previously modeled.

Model layering outside the MRGB follows the stratigraphic intervals shown in Table 4.1 for Layers 5 through 9. The four upper layers represent local units: valley fill, sedimentary and volcanic rocks not part of the regional flow system. They are inactive in most areas. Model layers representing the (absent) overlying formations are also inactive.

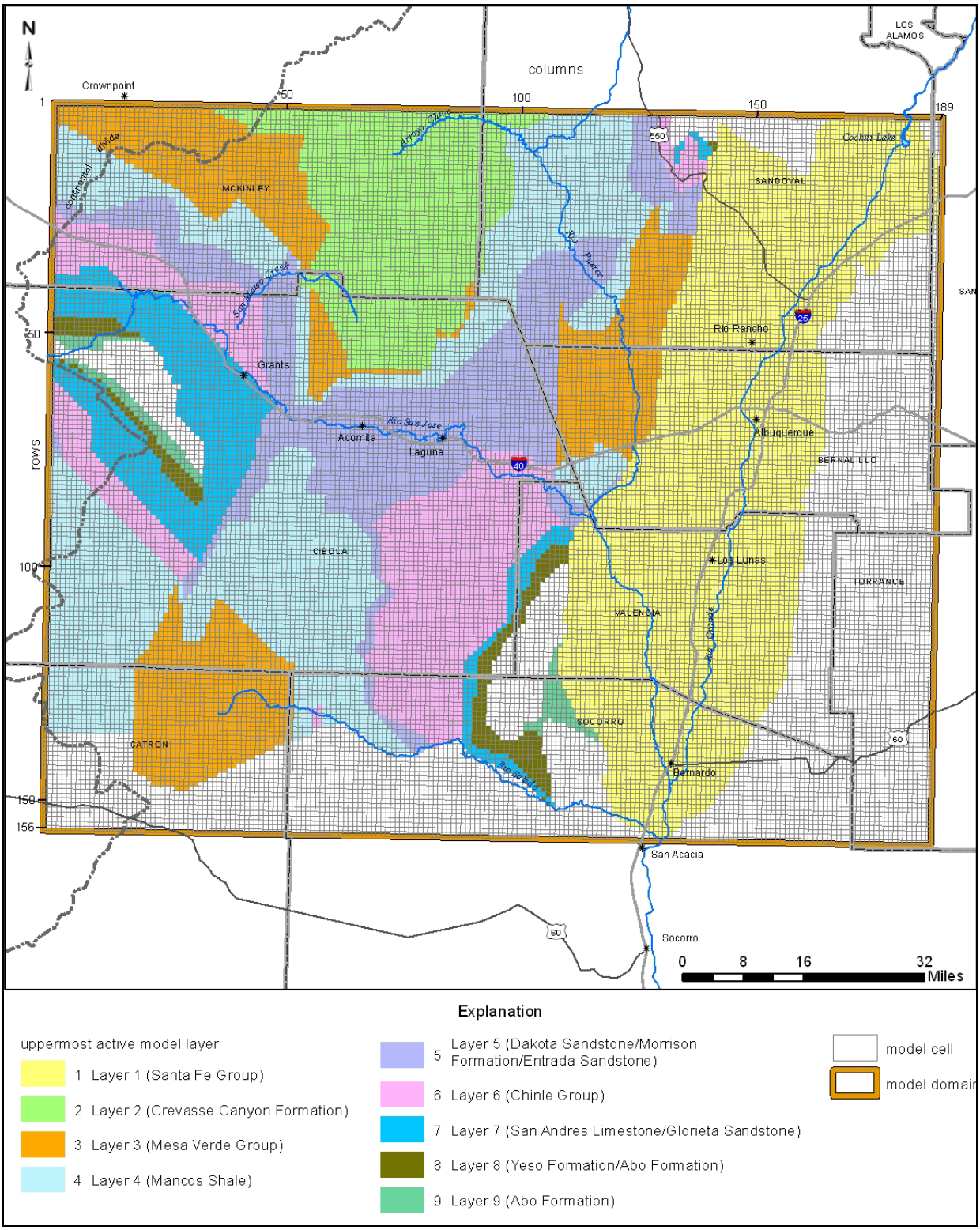

Figure 4.1. Model grid and uppermost active model layer.

Table 4.1. Descriptions of model layers

model layer	stratigraphic unit(s) west of MRGB	model layer thickness west of MRGB, ft	stratigraphic unit(s) in MRGB
1		inactive	alluvium
2		inactive	alluvium
3	Mesa Verde Group and local units	1,025	Santa Fe Group
4	Mancos Shale and local units	1,025	Santa Fe Group
5	Dakota Ss.-Morrison Fm.-Entrada Ss.	1,200	Santa Fe Group
6	Chinle Formation	1,400	Santa Fe Group
7	San Andres Limestone-Glorieta Ss.	250	Santa Fe Group
8	Yeso Fm./Abo Fm.	850	Dakota Ss.-Morrison Fm.-Entrada Ss.
9	Pennsylvanian and older bedrock	950	San Andres Limestone-Glorieta Ss. underlain by Abo/Yeso Fm. and Pennsylvania and older bedrock

MRGB - Middle Rio Grande Basin
Fm. - Formation
Ss. - Sandstone

The bottom of the model is defined as the bottom of the sedimentary sequence (Fig. 2.5).

Elevations of model layers were estimated based on a contour map of the Dakota – Morrison Formation contact (Fig. 2.4). Layer-top and bottom elevations were defined by subtracting average bed thicknesses from the Dakota-Morrison contact elevation. In the Rio Grande basin layers, top and bottom elevations were further modified in certain areas based on a contour map of the bottom elevation of the Santa Fe Group sediments (Fig. 2.3). Contours of the bottom elevations of model Layers 5, 7, and 9 are shown on Figures 4.2, 4.3, and 4.4, respectively.

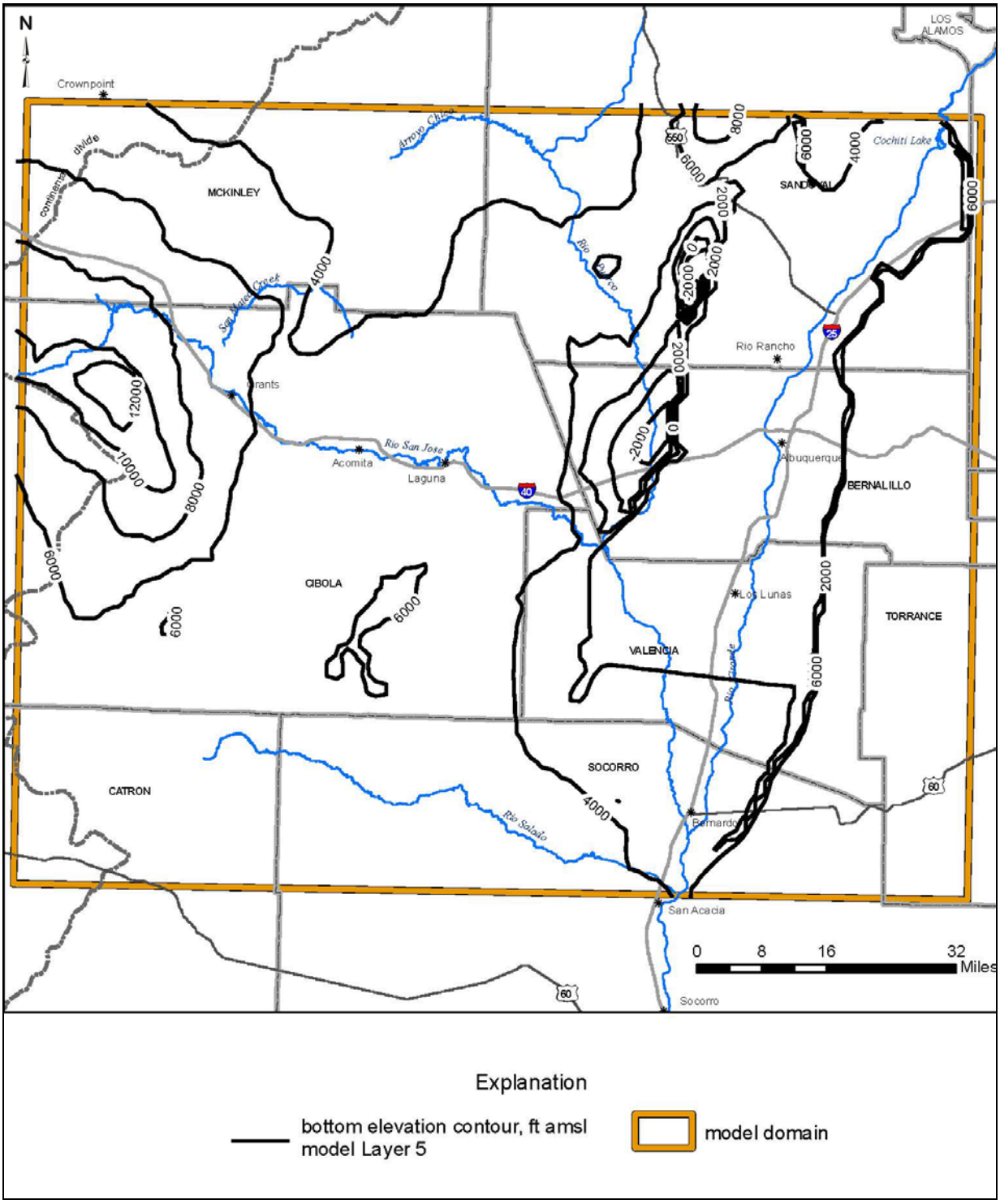

Figure 4.2. Bottom elevation of model Layer 5.

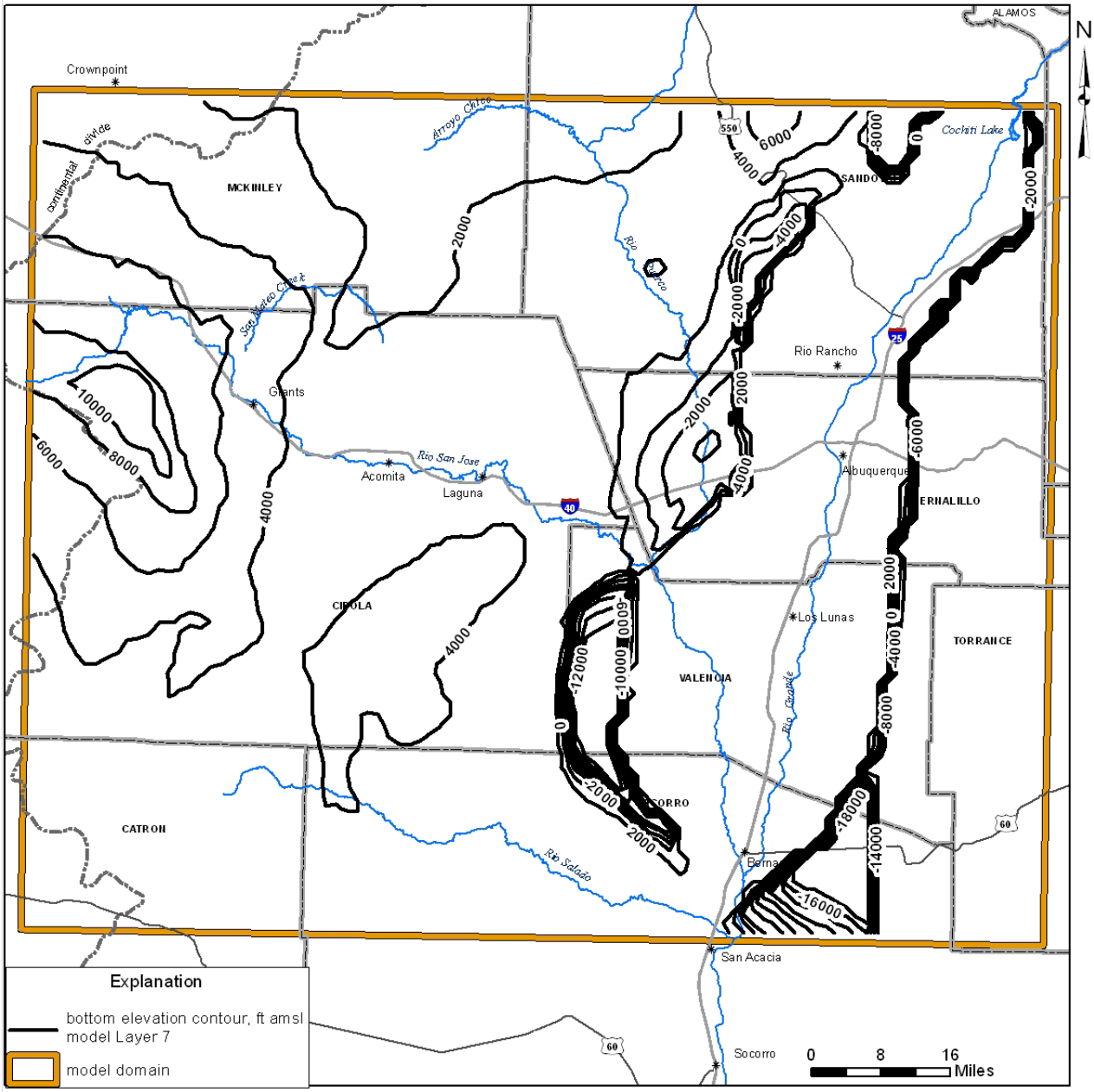

Figure 4.3. Bottom elevation of model Layer 7.

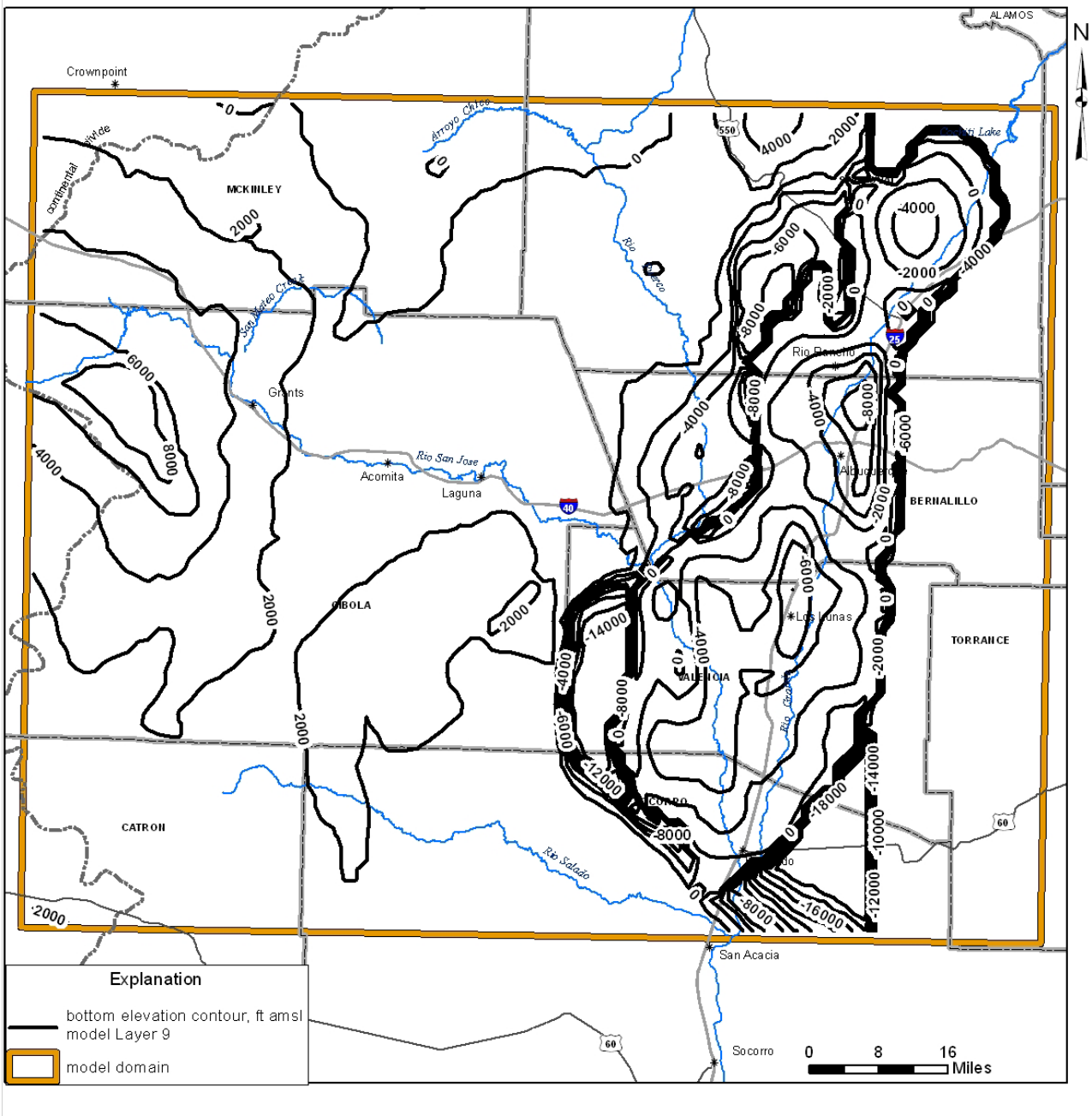

Figure 4.4. Bottom elevation of model Layer 9.

4.4 Aquifer Parameters

Modeled hydrogeologic units of the MRGB were taken unmodified from McAda and Barroll, 2002 except for the thickening of Layers 6 and 7 to represent the entire thickness of basin fill below Layer 5, and converting Layers 8 and 9 to represent bedrock units below. The modeled hydrogeologic units outside the MRGB are shown on Figures 4.5 through 4.9. Aquifer parameters were initially estimated from literature values and from previous models as described above. Parameters were adjusted during model calibration. Among the major adjustments were the delineation of a higher-conductivity zone in Layer 7 (San Andres Limestone) along the axis of the Rio San Jose, and a higher vertical-conductivity zone in Layers 6 and 7 along the steeply-dipping beds at the north end of the Lucero Uplift, near the confluence of the Rio San Jose with the Rio Puerco. Modeled aquifer parameters are presented on Table 4.2.

Additional aquifer parameters are defined using barriers to flow (MODFLOW module HFB) that represent fault barriers. Barriers defined include those representing faults within the Santa Fe Group sediments (McAda and Barroll, 2002), and a barrier along the bedrock-Santa Fe Group contact at the western edge of the Rio Grande sedimentary basin. Barrier conductances were adjusted during model calibration. An additional barrier was added in Layer 7 to represent the sharp drop in San Andres water levels east of Bluewater Lake. Modeled barrier conductances are presented on Table 4.3.

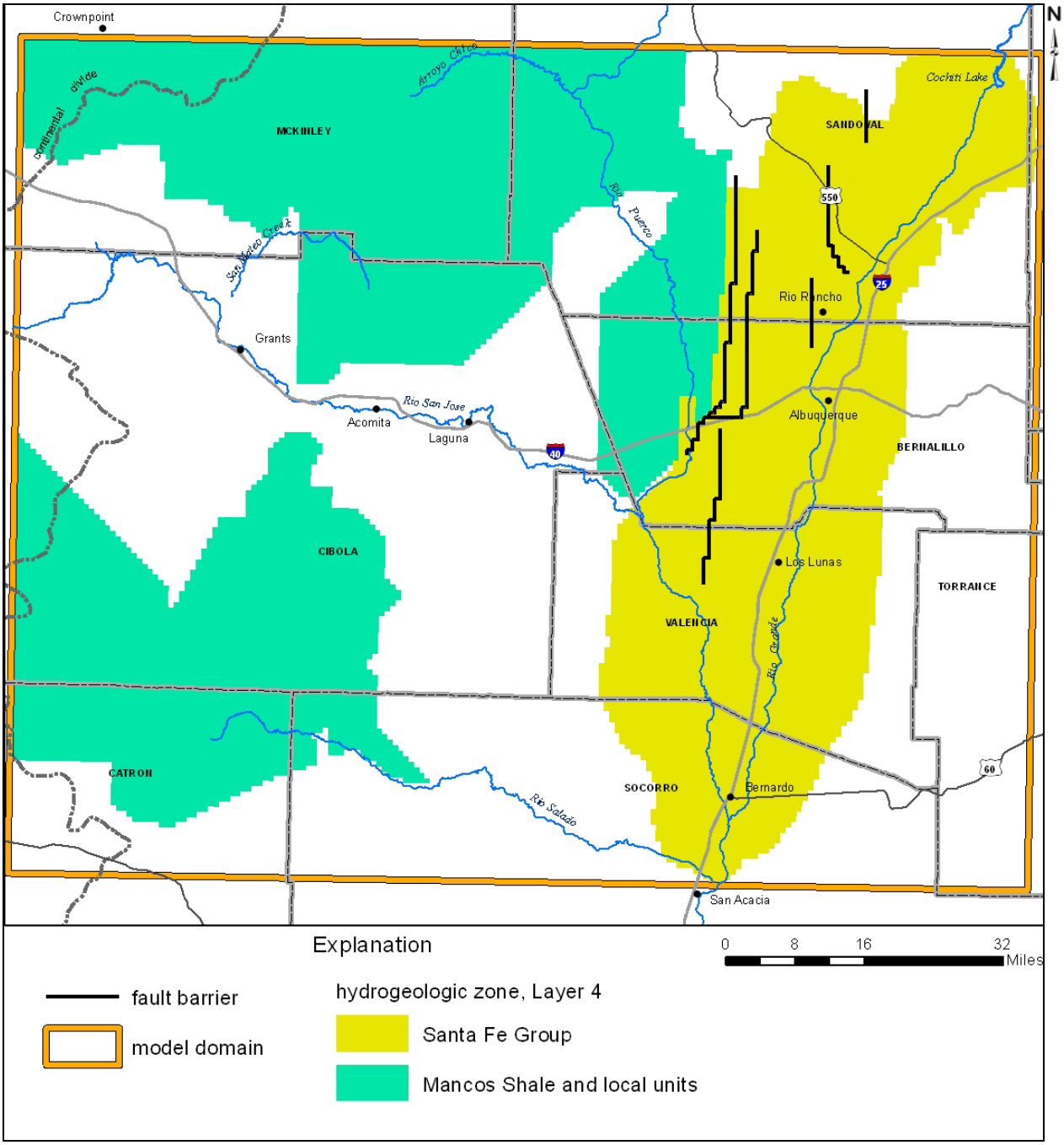

Figure 4.5. Model hydrogeologic zones, Layer 4.

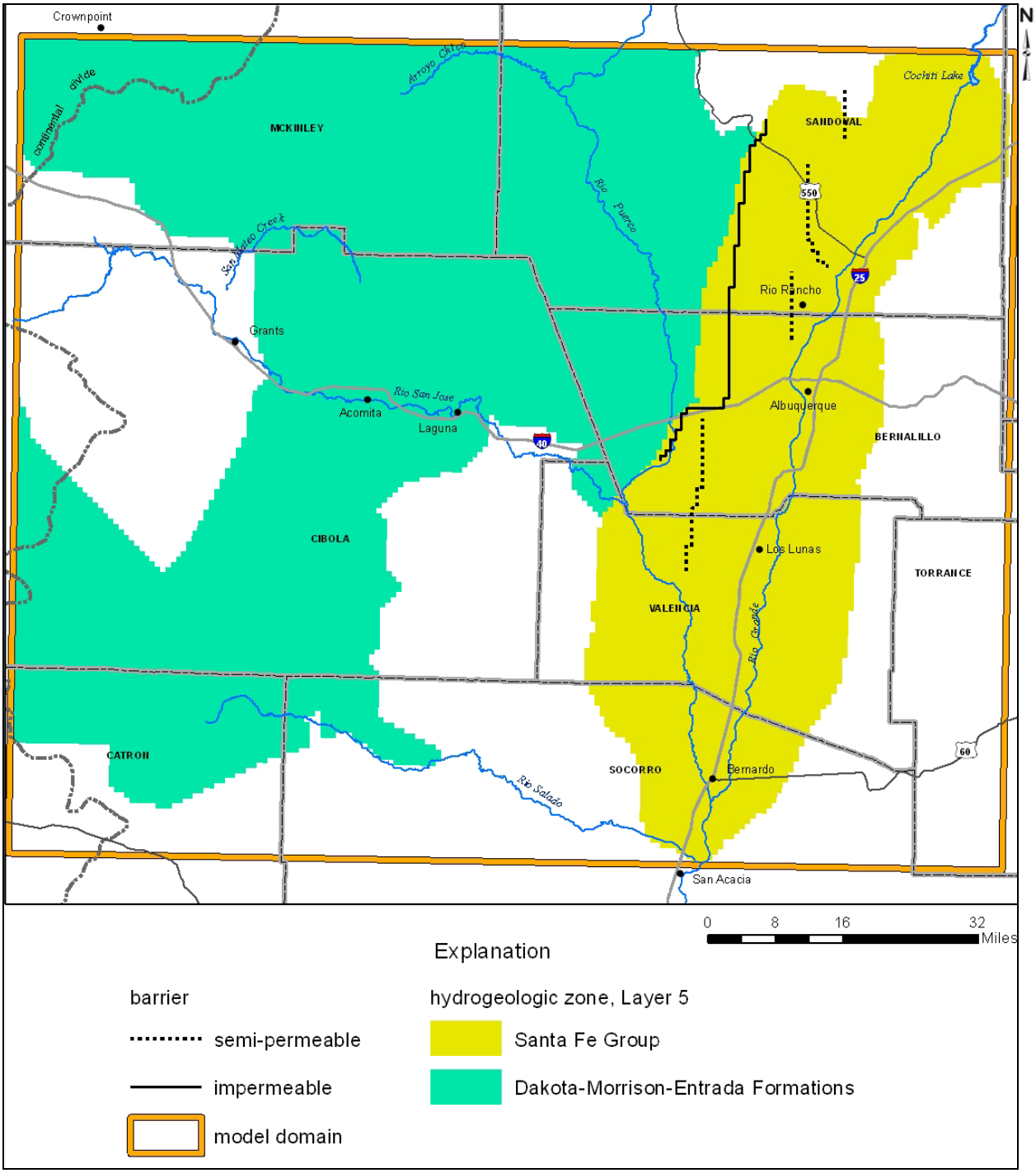

Figure 4.6. Model hydrogeologic zones, Layer 5.

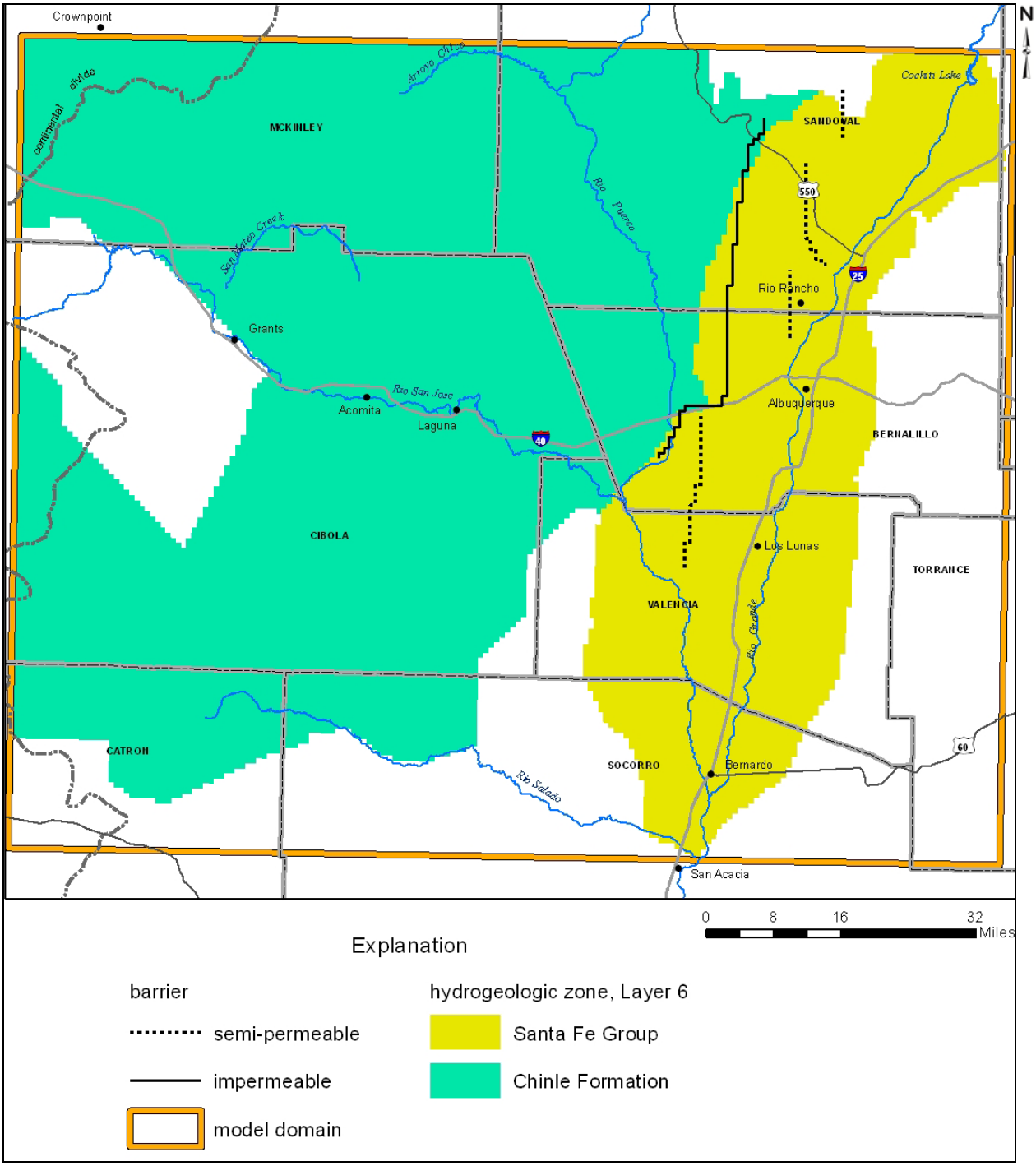

Figure 4.7. Model hydrogeologic zones, Layer 6.

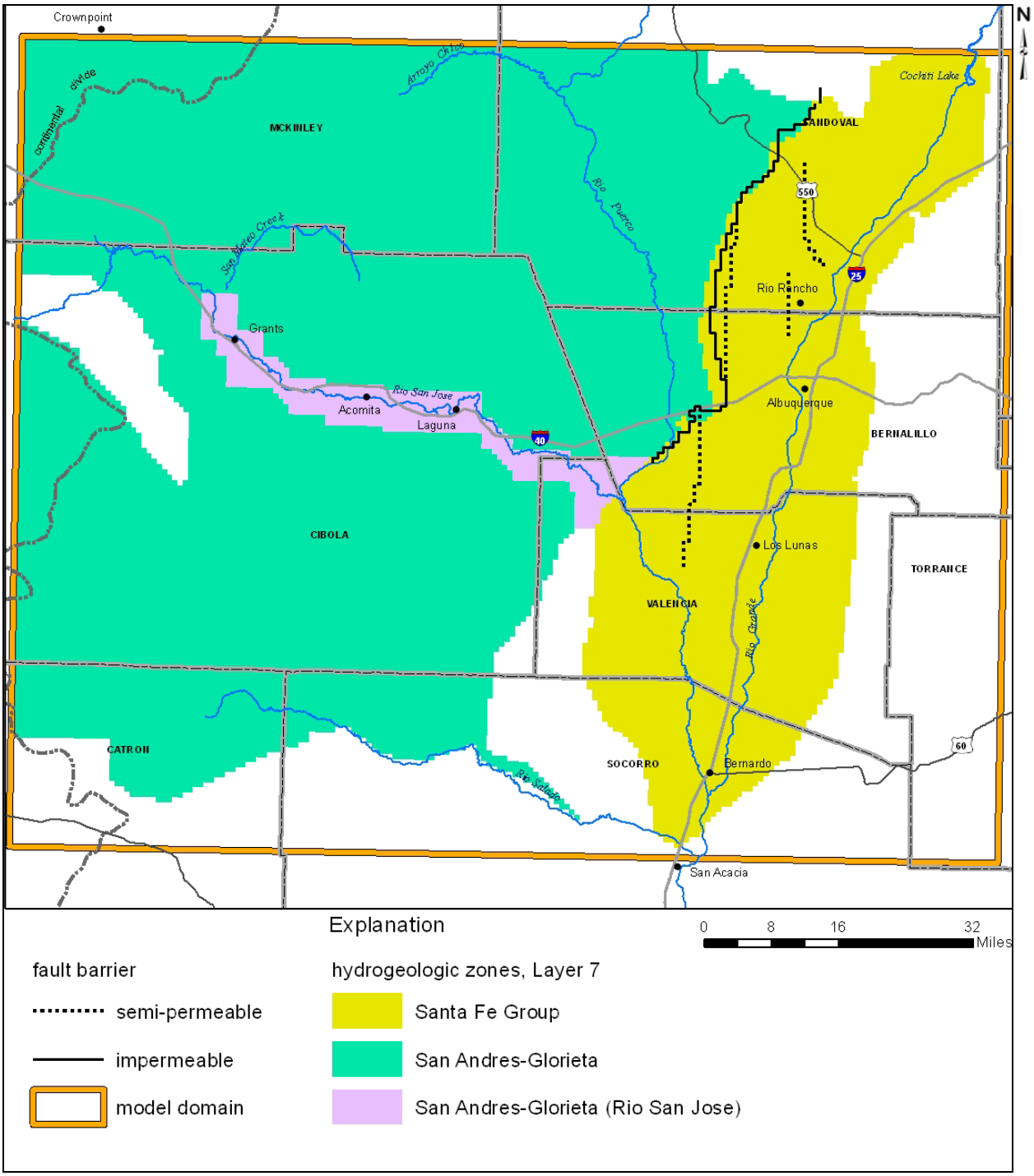

Figure 4.8. Model hydrogeologic zones, Layer 7.

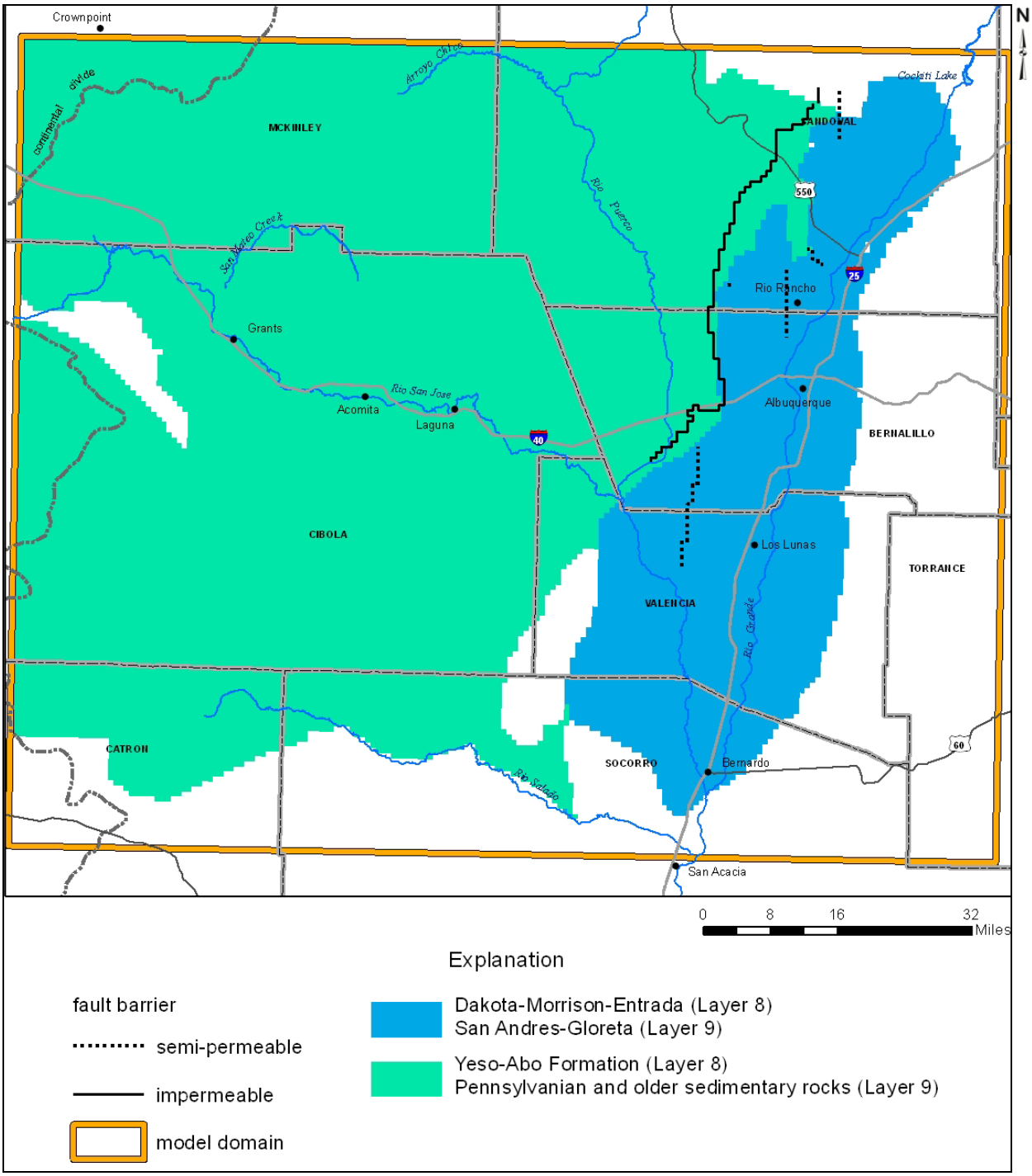

Figure 4.9. Model hydrogeologic zones, Layers 8 and 9.

Table 4.2. Model aquifer parameters

layer	description	thickness, ft	hydraulic conductivity, ft/day	transmissivity, ft^2/day	horizontal to vertical anisotropy ratio	vertical leakance, 1/day	specific storage	storage coefficient	specific yield
4	Mancos Shale \ local units	1,026	0.31	318	150	2.0E-06	2.00E-06	4.1E-03	0.005
5	Dakota Ss.-Morrison Fm.-Entrada Ss.	1,200	0.16	192	150	8.9E-07	2.00E-06	2.4E-03	0.005
6	Chinle Formation	1,400	1.0E-05	0.01	4000	1.8E-12	2.00E-06	2.8E-03	0.005
	Chinle Formation (Lower San Jose / Lucero Uplift)	1,400	1.0E-05	0.01	0.002	3.6E-06	2.00E-06	2.8E-03	0.005
7	San Andres Limestone-Glorieta Ss.	250	1.65	413	4000	1.7E-06	2.00E-07	5.0E-05	0.005
	San Andres Limestone-Glorieta Ss (Rio San Jose)	250	17.0	4,250	4000	1.7E-05	2.00E-07	5.0E-05	0.005
	San Andres Limestone-Glorieta Ss. (Lower San Jose / Lucero Uplift)	250	17.0	4,250	0.002	3.4E+01	2.00E-07	5.0E-05	0.005
8	Yeso Formation /Abo Formation	850	0.05	43	150	3.9E-07	2.00E-07	3.3E-04	0.005
9	Pennsylvanian and older bedrock	950	0.01	10	150	7.0E-08	2.00E-07	2.7E-04	0.005

Table 4.3. Flow barrier conductance

barrier description	leakance, 1/day
internal to MRGB	1.0E-04
Rio Puerco fault zone	1.0E-10
east of Bluewater, north of Bluewater Creek	1.0E-10

MRGB - Middle Rio Grande Basin

4.5 Boundary Conditions

Model boundary conditions for the MRGB are taken from McAda and Barroll (2002). The specified inflows on the west edge of the model domain, which are in the interior of the new model domain, were removed.

MRGB boundary conditions include mountain-front and stream-channel runoff (specified flow, MODFLOW module RCH), inflow and outflow to the Rio Grande and riverside drains (head-dependent flow, module RIV), outflow to interior drains (head-dependent outflow, module DRN), evapotranspiration (head-dependent outflow, module ETS), groundwater inflows from the north and east (specified inflow, module WEL) and pumping wells (specified outflow, module WEL).

Model boundary conditions outside the MRGB were specified as direct recharge (MODFLOW module RCH), stream-channel recharge and base flow discharge (module RIV2) and groundwater inflow and outflow (module GHB) at the north end of the model domain to represent the continuation of the aquifers into the San Juan Basin.

Estimated recharge rates (RCH) were taken from Frenzel (1992). Inflows from the Upper Rio Puerco Basin and outflows to the San Juan Basin (controlled by GHB cells) were specified based on model calibration and reasonable constraints. The stream network (RIV2) defined by Frenzel (1992) was extended to include the lower Rio San Jose, San Mateo Creek, Rio Puerco, and Rio Salado.

Model boundary condition types and locations are shown on Figure 4.10. Model boundary conditions and the resulting simulated water balance are summarized in Table 4.4.

In addition to the natural boundary conditions, historical pumping from wells was represented using module WEL. In addition to MRGB pumping (McAda and Barroll, 2002), pumping outside the MRGB (Frenzel, 1992; BGW, 2012[1]) was represented at the well locations shown on Table 4.5. Simulated pumping rates are shown on Figure 4.11 for the higher rates and Figure 4.12 for the lower rates.

Pumping from deep wells near the MRGB is represented using the MODFLOW module LAK2 (Jones, 2011), to simulate both the Sandoval County aquifer test and potential future deep well pumping. LAK2 is used to simulate in-well pumping water levels.

[1] The data described was furnished by the New Mexico Office of the State Engineer (NMOSE) and is accepted for use by JSAI with the expressed understanding that the NMOSE and BGW make no warranties, expressed or implied, concerning the accuracy, completeness, reliability, usability, or suitability of the data. The furnishing of the data by the NMOSE is not a sale transaction and no consideration has been exchanged. The NMOSE and BGW shall not be liable to JSAI by reason of any use made thereof.

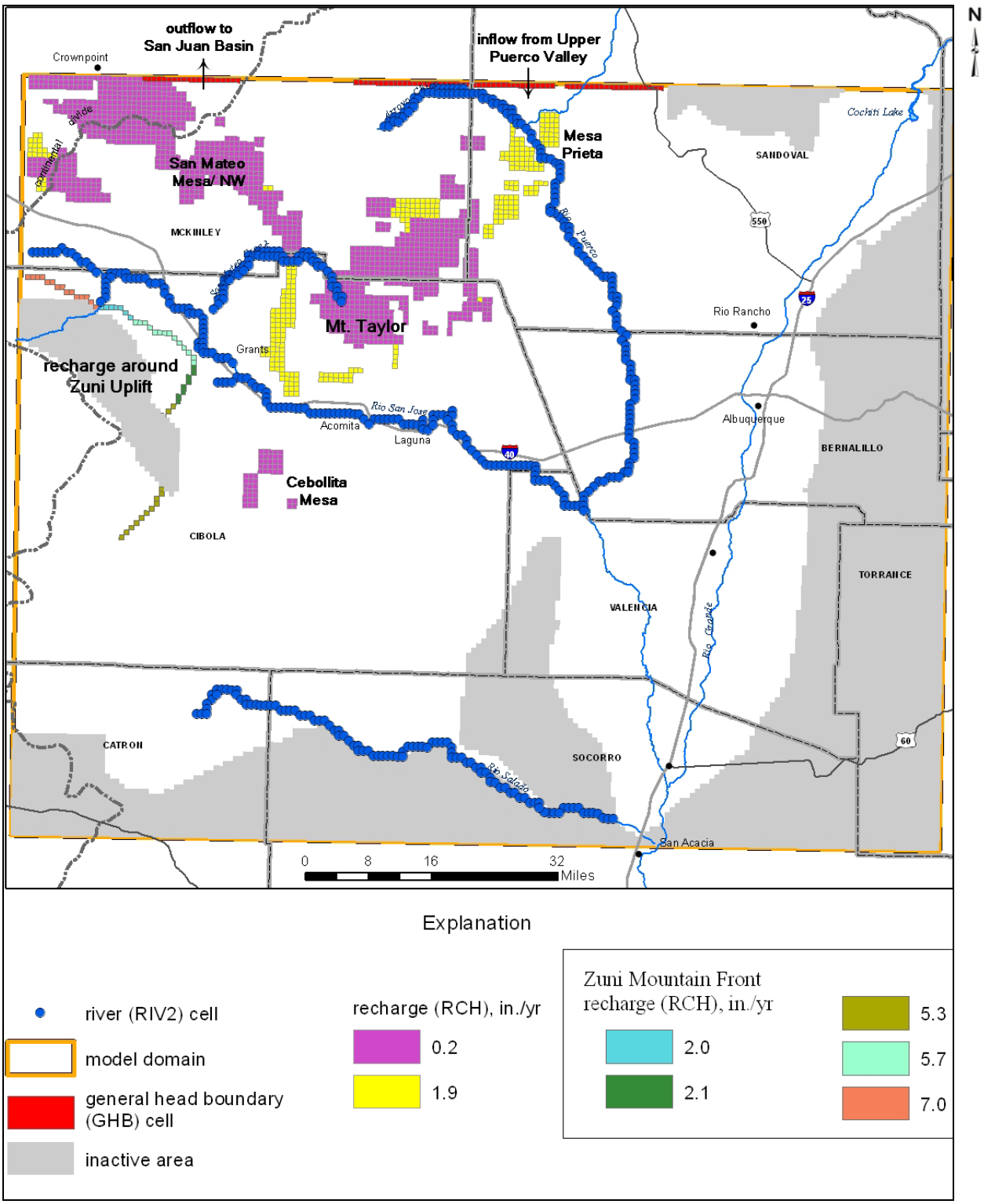

Figure 4.10. Model boundary conditions.

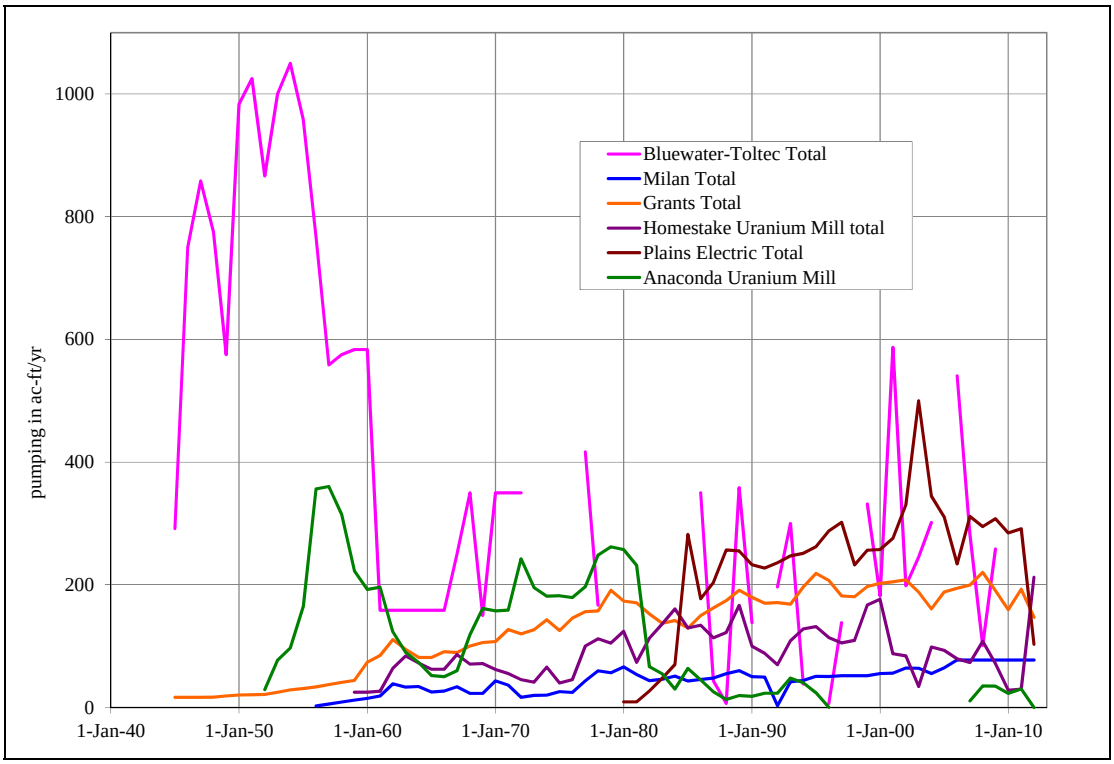

Figure 4.11. Groundwater pumping outside of MRGB, larger withdrawals.

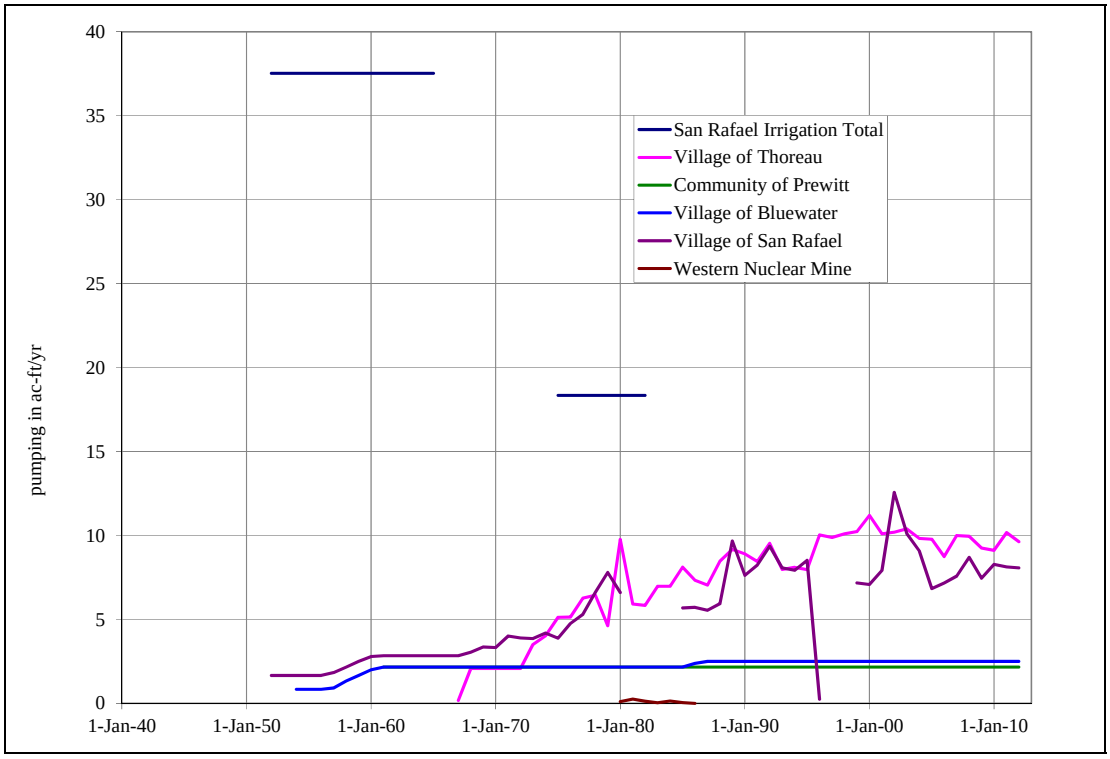

Figure 4.12. Groundwater pumping outside of MRGB, smaller withdrawals.

Table 4.4. Model boundary conditions and simulated water balance

INFLOW	**MODFLOW module**	**recharge (ac-ft/yr)**	**boundary condition type**
recharge around Mount Taylor			
Mount Taylor (direct)	RCH	9,339	specified-flow
Mount Taylor (runoff to San Mateo Creek)	RIV2	4,535	head-dependent / specified-flow
San Mateo Mesa, northwest	RCH	1,571	specified-flow
Mesa Prieta, northeast	RCH	4,709	specified-flow
Cebollita Mesa	RCH	181	specified-flow
TOTAL		**20,335**	
recharge around Zuni Uplift			
mountain-front recharge	RCH	7,088	specified-flow
runoff to Cottonwood Creek	RIV2	2,825	head-dependent / specified-flow
runoff to Bluewater Creek	RIV2	6,593	head-dependent / specified-flow
TOTAL		**16,506**	
groundwater inflow from North Puerco Valley	GHB	8,040	head-dependent
TOTAL INFLOW		**44,881**	
OUTFLOW	MODFLOW module	discharge (ac-ft/yr)	
discharge to surface channels	RIV2	35,067	head-dependent / specified-flow
groundwater outflow to San Juan Basin	GHB	2,846	head-dependent
groundwater outflow to MRGB		6,963	
TOTAL OUTFLOW		**44,876**	

ac-ft/yr - acre-feet per year
MRGB - Middle Rio Grande Basin

Table 4.5. Model pumping locations outside the MRGB

well No.	owner	easting	northing	aquifer	depth (ft)	layer	row	column
1	Village of Thoreau Water & Sanitation District; B 00386	205058	3924647	artesian	1370	7	27	6
2	Community of Prewitt	222400	3917100	unknown		7	35	24
3	Village of Bluewater	229239	3904636	shallow	345	7	47	31
4	Village of Milan B 000023	235991	3895627	shallow	125	7	56	38
5	Village of Milan B 000024	236608	3896205	shallow	144	7	55	38
6	Village of Milan B 000035	235854	3897819	shallow	155	7	54	37
7	Village of Milan B 000050	234927	3900650	shallow	175	6	51	36
8	City of Grants B 000038	238352	3894165	artesian	300	7	57	40
9	City of Grants B 000040	237987	3894983	shallow	367	7	56	40
10	City of Grants B 000039	239510	3893331	shallow	314	7	58	41
11	Village of San Rafael; B 0000136/7	237569	3890004	shallow	150	7	61	39
12	Anaconda Uranium Mill B 000003	231683	3905358		360	6	46	33
13	Homestake Uranium Mill B 000028	240236	3903679	shallow	78	6	48	42
14	Homestake Uranium Mill B 000028 POD 1339	239329	3903609	shallow		6	48	41
15	Homestake Uranium Mill B 47/48	236542	3900996	shallow	312	7	50	38
16	Homestake Uranium Mill DP-200				35	1	50	42
17	Plains Electric B 000087 POD10	219659	3924204	shallow/artesian	1,550	7	28	21
18	Plains Electric B44/45	237179	3902778	shallow	542	6	49	39
19	Plains Electric B7	228661	3907973	shallow	350	6	44	30
20	Plains Electric B18/19	235297	3899438	shallow	275	6	52	37
21	Western Nuclear Mine				25	5	18	14
22	Bluewater-Toltec Irr. B 00001	238021	3899637	shallow		7	52	40
23	Bluewater-Toltec Irr. B 00002	233286	3903401	shallow	16	7	48	35
24	Bluewater-Toltec Irr. B 00003	231683	3905358	shallow	360	7	46	33
25	Bluewater-Toltec Irr. B 00006	233585	3903487	shallow	245	7	48	35
26	Bluewater-Toltec Irr. B 00007	228661	3907973	shallow	350	7	44	30
27	Bluewater-Toltec Irr. B 00008	228108	3906876	shallow	350	7	45	30
28	Bluewater-Toltec Irr. B 00009	230806	3903377	shallow	360	7	48	32
29	Bluewater-Toltec Irr. B 00016	234737	3901051	shallow	150	7	50	36
30	Bluewater-Toltec Irr. B 00021	236608	3896005	shallow	170	7	55	38
31	Bluewater-Toltec Irr. B 00022	236592	3895807	shallow	200	7	56	38
32	Bluewater-Toltec Irr. B 00023	235991	3895627	shallow	125	7	56	38
33	Bluewater-Toltec Irr. B 00024	236608	3896205	shallow	170	7	55	38
34	Bluewater-Toltec Irr. B 00030	227950	3907887		465	7	44	29
35	Bluewater-Toltec Irr. B 00036	227462	3908397		505	7	43	29
36	Bluewater-Toltec Irr. B 00044	237179	3902778	shallow	542	7	49	39
37	Bluewater-Toltec Irr. B 00045	234971	3902845	shallow	369	7	49	36
38	Bluewater-Toltec Irr. B 00047	235521	3900224	shallow	1050	8	51	37
39	Bluewater-Toltec Irr. B 00048	236542	3900996	shallow	312	7	50	38
40	Bluewater-Toltec Irr. B 00049	234937	3901051	shallow	188	7	50	36
41	Bluewater-Toltec Irr. B 00050	234927	3900650	shallow	175	7	51	36
42	Bluewater-Toltec Irr. B 00051	234727	3900650	shallow	135	7	51	36
43	Bluewater-Toltec Irr. B 00052	233269	3902599			7	49	35
44	Bluewater-Toltec Irr. B 00087 B	220425	3923338			7	28	22
45	Bluewater-Toltec Irr. B 00979	231717	3903452	shallow	275	7	48	33
46	San Rafael Irr. B 00014	237212	3887710	shallow	110	1	64	39
47	San Rafael Irr. B 00011	238084	3889687	shallow	75	1	62	40
48	San Rafael Irr. B 00937	238211	3883751	shallow	216	1	68	40
49	San Rafael Irr. B 00010	236700	3883698	shallow	165	1	68	39
50	San Rafael Irr. B 00773	237360	3888803	shallow	200	1	63	39
51	San Rafael Irr. B 00029	237672	3888486	shallow	200	1	63	39
52	San Rafael Irr. B 00055	237872	3889497	shallow		1	62	40

MRGB - Middle Rio Grande Basin

4.6 Model Calibration

Model calibration targets include the following:

- Measured "steady state' water levels in the bedrock units, outside of the MRGB.
- Measured historical water-level hydrographs within the MRGB, selected from the MRGB model calibration (McAda and Barroll, 2002).
- Measured historical water-level hydrographs outside of the MRGB, compiled from the USGS database.
- Results of the Sandoval County aquifer test (INTERA, 2008).

4.6.1 Steady-State

Locations of steady-state calibration targets are shown on Figure 4.13.

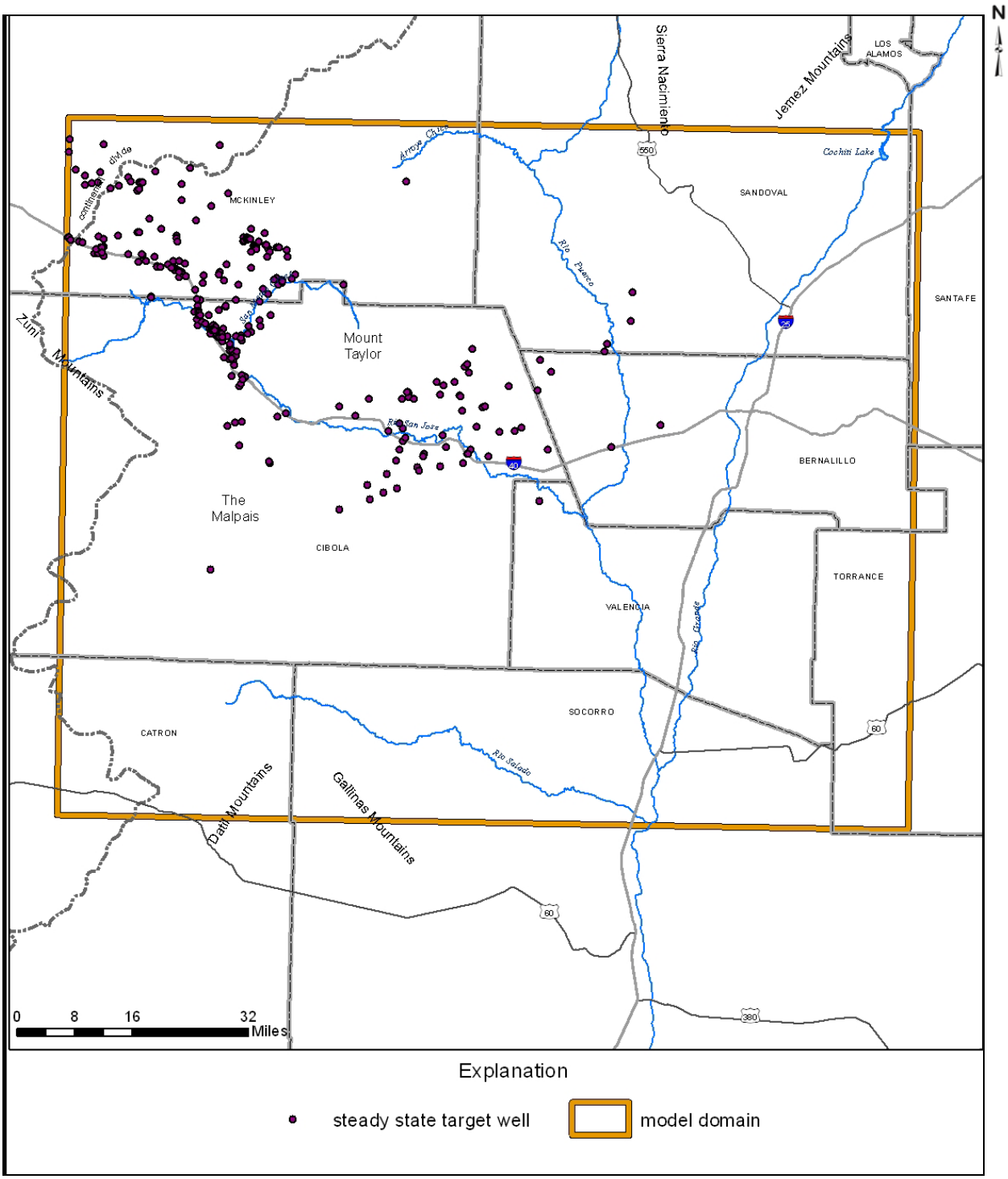

Figure 4.13. Steady-state calibration targets.

Measured and simulated (steady-state) water levels are compared graphically on Figure 4.14. Agreement between measured and simulated water levels is good, recognizing the limited accuracy of the measured data, and the fact that measurements were taken at different times and under non-steady conditions.

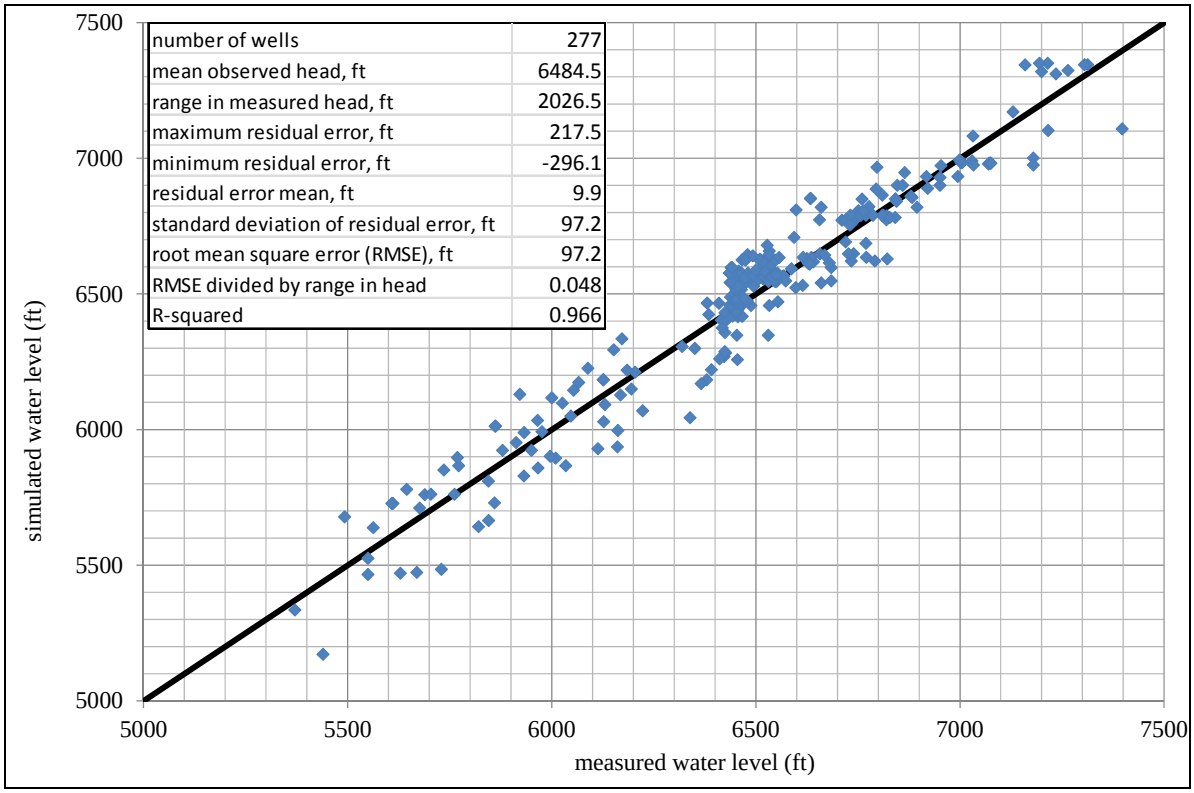

Figure 4.14. Measured and simulated steady-state water levels.

4.6.2 Historical Transient Calibration

Locations of historical calibration targets are shown on Figure 4.15, including selected MRGB targets (McAda and Barroll, 2002) and targets outside the MRGB, compiled from the USGS (http://waterdata.usgs.gov/nwis) database and organized by location into numbered groups. Information on the target wells outside the MRGB is listed on Table 4.6.

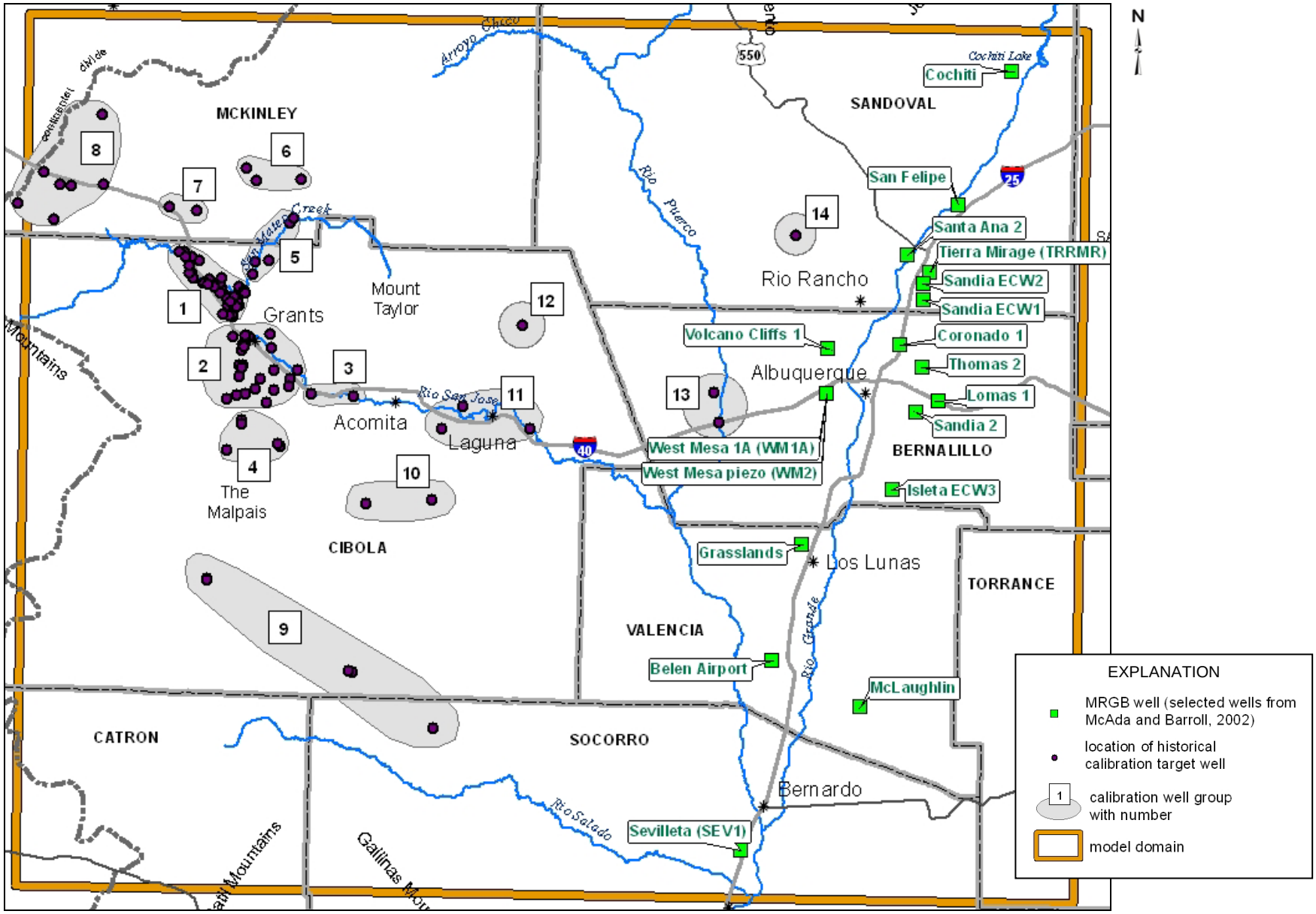

Figure 4.15. Historical calibration targets.

Table 4.6. Historical calibration targets

USGS well ID	layer	row	column	T R S.qqq	latitude	longitude	datum	X_UTM83	Y_UTM83	elevation
351434107552601	L1	48	35	12N.10W.30.242	35 14 34	107 55 26	NAD27	233885.959	3903891.6	Frenzel data
351304107543701	L1	51	37	12N.10W.29.434	35 13 04	107 54 39	NAD83	235048.833	3901077.4	6,552.00 ft above NGVD29
351255107544001	L1	51	37	11N.10W.05.214	35 12 55	107 54 40	NAD27	234959.527	3900806.4	Frenzel data
351303107532201	L1	51	39	11N.10W.04.222	35 13 03	107 53 21	NAD27	236964.813	3900994.6	Frenzel data
351213107531701	L1	52	39	11N.10W.10.111	35 12 13	107 53 16	NAD27	237046.454	3899450	Frenzel data
351107107535201	L1	54	38	11N.10W.16.142	35 11 07	107 53 52	NAD27	236076.453	3897442.5	Frenzel data
351630107572801	L1	44	32	12N.11W.14.213	35 16 26.1	107 58 03.2	NAD83	230070.633	3907459	6,615.00 ft above NGVD29
350910107515401	L1	58	41	11N.10W.26.321	35 09 13	107 51 54	NAD27	238960.787	3893842.7	Frenzel data
350937107493201	L1	57	44	11N.09W.30.211	35 09 37	107 49 30	NAD27	242626.632	3894478.1	Frenzel data
350514107502701	L1	65	43	10N.10W.24.212	35 05 16	107 50 27	NAD27	240954.375	3886475.9	Frenzel data
350418107510101	L1	67	42	10N.10W.25.114	35 04 17	107 51 00	NAD27	240066.406	3884681.6	Frenzel data
350603107485801	L1	64	45	10N.09W.17.113	35 06 03	107 48 58	NAD27	243249.853	3887860.2	6,439.00 ft above NGVD29
350408107485401	L1	67	45	10N.09W.29.132	35 04 08	107 48 54	NAD27	243251.005	3884313.4	Frenzel data
350300107491201	L1	69	44	10N.09W.31.324	35 03 00	107 49 42	NAD27	241975.338	3882252.3	Frenzel data
350516107470001	L1	65	48	10N.09W.21.222	35 05 16	107 47 00	NAD27	246198.004	3886327.8	Frenzel data
351403107531801	L1	49	39	12N.10W.27.343	35 14 03	107 53 18	NAD27	237094.5	3902841.4	Frenzel data
351343107523701	L1	49	40	12N.10W.34.232	35 13 43	107 52 37	NAD27	238113.378	3902195	Frenzel data
351640107494801	L1	44	44	12N.09W.07.343	35 16 40	107 49 48	NAD27	242542.689	3907526.8	Frenzel data
351237107532201	L1	51	39	11N.10W.04.422	35 12 36	107 53 20	NAD27	236965.892	3900161.7	Frenzel data
350851107522401	L1	58	40	11N.10W.27.443	35 08 51	107 52 24	NAD27	238181.85	3893186.7	Frenzel data
350839107522401	L1	59	40	11N.10W.34.223	35 08 39	107 52 24	NAD27	238171.165	3892816.8	Frenzel data
350630107523701	L1	63	40	10N.10W.10.414	35 06 30	107 52 37	NAD27	237727.125	3888850.9	Frenzel data
350631107525801	L1	63	39	10N.10W.10.321	35 06 31	107 52 58	NAD27	237196.179	3888897.1	Frenzel data
350633107523701	L1	63	40	10N.10W.10.412	35 06 33	107 52 37	NAD27	237729.797	3888943.4	Frenzel data
350523107525501	L1	65	39	10N.10W.15.344	35 05 23	107 52 56	NAD27	237186.164	3886800	Frenzel data

Table 4.6. Historical calibration targets (continued)

USGS well ID	layer	row	column	T R S.qqq	latitude	longitude	datum	X_UTM83	Y_UTM83	elevation
350815107491901	L1	60	45	11N.09W.31.423	35 08 15	107 49 19	NAD27	242833.323	3891943.2	Frenzel data
350609107460701	L1	63	49	10N.09W.31.423	35 06 09	107 46 07	NAD27	247585.97	3887923.7	Frenzel data
351719107594901	L7	43	29	12N.11W.09.221	35 17 19	107 59 49	NAD27	227389.881	3909175.2	Frenzel data
351645107590001	L7	44	30	12N.11W.10.431	35 16 45	107 59 00	NAD27	228596.581	3908090	Frenzel data
351505107585001	L7	47	30	12N.11W.22.414	35 15 05	107 58 50	NAD27	228756.659	3905000.5	Frenzel data
351516107585701	L7	46	30	12N.11W.22.234	35 15 16	107 58 57	NAD27	228589.881	3905344.8	Frenzel data
351417107573301	L7	48	32	12N.11W.26.244	35 14 17	107 57 33	NAD27	230659.228	3903462.9	Frenzel data
351441107552401	L7	48	33	12N.11W.25.214	35 14 38	107 56 48	NAD27	231816.314	3904076.2	Frenzel data
351354107552401	L7	49	35	12N.10W.32.111	35 13 54	107 55 24	NAD27	233900.206	3902657.4	6,566.00 ft above NGVD29
351423107554601	L7	48	35	12N.10W.30.412	35 14 20	107 55 46	NAD27	233367.535	3903475.1	Frenzel data
351419107553101	L7	48	35	12N.10W.30.421	35 14 19	107 55 31	NAD27	233745.907	3903433.1	6,576.00 ft above NGVD29
351213107542701	L7	52	37	11N.10W.08.221	35 12 13	107 54 28	NAD27	235225.131	3899503.1	Frenzel data
351104107534701	L7	51	38	11N.10W.04.211	35 13 03.7	107 53 47.7	NAD83	236346.006	3901030.2	6,542.00 ft above NGVD29
351519107513901	L7	46	41	12N.10W.23.233	35 15 19	107 51 39	NAD27	239665.401	3905111.1	6,592.00 ft above NGVD29
351122107535901	L7	54	38	11N.10W.16.121	35 11 22	107 53 59	NAD27	235912.833	3897910	Frenzel data
351157107532801	L7	53	38	11N.10W.09.241	35 11 58	107 53 37	NAD27	236501.767	3899003.2	Frenzel data
350111107523501	L7	73	39	09N.10W.10.414	35 01 11	107 52 35	NAD27	237494.011	3879018.7	Frenzel data
352532107524901	L7	28	40	14N.10W.22.414	35 25 29.1	107 52 51.4	NAD83	238438.306	3923961.4	7,030.00 ft above NGVD29
351715108003001	L7	43	28	12N.11W.09.114	35 17 15	108 00 30	NAD27	226350.044	3909083.3	6,662.00 ft above NGVD29
351445107584201	L7	47	30	12N.11W.27.222	35 14 45	107 58 42	NAD27	228940.405	3904378	Frenzel data
351211107532901	L7	52	38	11N.10W.09.211	35 12 11	107 53 29	NAD27	236715.81	3899397.9	6,535.00 ft above NGVD29
350923107522701	L7	57	40	11N.10W.27.241	35 09 24.5	107 52 26.3	NAD83	238209.278	3894215	6,480.00 ft above NGVD29
350336107531501	L7	68	38	10N.10W.27.333	35 03 36	107 53 15	NAD27	236609.29	3883516.5	6,526.00 ft above NGVD29

Table 4.6. Historical calibration targets (continued)

USGS well ID	layer	row	column	T R S.qqq	latitude	longitude	datum	X_UTM83	Y_UTM83	elevation
350346107521201	L7	68	40	10N.10W.26.331	35 03 44.0	107 52 12.6	NAD83	238253.439	3883711.3	6,454.00 ft above NGVD29
350053107523301	L7	73	39	09N.10W.15.212	35 00 53	107 52 33	NAD27	237528.727	3878462.5	6,529.00 ft above NGVD29
345815107541501	L7	78	37	09N.10W.35.110	34 58 15	107 54 15	NAD27	234800.875	3873668.3	Frenzel data
350108107183501	L7	73	91	09N.05W.12.442	35 01 06	107 18 36	NAD27	289181.518	3877521.2	Frenzel data
353016108100401	L7	18	14	15N.13W.25.142	35 30 16	108 10 04	NAD27	212615.793	3933606.7	7,485.00 ft above NGVD29
351416107571001	L7	48	32	12N.11W.25.313	35 14 17.0	107 57 29.7	NAD83	230798.634	3903454.9	6,592.00 ft above NGVD29
351452107552301	L7	47	35	12N.10W.20.333	35 14 52	107 55 23	NAD27	233978.157	3904444.1	6,570.00 ft above NGVD29
351105107194801	L7	55	89	11N.05W.14.241	35 11 05	107 19 48	NAD27	287788.083	3896020.6	Frenzel data
343158107290801	L7	127	75	04N.06W.32.214	34 31 58	107 29 08	NAD27	271826.797	3824045.5	Frenzel data
352126108193801	L7	0	0	13N.14W.16.144	35 21 26	108 19 38	NAD27	197597.431	3917747.2	Frenzel data
352434108164201	L7	29	4	14N.14W.25.342	35 24 34	108 16 42	NAD27	202233.945	3923393.4	Frenzel data
352324108145001	L7	31	6	13N.13W.06.224	35 23 24	108 14 50	NAD27	204989.368	3921142.5	Frenzel data
352315108132501	L7	31	8	13N.13W.04.143	35 23 15	108 13 25	NAD27	207125.793	3920794.9	Frenzel data
352002108152601	L7	37	5	13N.13W.30.122	35 20 02	108 15 26	NAD27	203875.621	3914946.3	Frenzel data
352330108093402	L7	31	14	13N.13W.01.222	35 23 30	108 09 34	NAD27	212971.31	3921068.9	Frenzel data
352135108014801	L7	35	26	13N.11W.17.123	35 21 35	108 01 50	NAD83	224629.753	3917152.9	6,802.00 ft above NGVD29
352532108524901	L7	27	40	14N.10W.22.414	35 25 32	107 52 49	NAD27	238445.618	3924053.9	Frenzel data
352433107462101	L7	29	49	14N.09W.28.441	35 24 33	107 46 21	NAD27	248182.39	3921955.6	6,982.00 ft above NGVD29
352330108093401	L7	31	14	13N.13W.01.222	35 23 29.4	108 09 38.5	NAD83	212913.551	3921049.1	7,005.00 ft above NGVD29
352115107582801	L7	35	31	13N.11W.14.322	35 21 15	107 58 28	NAD27	229655.293	3916386.8	Frenzel data
351117107542301	L7	54	37	11N.10W.17.222	35 11 17	107 54 23	NAD27	235301.111	3897773.6	6,525.00 ft above NGVD29
350911107535301	L7	58	38	11N.10W.28.322	35 09 11	107 53 53	NAD27	235946.911	3893868.4	6,550.00 ft above NGVD29
350829107524301	L7	59	39	11N.10W.34.231	35 08 29	107 52 43	NAD27	237681.27	3892522.6	Frenzel data

Table 4.6. Historical calibration targets (continued)

USGS well ID	layer	row	column	T R S.qqq	latitude	longitude	datum	X_UTM83	Y_UTM83	elevation
350615107524601	L7	63	39	10N.10W.10.433	35 06 13	107 52 45	NAD27	237509.367	3888332.9	Frenzel data
350311107542101	L7	69	37	10N.10W.33.1333	35 03 11	107 54 21	NAD27	234914.334	3882794.7	6,750.00 ft above NGVD29
350352107442601	L7	68	52	09N.10W.25.324	35 03 52	107 44 26	NAD27	250027.804	3883631.1	Frenzel data
345850107475401	L7	77	47	09N.09W.28.1344	34 58 50	107 47 54	NAD27	244496.343	3874471	6,655.00 ft above NGVD29
344548107560801	L7	101	34	06N.10W.07.141	34 45 48	107 56 08	NAD27	231259.308	3850731.7	Frenzel data
345325107374201	L7	87	62	08N.08W.25.414	34 53 25	107 37 42	NAD27	259755.941	3864034.5	Frenzel data
350053107290101	L7	73	75	09N.06W.16.111	35 00 53	107 29 01	NAD27	273327.593	3877501.2	5,990.00 ft above NGVD29
345402107295701	L7	86	74	08N.06W.20.333	34 54 02	107 29 57	NAD27	271591.224	3864872.2	Frenzel data
343714107384301	L7	117	60	05N.08W.35.123	34 37 14	107 38 43	NAD27	257419.043	3834154.9	Frenzel data
340107107211601	L7	0	0	03S.05W.27.311	34 01 07.1	107 21 17.7	NAD83	282552.979	3766723.5	6,872.00 ft above NGVD29
340506107061001	L1	0	0	03S.03W.01.212	34 05 07.9	107 06 12.6	NAD83	305924.894	3773636.3	6,120.00 ft above NGVD29
340741107085101	L8	0	0	02S.03W.22.111	34 07 40.8	107 08 52.7	NAD83	301920.113	3778432.2	6,020.00 ft above NGVD29
343715107391501	L7	117	59	05N.08W.35.123	34 37 15	107 39 15	NAD27	256604.665	3834207.1	6,977.0 ft above NGVD29
344545107560801	L7	101	34	06N.10W.07.1413	34 45 45	107 56 08	NAD27	231256.604	3850639.3	7,130.0 ft above NGVD29
345329107374001	L7	87	62	08N.08W.25.4231	34 53 29	107 37 40	NAD27	259809.96	3864156.5	6,400.0 ft above NGVD29
345901107480901	L7	77	46	09N.09W.28.113	34 59 01	107 48 09	NAD27	244125.386	3874820.7	6,640.0 ft (Google Earth)
350306107263401	L1	69	79	10N.06W.35.322	35 03 06	107 26 34	NAD27	277154.662	3881507.4	5,945.0 ft above NGVD29
350347107392301	L1	68	60	10N.08W.26.341	35 03 47	107 39 23	NAD27	257701.12	3883269.2	6,150.00 ft above NGVD29
350431107470301	L5	67	48	10N.09W.21.444	35 04 31	107 47 03	NAD27	246083.252	3884943.2	6,400.00 ft above NGVD29
350758107524501	L7	60	39	11N.10W.34.433	35 07 58	107 52 45	NAD27	237602.986	3891568.7	6,590.00 ft above NGVD29
350819107523201	L7	59	40	11N.10W.34.4122	35 08 19	107 52 32	NAD27	237950.83	3892206.4	6,520.00 ft above NGVD29

Table 4.6. Historical calibration targets (concluded)

USGS well ID	layer	row	column	T R S.qqq	latitude	longitude	datum	X_UTM83	Y_UTM83	elevation
351125107550401	L7	54	36	11N.10W.08.344	35 11 25	107 55 04	NAD27	234271.007	3898050.6	6,526.00 ft above NGVD29
351237107541901	L7	51	37	11N.10W.04.311	35 12 38	107 54 18	NAD27	235500.634	3900266.2	6,543.00 ft above NGVD29
351323107552401	L7	50	35	12N.10W.32.313	35 13 23	107 55 24	NAD27	233872.064	3901702	6,578.00 ft above NGVD29
351331107523401	L7	50	40	12N.10W.34.412	35 13 31	107 52 34	NAD27	238178.526	3901823	6,557.00 ft above NGVD29
351357107561001	L7	49	34	12N.10W.31.121	35 13 57	107 56 10	NAD27	232739.709	3902784.2	6,575.00 ft above NGVD29
351416107565801	L7	48	33	12N.11W.25.413	35 14 16	107 56 58	NAD27	231543.316	3903405.7	6,595.00 ft above NGVD29
351514107590701	L7	46	30	12N.11W.22.322	35 15 14	107 59 07	NAD27	228335.216	3905290.8	6,635.00 ft above NGVD29
351554107591501	L7	45	30	12N.11W.15.341	35 15 54	107 59 15	NAD27	228170.11	3906529.6	6,627.00 ft above NGVD29
351630107513101	L1	44	41	12N.10W.14.212	35 16 30	107 51 31	NAD27	239930.721	3907293.3	6,621.00 ft above NGVD29
351651107594501	L8	43	29	12N.11W.09.424	35 16 49.7	107 59 44.4	NAD83	227534.847	3908263.3	6,642.00 ft above NGVD29
352023107473201	L5	37	47	13N.09W.21.4123	35 20 23	107 47 34	NAD83	246178.646	3914297.8	6,785.00 ft above NGVD29
352037107465701	L5	36	48	13N.09W.22.112	35 20 46.3	107 47 02.1	NAD83	247004.398	3914993.2	6,830.00 ft above NGVD29
352418107513401	L5	30	41	14N.10W.35.221	35 24 18	107 51 34	NAD27	240271.602	3921718.4	7,010.00 ft above NGVD29
350204106562301	L3	72	125	9N.01W.4.424	35 02 04	106 56 23	NAD27	323006.154	3878588.8	5,280.00 ft above NGVD29
350454106570401	L3	66	124	10N.01W.21.134	35 04 54	106 57 04	NAD27	322069.59	3883846.8	5,320.00 ft above NGVD29
352019106474801	L7	38	138	13N.01E.24.313	35 20 19	106 47 48	NAD83	336720.517	3912075.8	6,165.00 ft above NGVD29

Measured and simulated water levels in the MRGB wells are shown on Figures 4.16 through 4.31. Results match those of McAda and Barroll (2002); however, some exceptions are found: the simulated water level in Tierra Mirage (Fig. 4.17) is much closer to the measured than simulated by the 2002 model. The simulated water level in McLaughlin (Fig. 4.20) is slightly below measured, while in the 2002 model it was slightly above. Simulated water level in West Mesa 1A (Fig. 4.26), West Mesa Piezo 2 (Fig. 4.28), San Felipe (Fig. 4.29), and Santa Ana 2 (Fig. 4.30) are lower than simulated by the 2002 model,

Measured and simulated water levels in well Group 1 (Fig. 4.15), along the Rio San Jose upstream of the confluence with San Mateo Creek, are shown on Figures 4.32 through 4.37.

Measured and simulated water levels in well Group 2 (Fig. 4.15), along the Rio San Jose downstream of the confluence with San Mateo Creek, are shown on Figures 4.38 through 4.41. Simulated water levels in Group 2 are generally low.

Measured and simulated water levels in well Group 3 (Fig. 4.15), along the Rio San Jose downstream of Group 2, near Acoma, are shown on Figure 4.39. One of the simulated water levels is more than 200 ft too low.

This is a problem with the simulation of the San Andres-Glorietta water level, which in this area is apparently about the same as the elevation of the Rio San Jose upstream, where the San Andres outcrops. The model does not properly simulate the compartmentalization of the aquifer in this area, simulating a gradient rather than a flat water table with sharp “stair step” changes (compartmentalization). The current model simulates a high-conductivity aquifer along Rio San Jose, bounded by a medium-permeability zone; the juxtaposition of the two zones causes a much steeper gradient to be simulated in the high-permeability compartment. To correctly simulate the compartment, the model will need to better isolate the high-permeability from the medium-permeability zone. A flow barrier (HFB) defined around the compartment is a possible solution.

Measured and simulated water levels in well Group 4 (Fig. 4.15), south of Grants, are shown on Figure 4.43.

Measured and simulated water levels in well Group 5 (Fig. 4.15), along San Mateo Creek, are shown on Figure 4.44.

Measured and simulated water levels in well Group 6 (Fig. 4.15), north of the San Mateo Mountains, are shown on Figure 4.45.

Measured and simulated water levels in well Group 7 (Fig. 4.15), northwest of Grants, are shown on Figure 4.46.

Measured and simulated water levels in well Group 8 (Fig. 4.15), in the northwest part of the model domain near the continental divide, are shown on Figure 4.47.

Measured and simulated water levels in well Group 9 (Fig. 4.15), in the southwest part of the model domain, are shown on Figure 4.48.

Measured and simulated water levels in well Group 10 (Fig. 4.15), southeast of Acoma, are shown on Figure 4.49.

Measured and simulated water levels in well Group 11 (Fig. 4.15), along the lower Rio San Jose, are shown on Figure 4.50

Measured and simulated water levels in well Group 12 (Fig. 4.15), northeast of Acoma, are shown on Figure 4.51.

Measured and simulated water levels in well Group 13 (Fig. 4.15), along the lower Rio Puerco, are shown on Figure 4.52.

Measured and simulated water levels in well Group 14 (Fig. 4.15), a Santa Fe Group well in the MRGB, are shown on Figure 4.53.

MRGB Wells

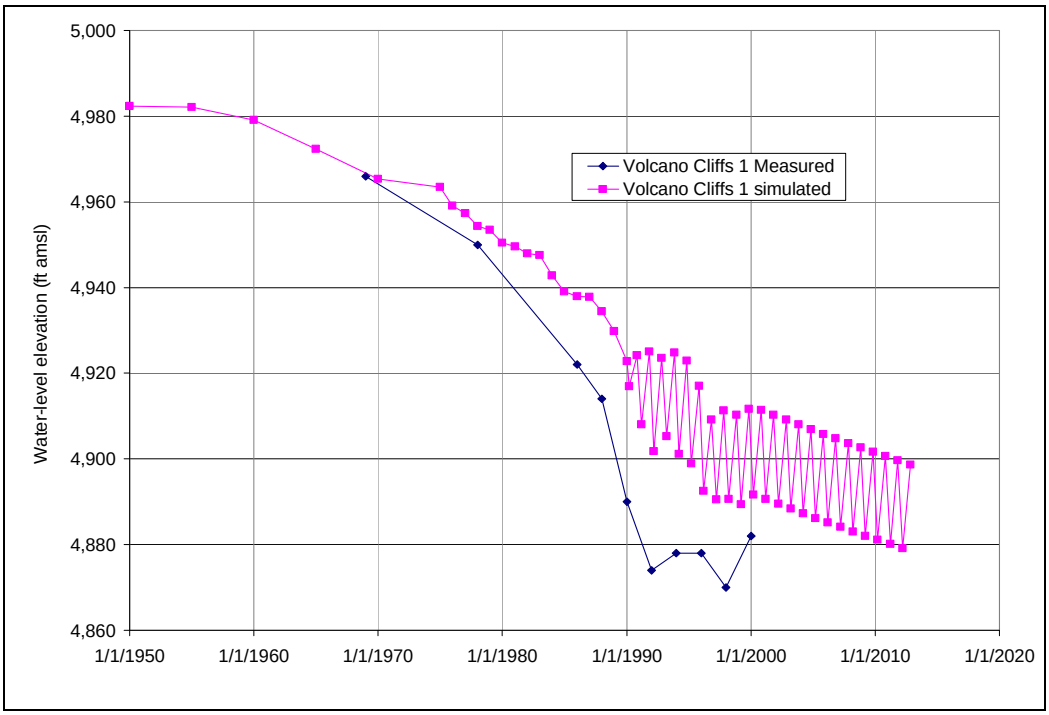

Figure 4.16. Measured and simulated water level in well "Volcano Cliffs 1".

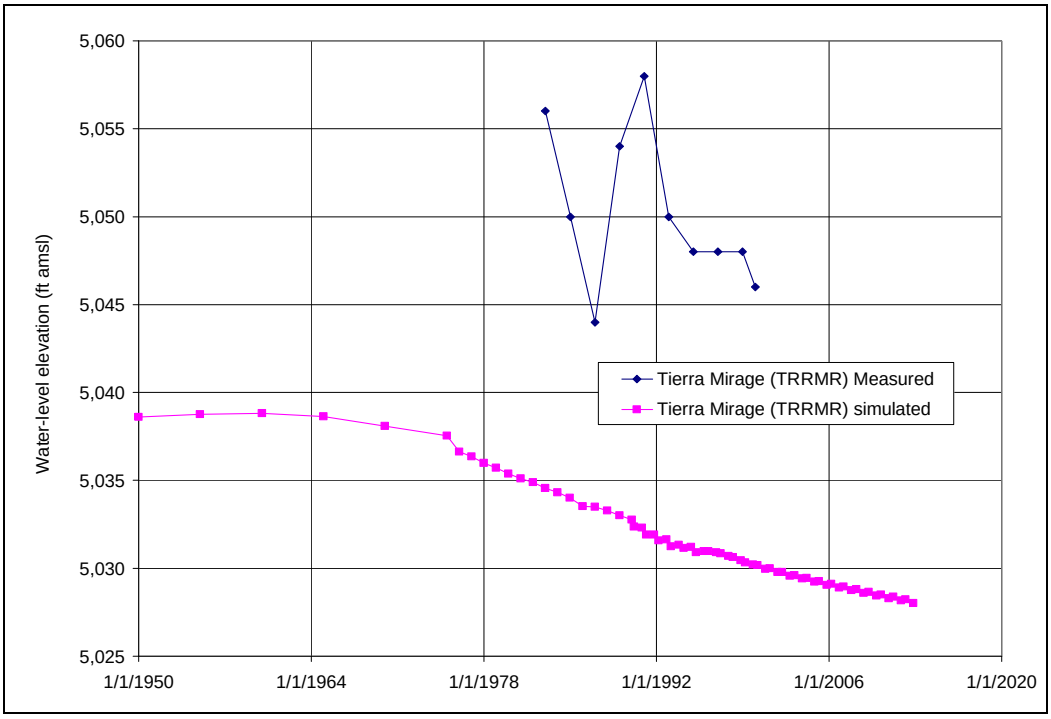

Figure 4.17. Measured and simulated water level in well "Tierra Mirage".

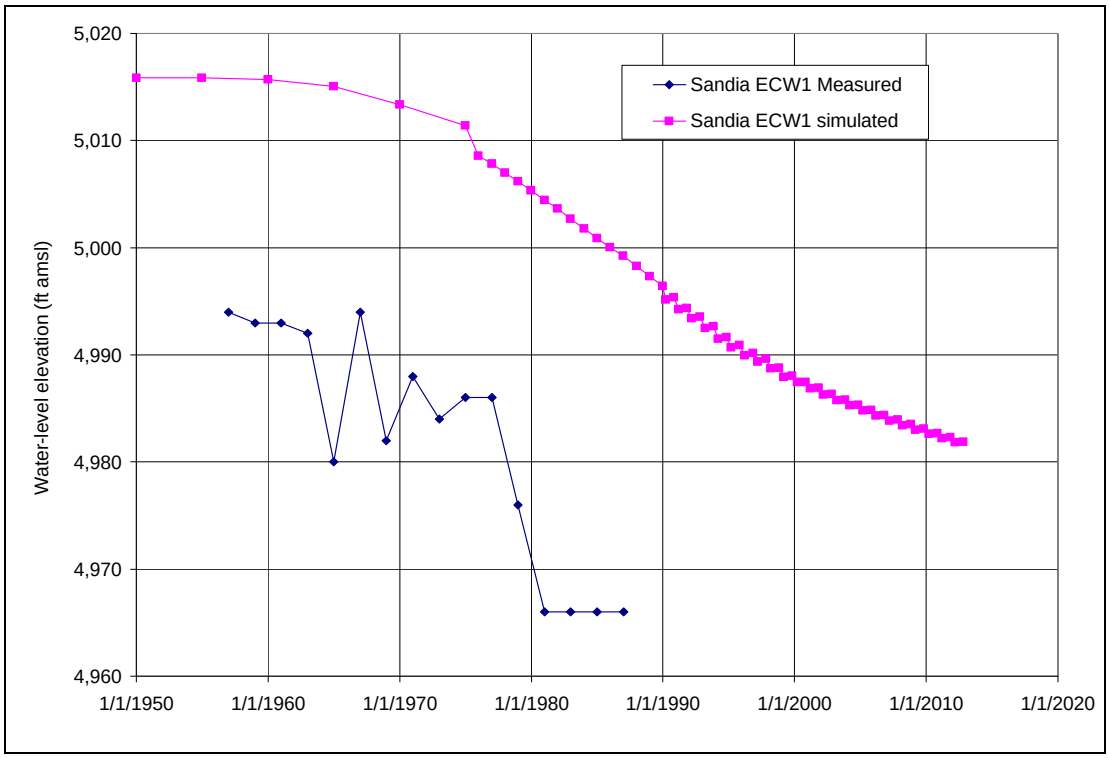

Figure 4.18. Measured and simulated water level in well "Sandia ECW1".

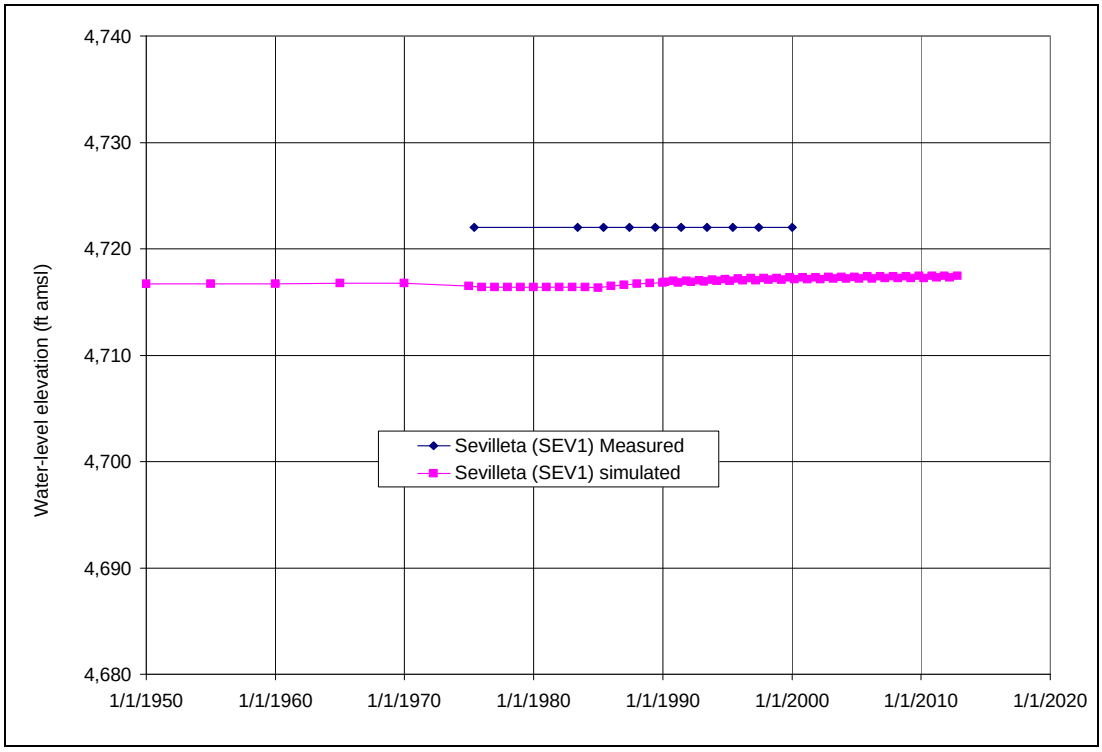

Figure 4.19. Measured and simulated water level in well "Sevilleta 1".

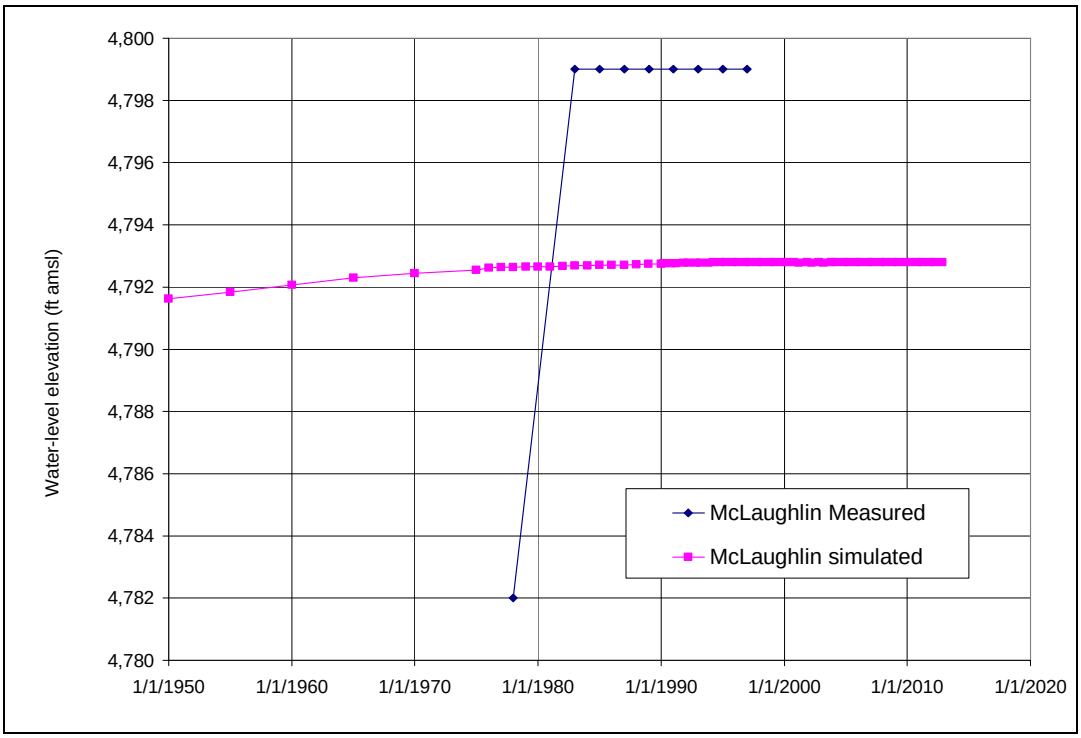

Figure 4.20. Measured and simulated water level in well "McLaughlin".

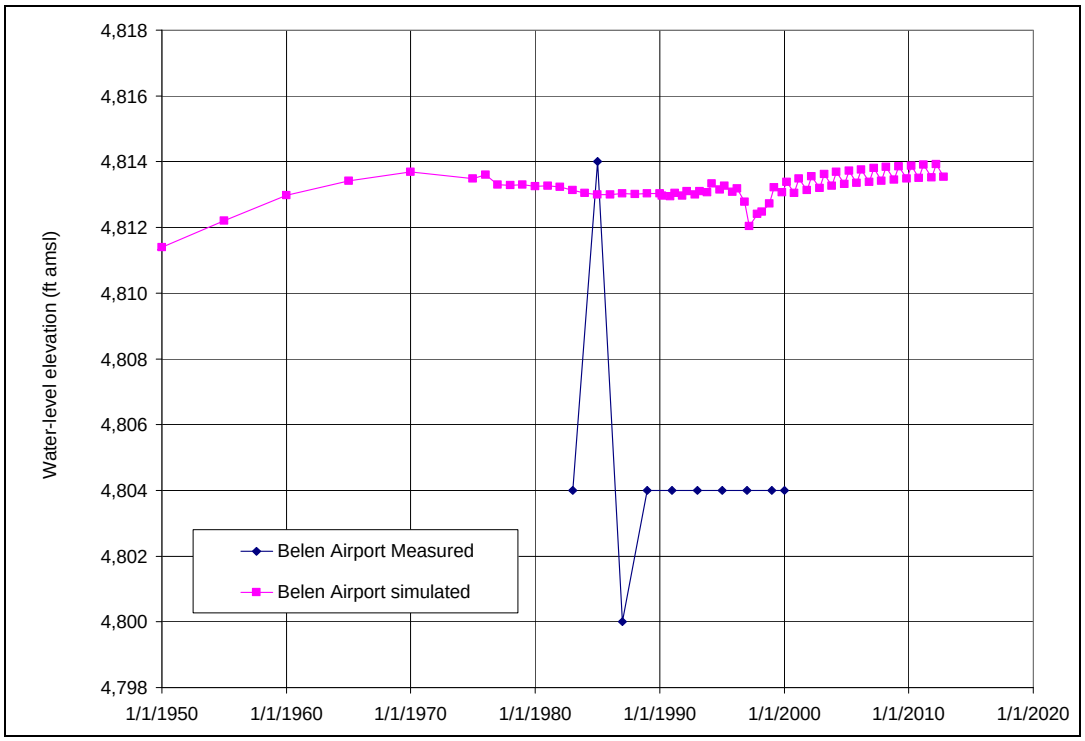

Figure 4.21. Measured and simulated water level in well "Belen Airport".

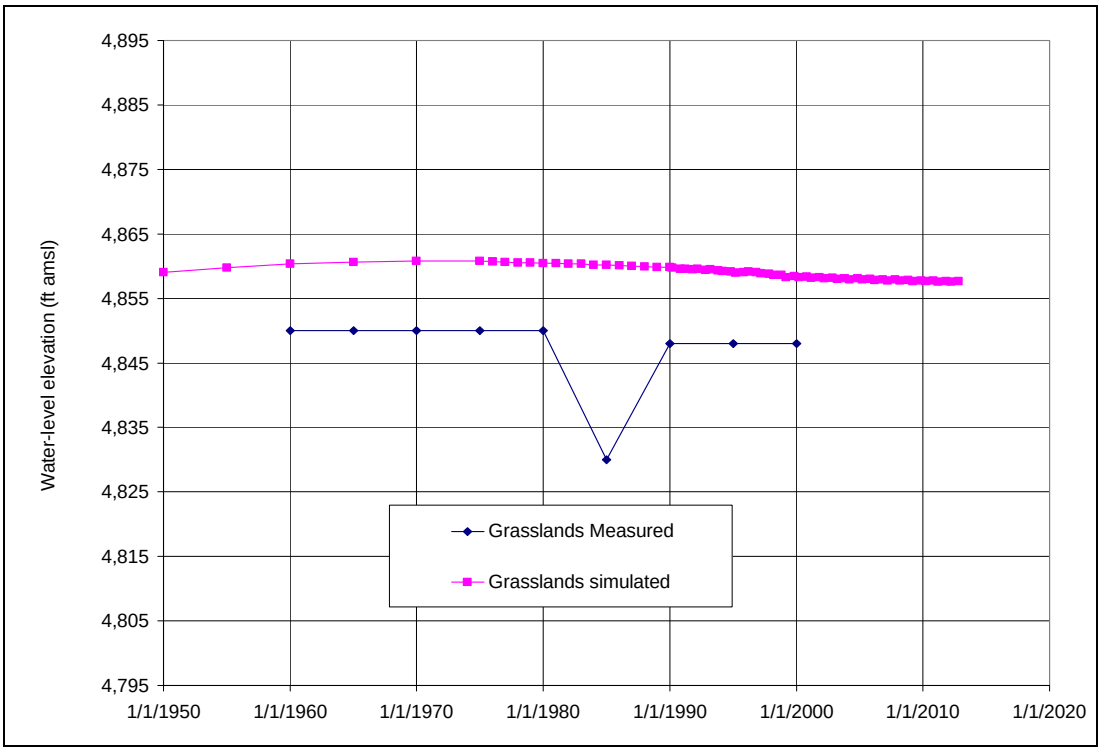

Figure 4.22. Measured and simulated water levels in well "Grasslands".

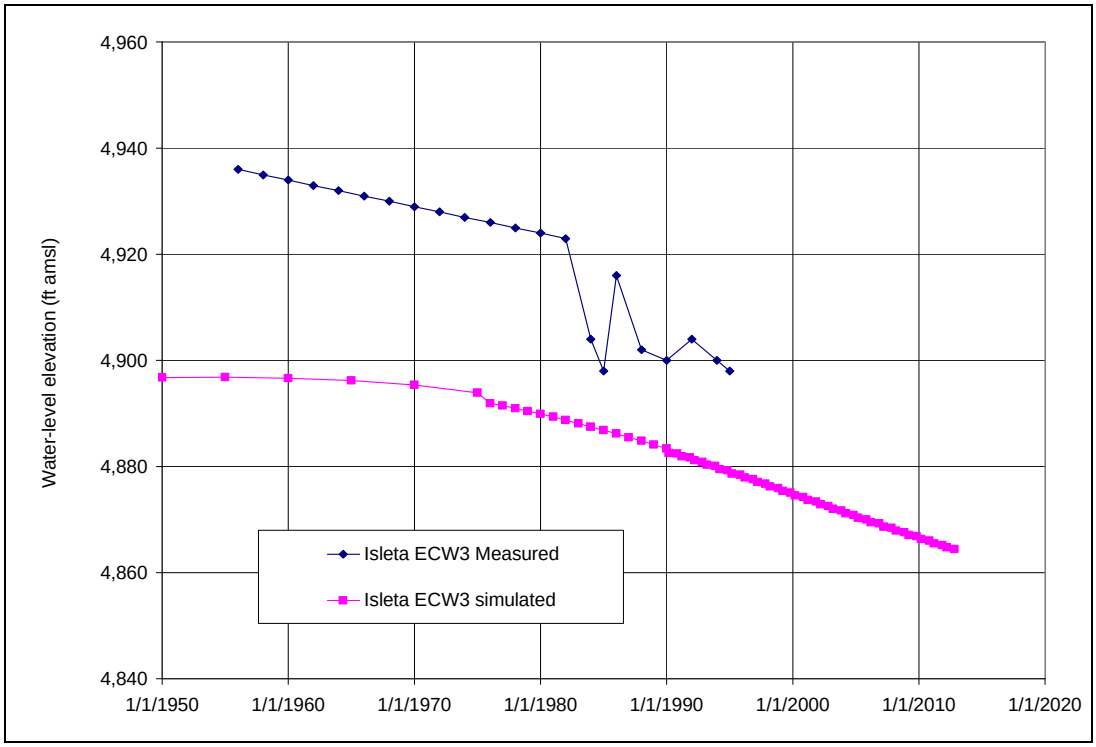

Figure 4.23. Measured and simulated water levels in well "Isleta ECW3".

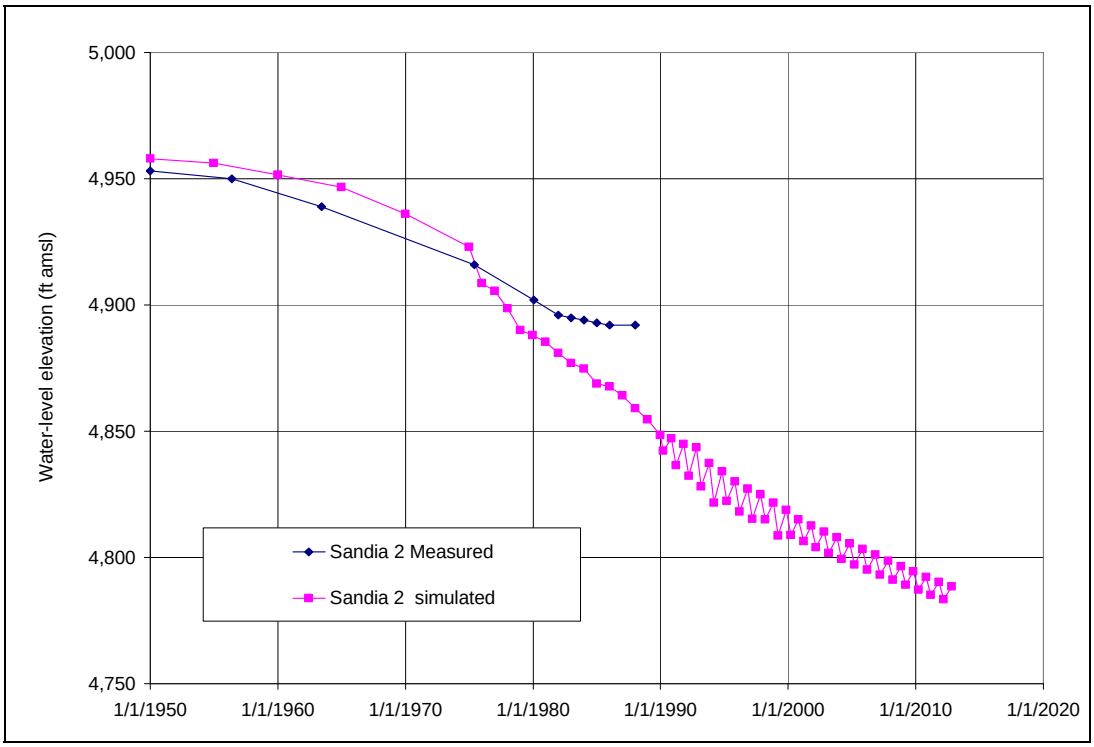

Figure 4.24. Measured and simulated water level in well "Sandia 2".

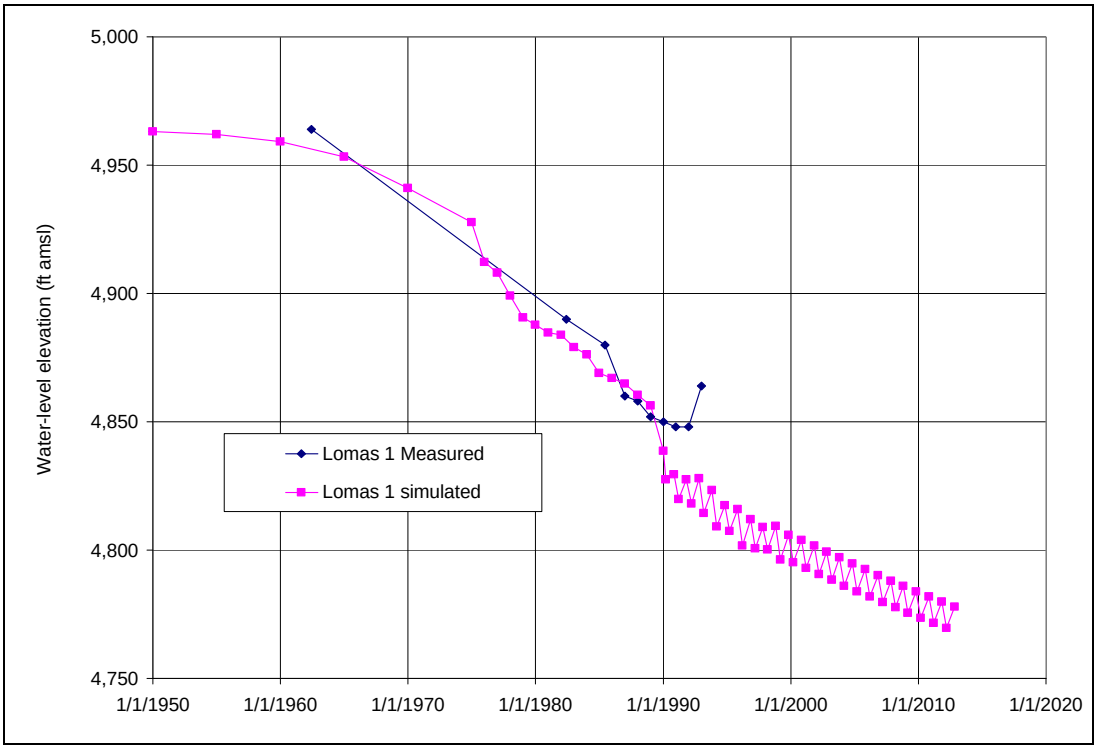

Figure 4.25. Measured and simulated water level in well "Lomas 1".

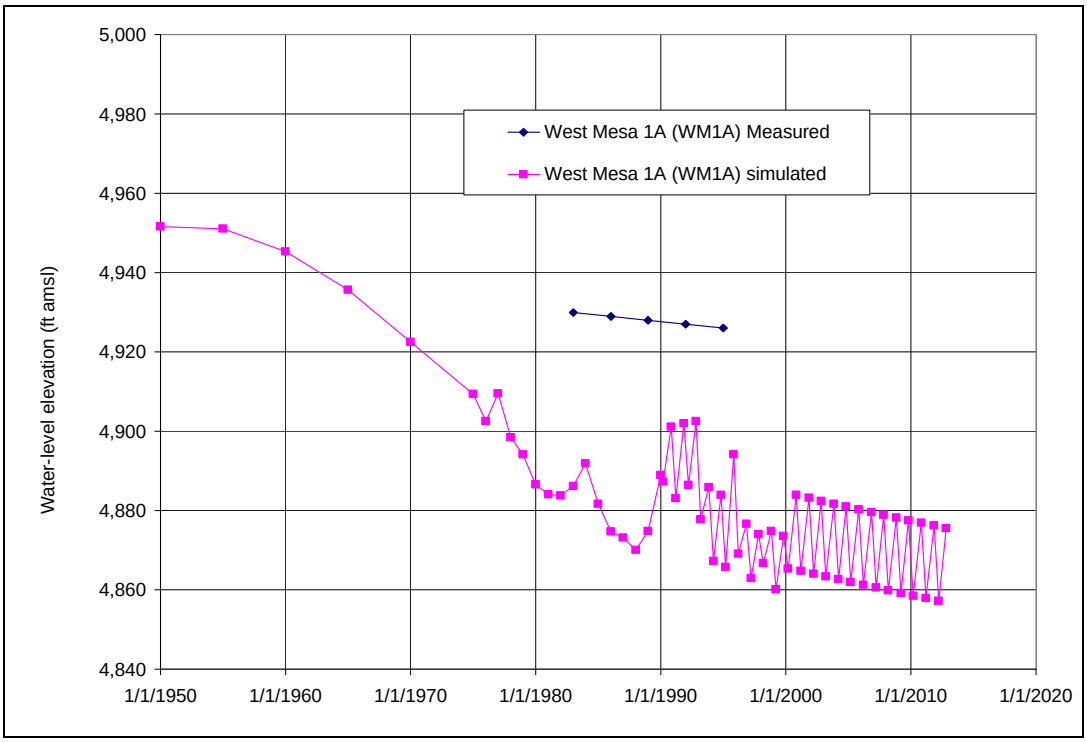

Figure 4.26. Measured and simulated water level in well "West Mesa 1A".

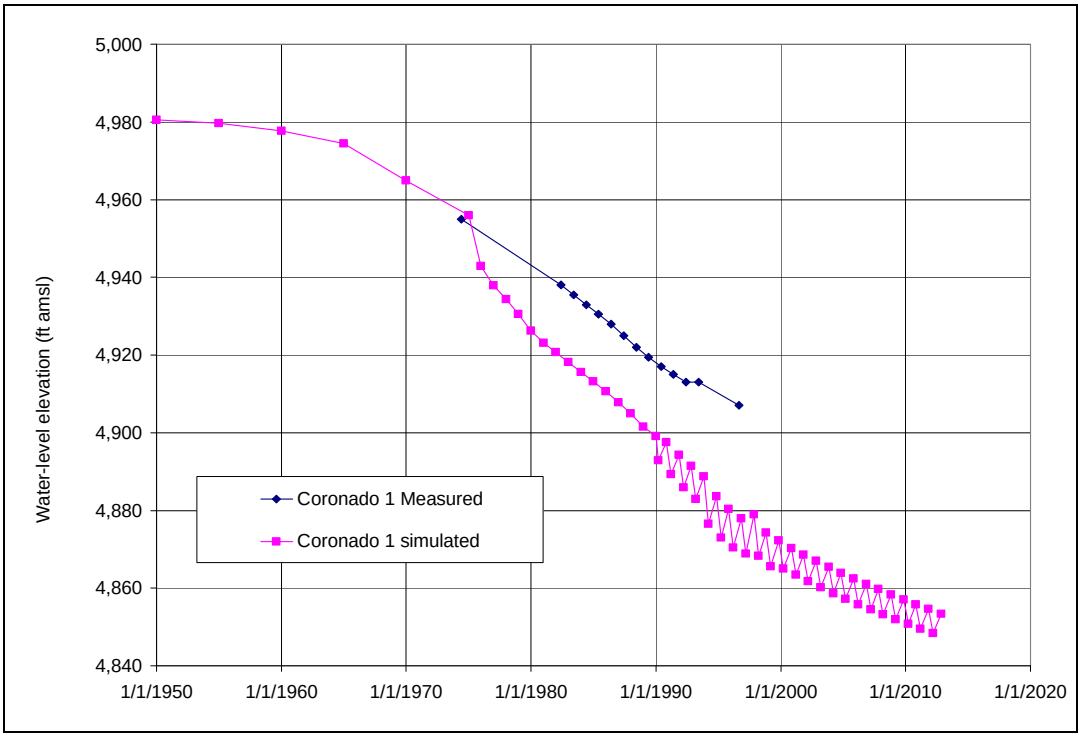

Figure 4.27. Measured and simulated water level in well "Coronado 1".

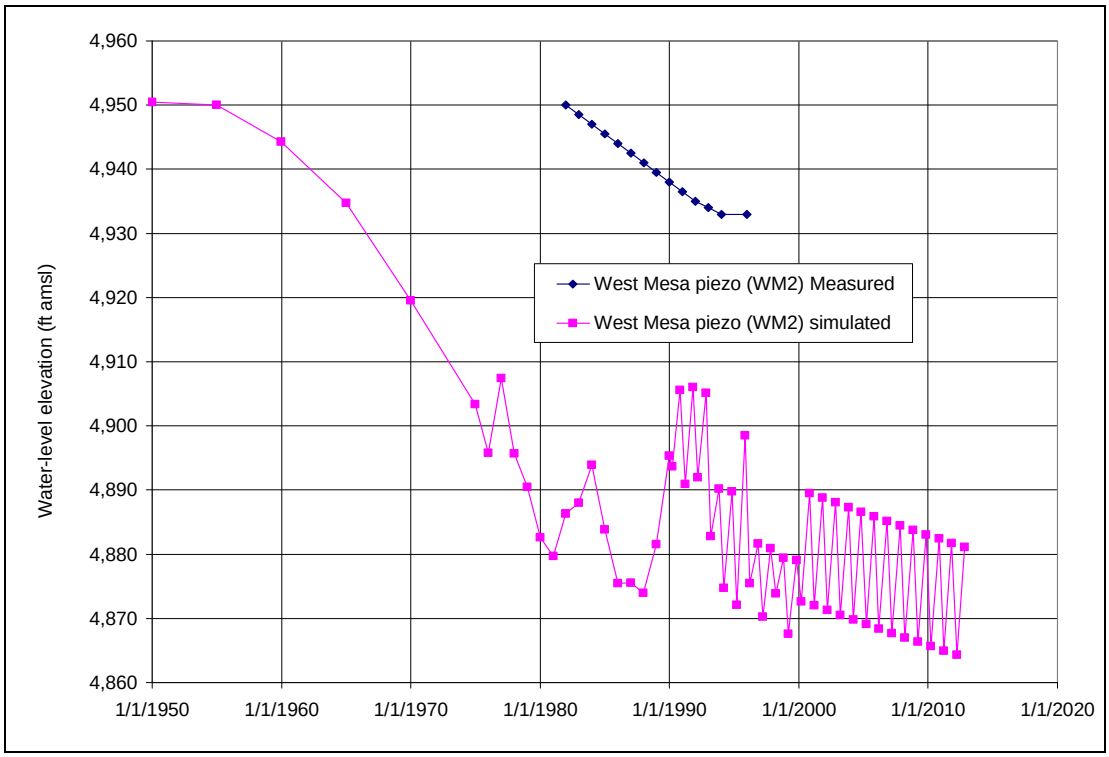

Figure 4.28. Measured and simulated water levels in well "West Mesa Piezo 2".

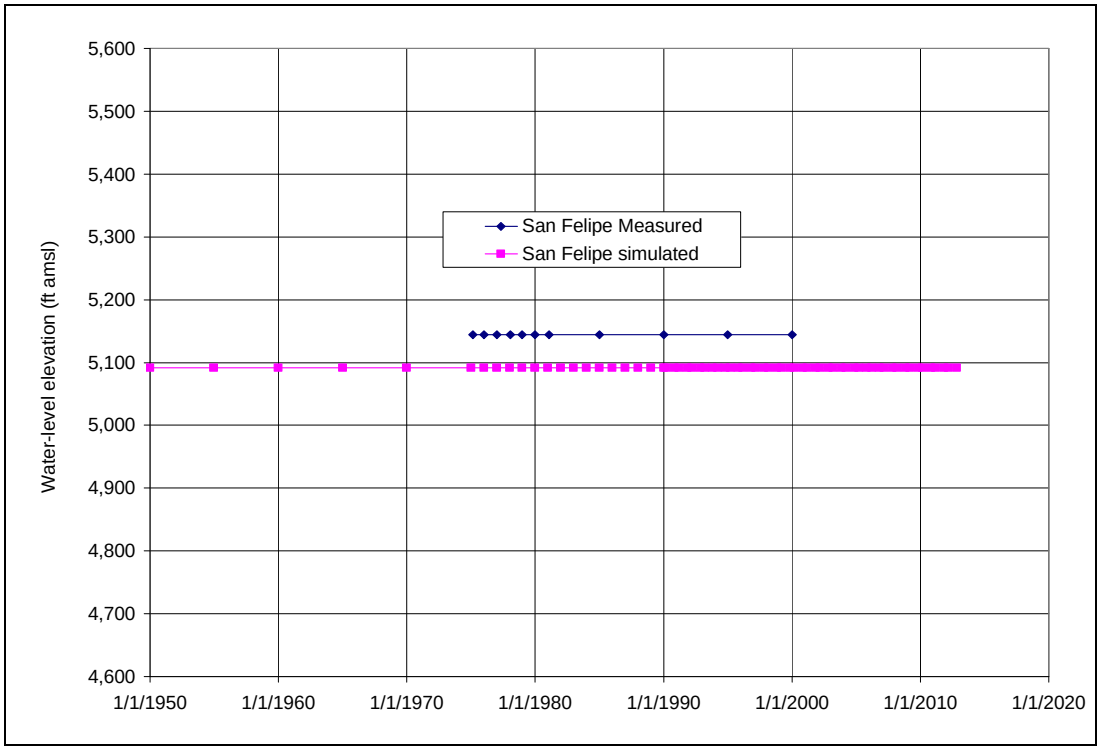

Figure 4.29. Measured water level in "San Felipe."

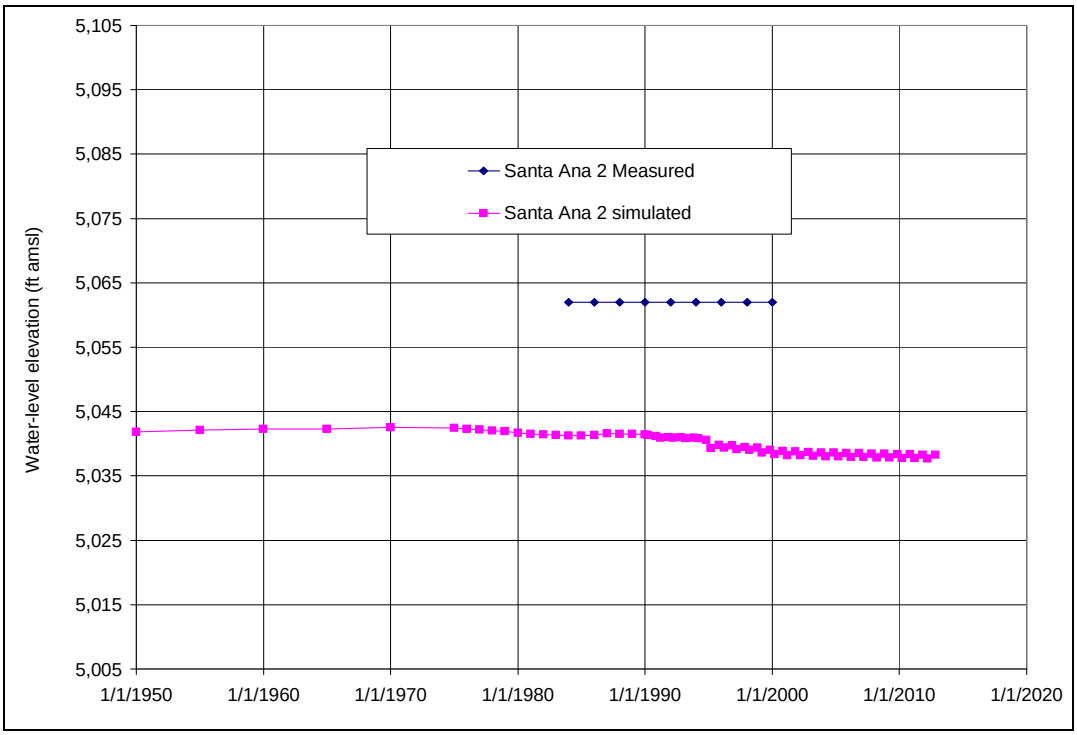

Figure 4.30. Measured and simulated water level in well "Santa Ana 2."

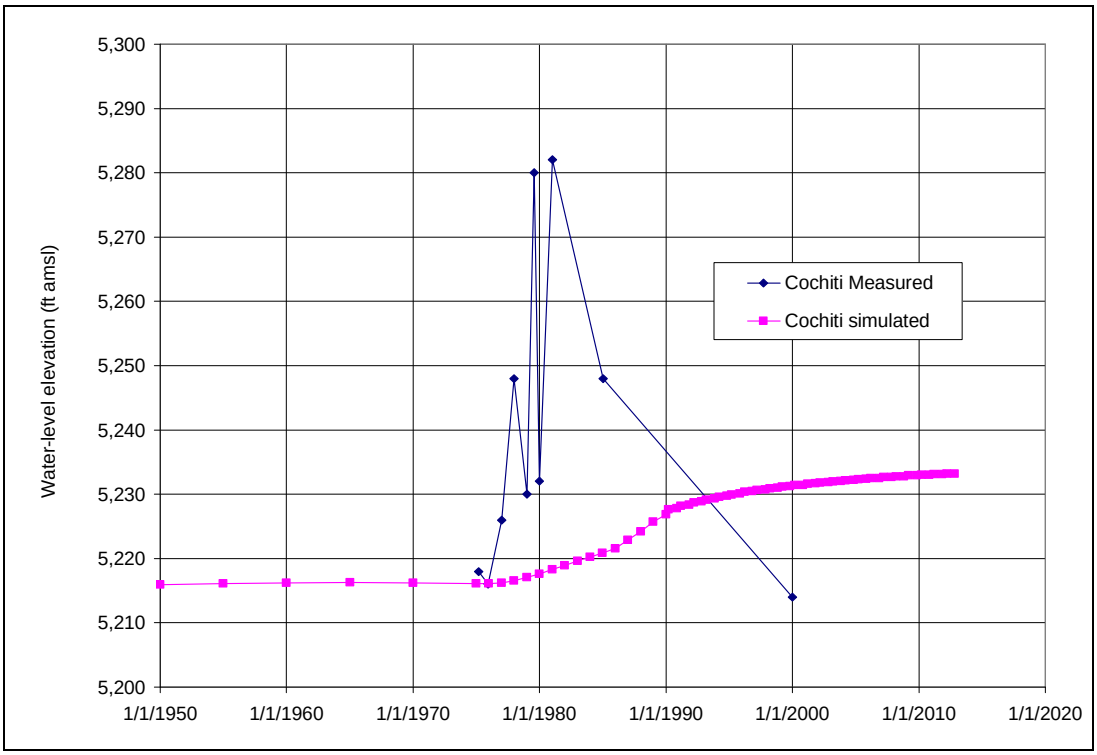

Figure 4.31. Measured water level in well "Cochiti."

Group 1 Wells

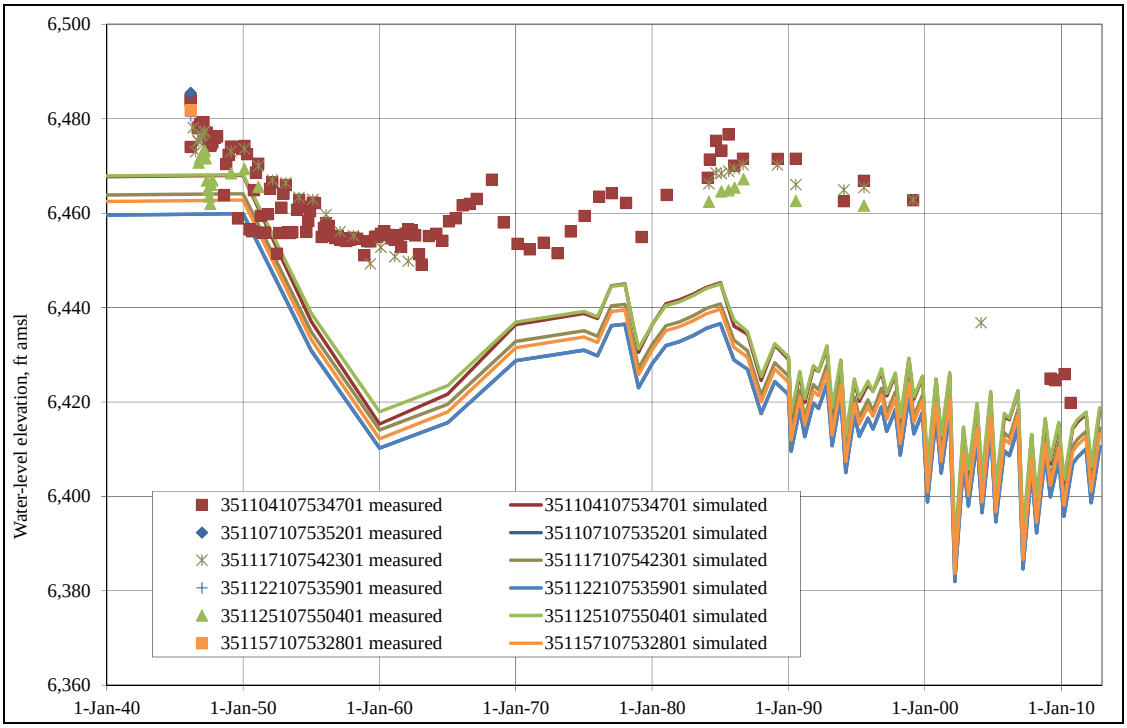

Figure 4.32. Measured and simulated water levels in Group 1 wells (1 of 6).

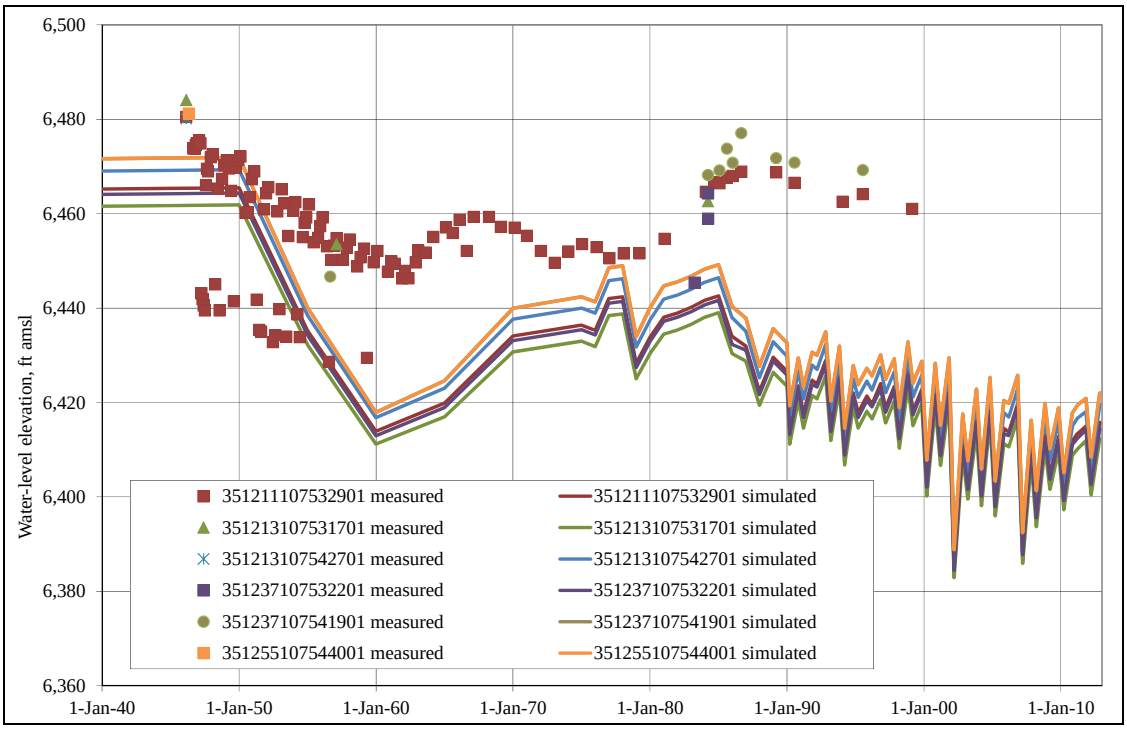

Figure 4.33. Measured and simulated water level in Group 1 wells (2 of 6).

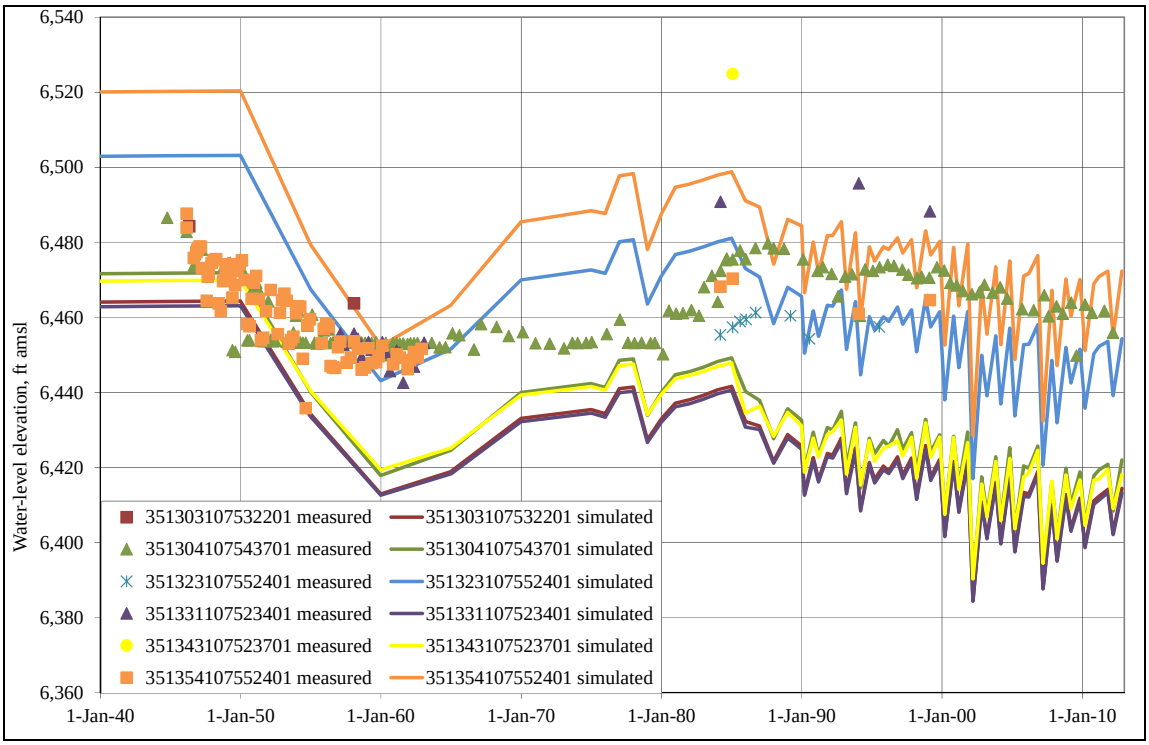

Figure 4.34. Measured and simulated water level in Group 1 wells (3 of 6).

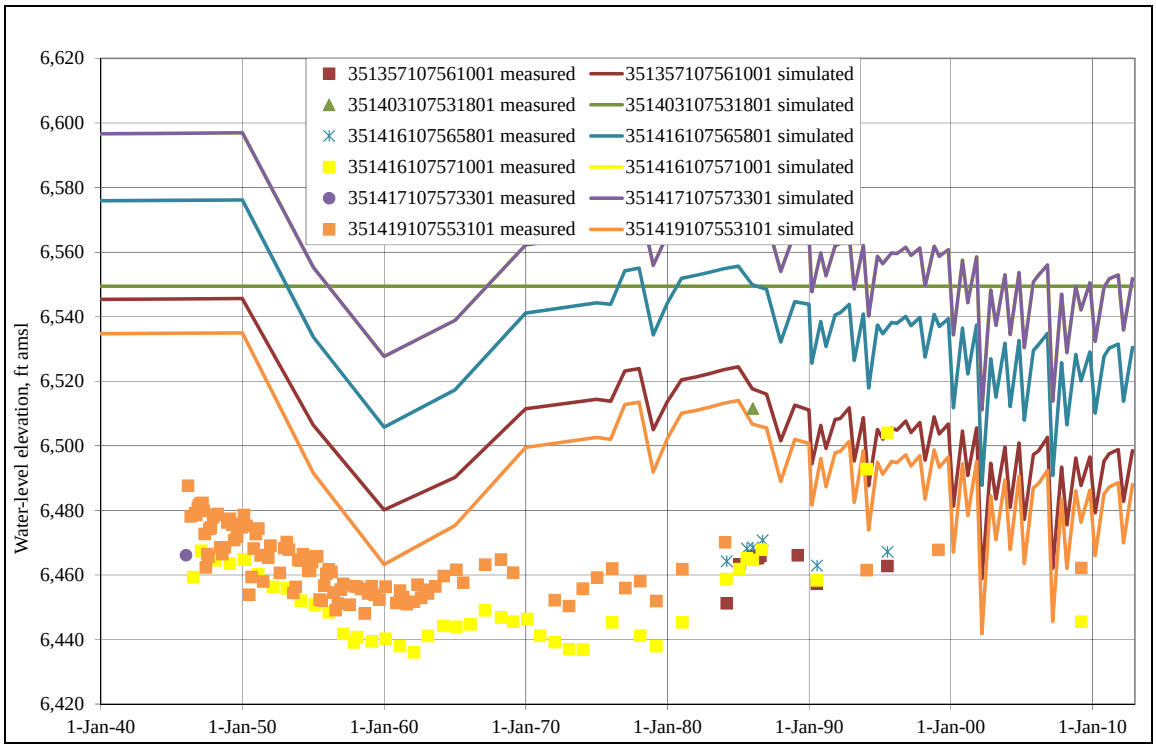

Figure 4.35. Measured and simulated water level in Group 1 wells (4 of 6).

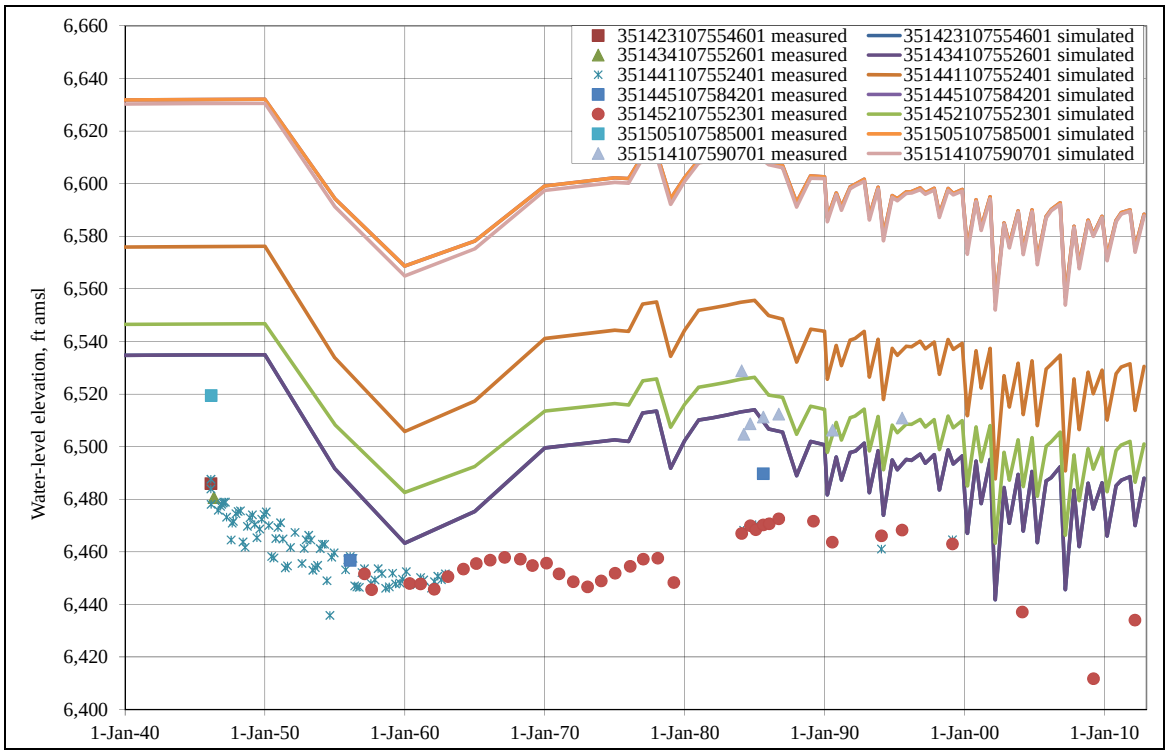

Figure 4.36. Measured and simulated water level in Group 1 wells (5 of 6).

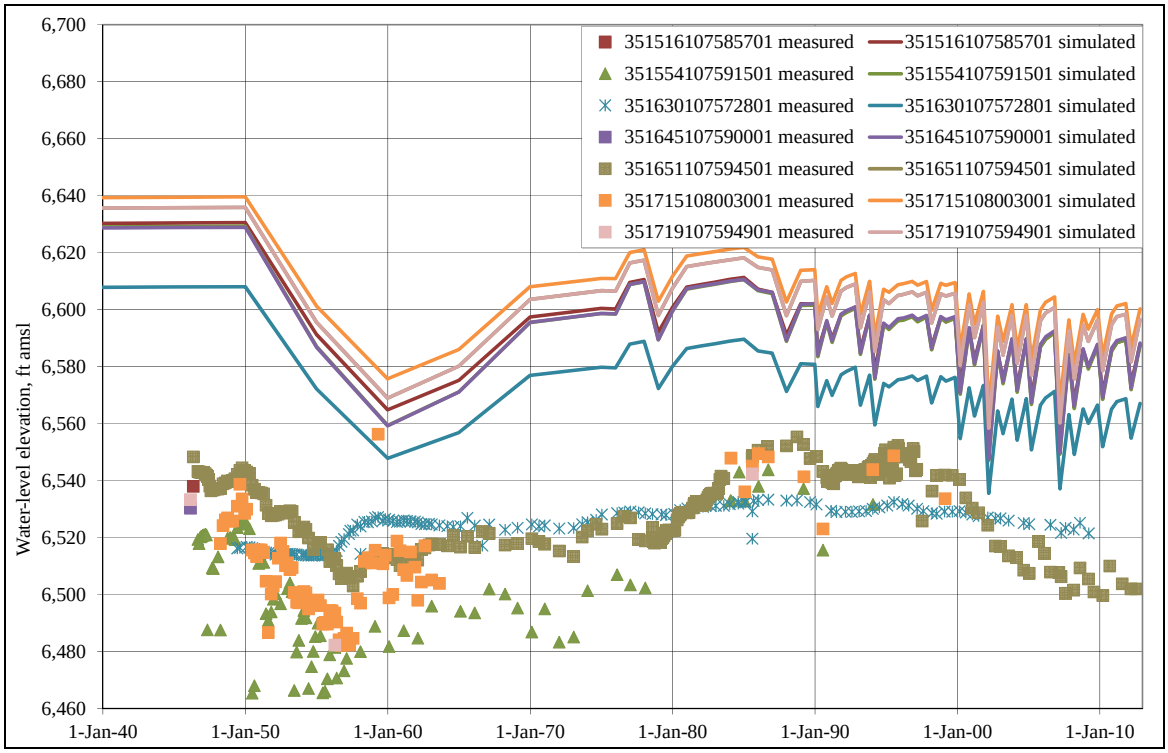

Figure 4.37. Measured and simulated water level in Group 1 wells (6 of 6).

Group 2 Wells

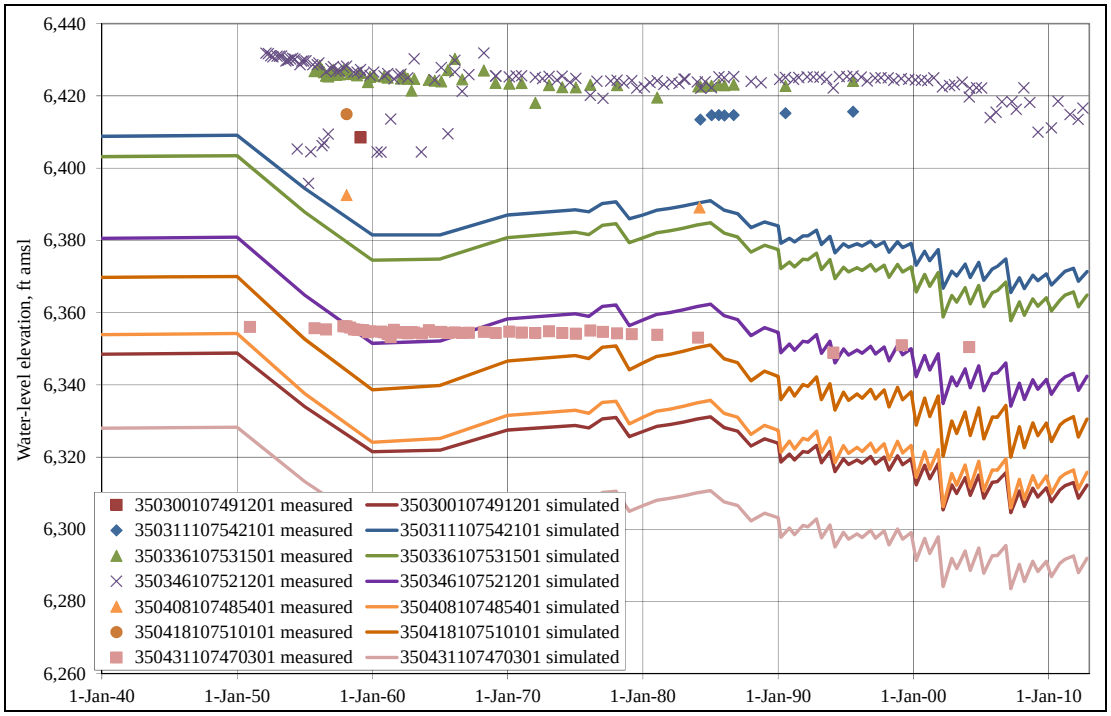

Figure 4.38. Measured and simulated water levels in Group 2 wells (1 of 4).

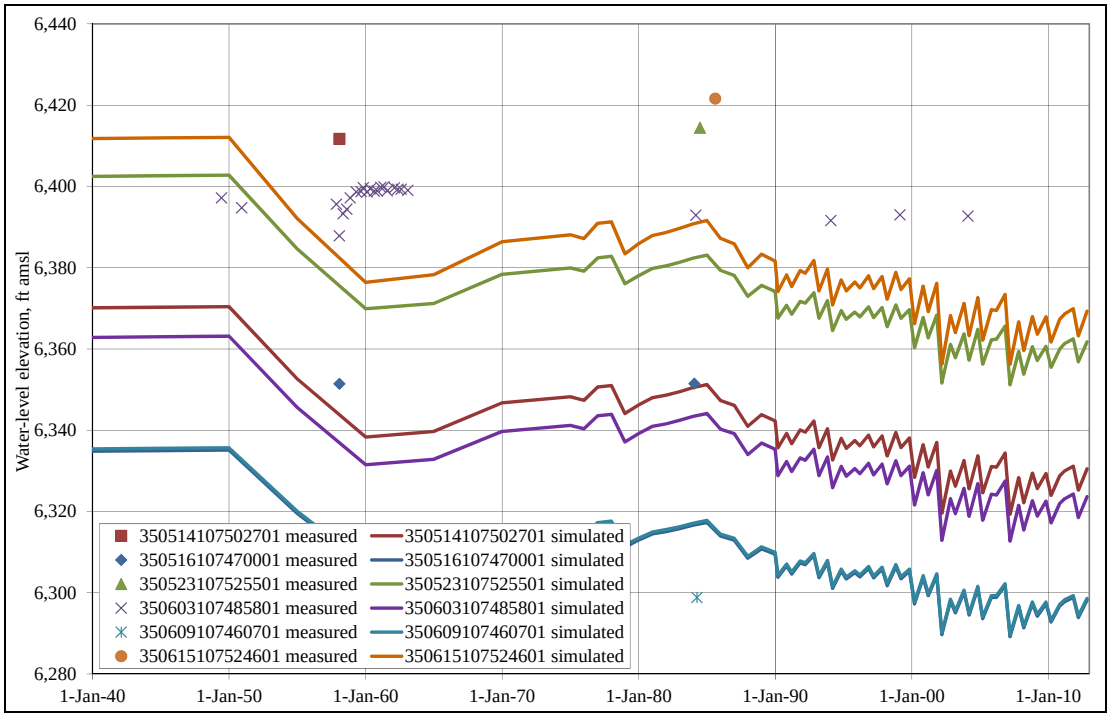

Figure 4.39. Measured and simulated water levels in Group 2 wells (2 of 4).

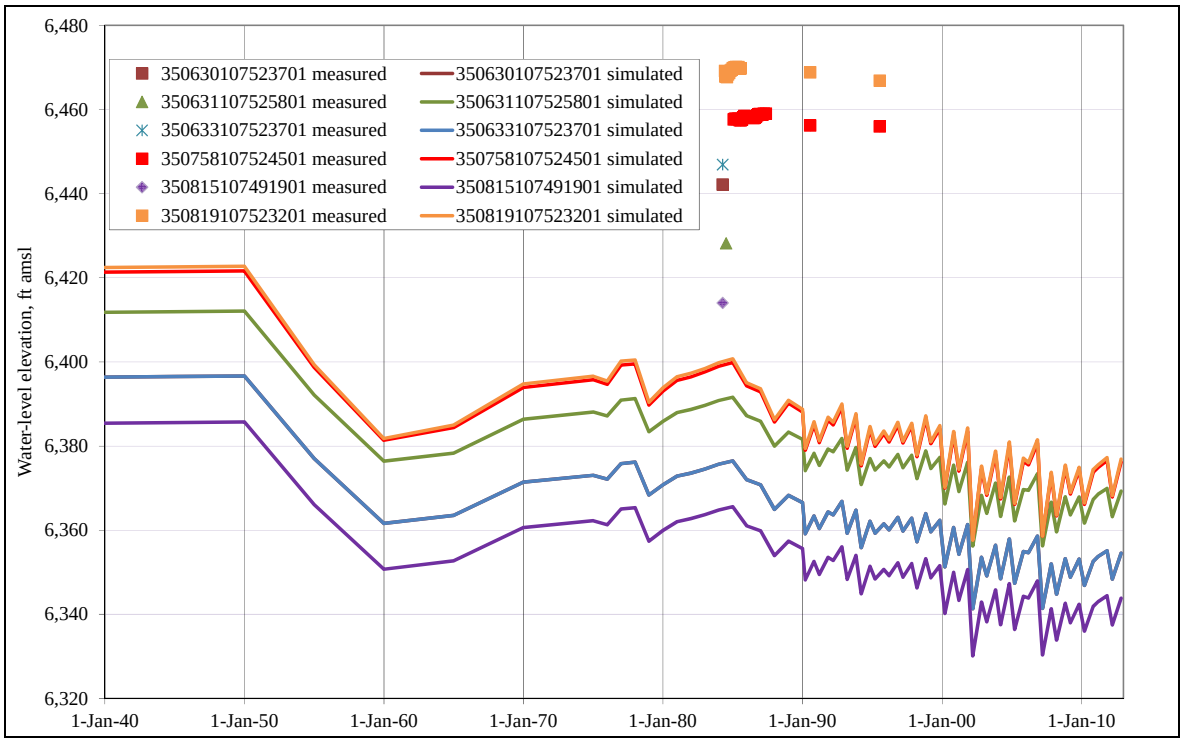

Figure 4.40. Measured and simulated water level in Group 2 wells (3 of 4).

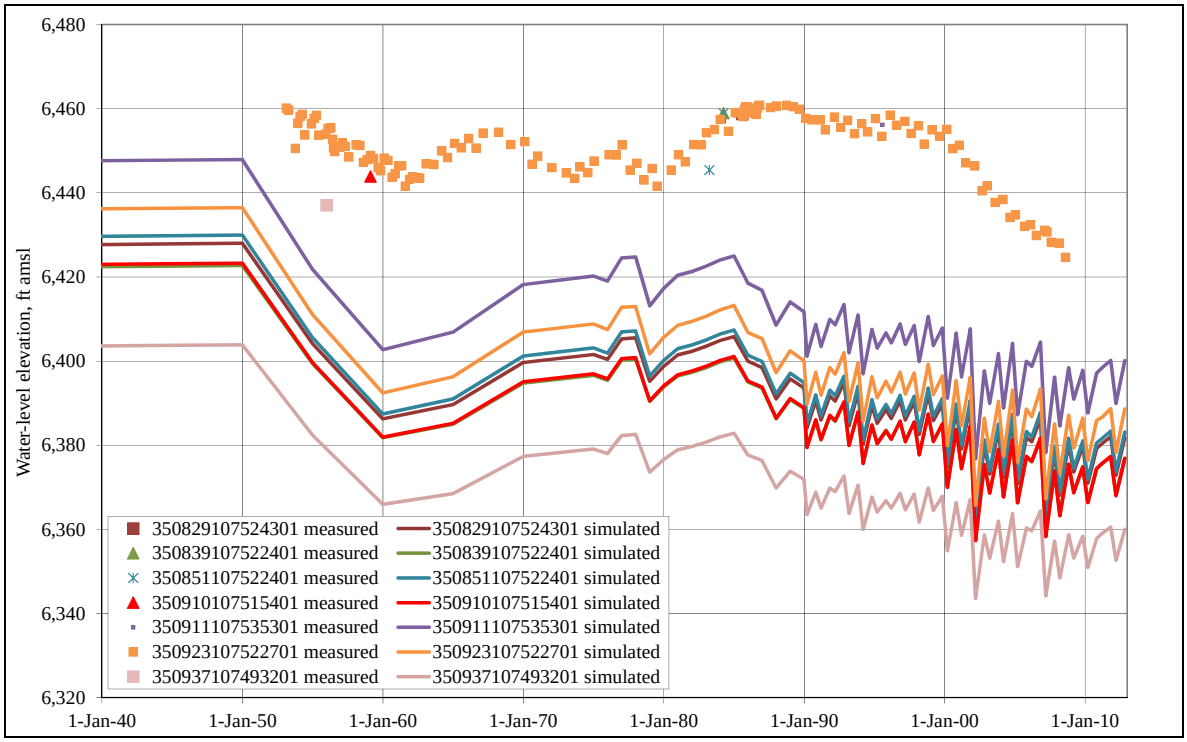

Figure 4.41. Measured and simulated water level in Group 2 wells (4 of 4).

Group 3 Wells

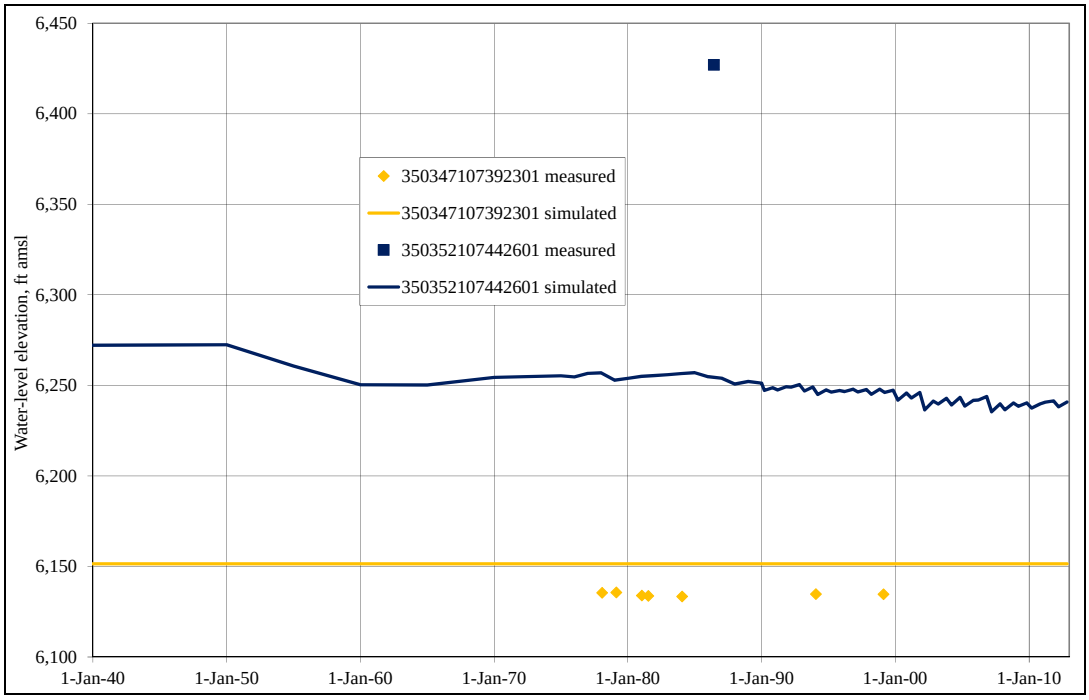

Figure 4.42. Measured and simulated water level in Group 3 wells.

Group 4 Wells

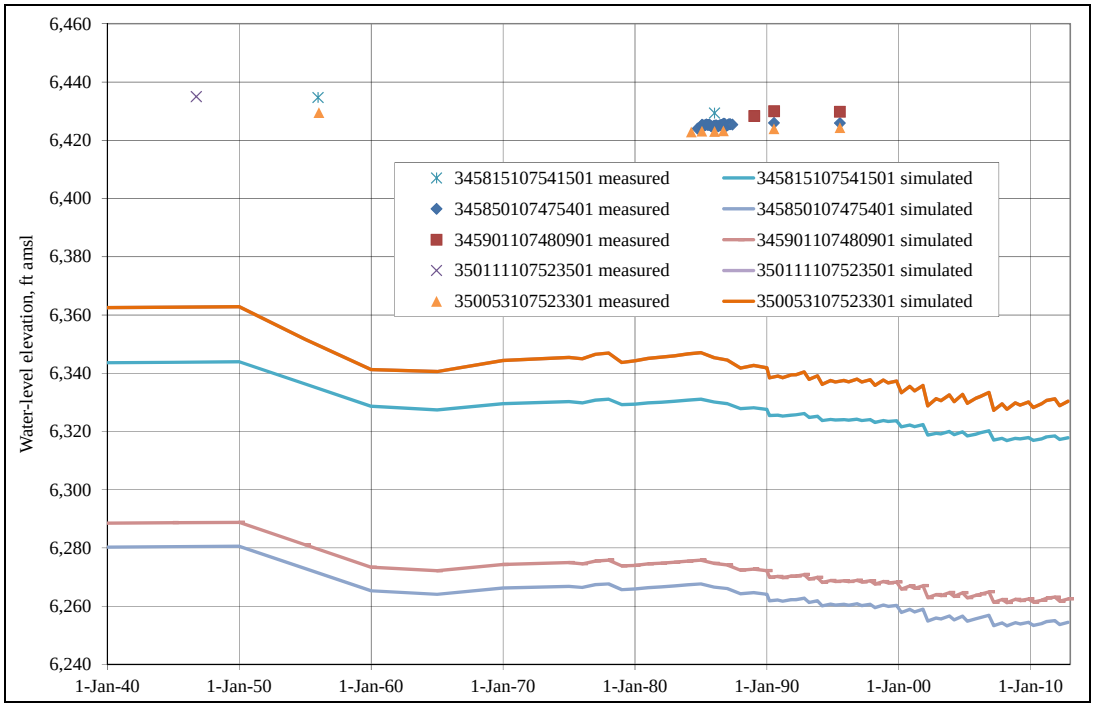

Figure 4.43. Measured and simulated water levels in Group 4 wells.

Group 5 Wells

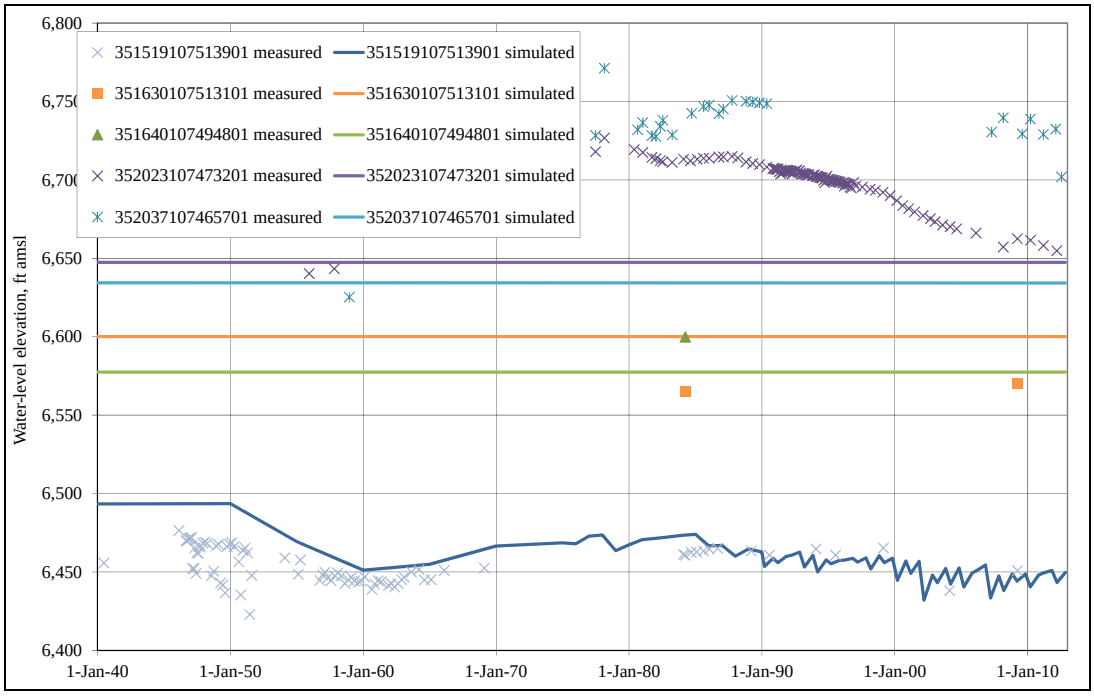

Figure 4.44. Measured and simulated water level in Group 5 wells.

Group 6 Wells

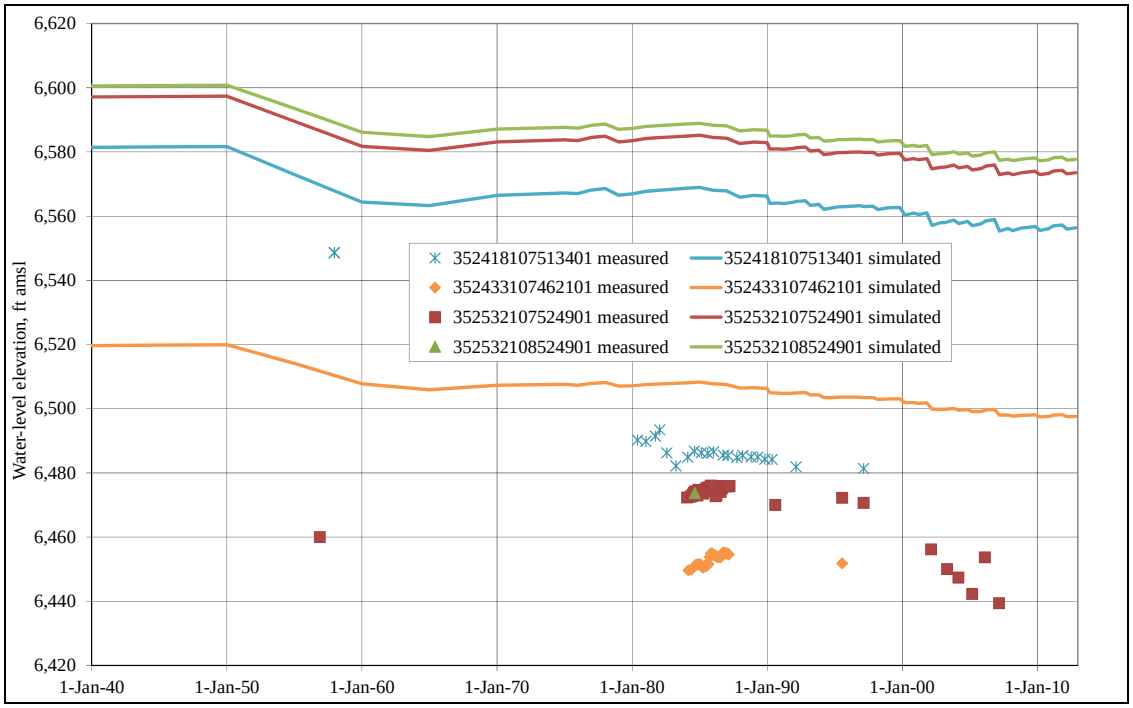

Figure 4.45. Measured and simulated water level in Group 6 wells.

Group 7 Wells

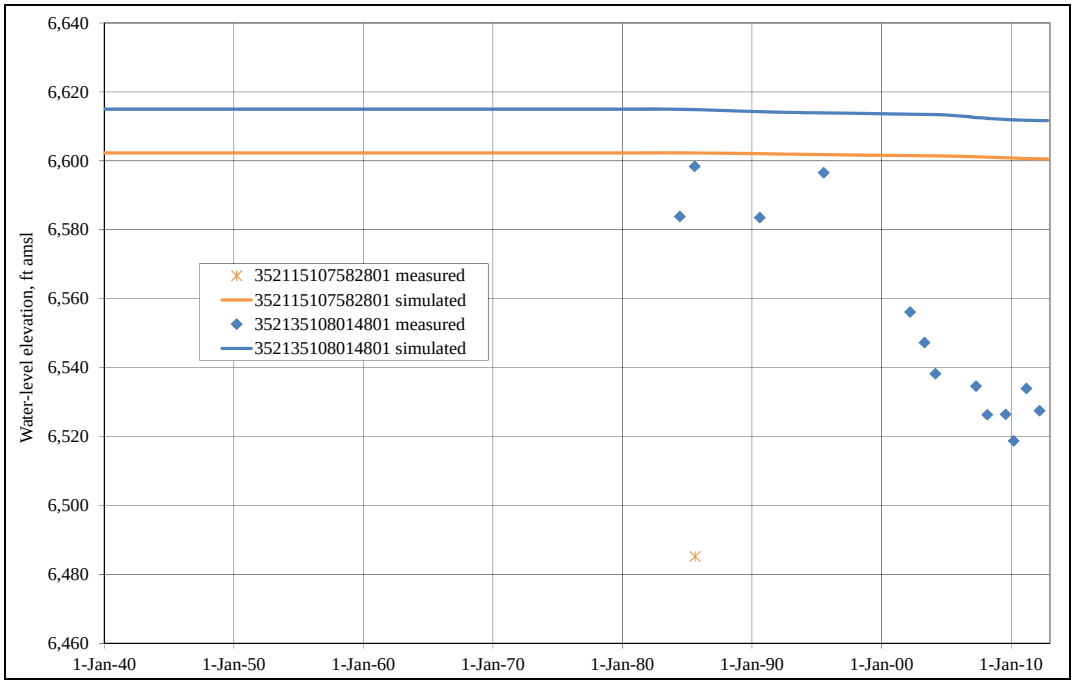

Figure 4.46. Measured and simulated water level in Group 7 wells.

Group 8 Wells

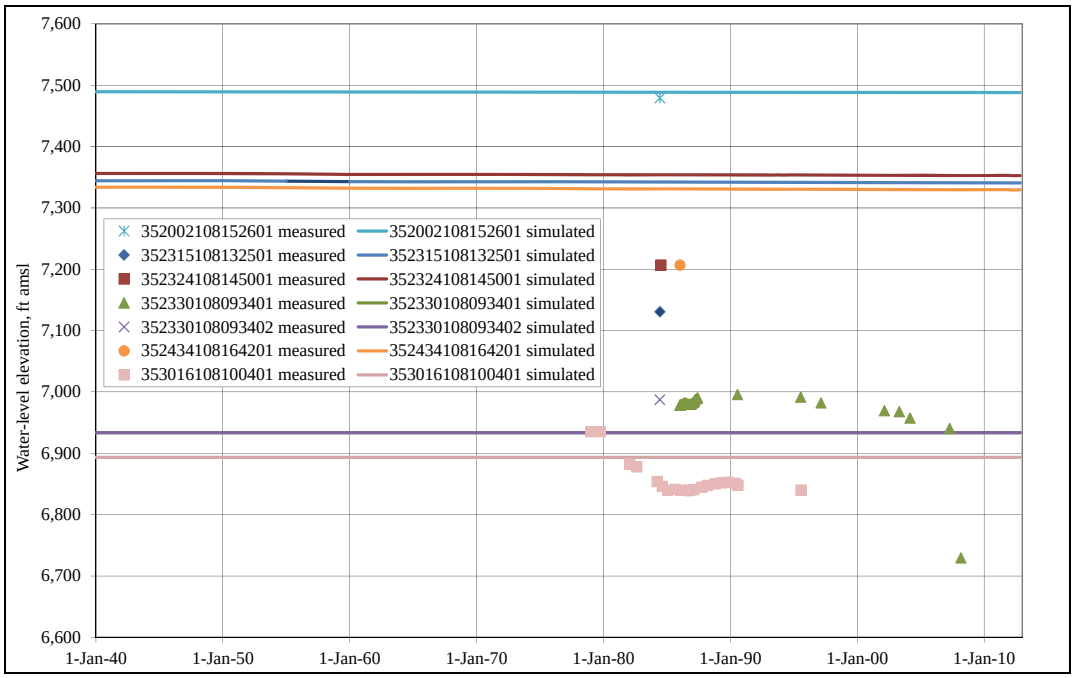

Figure 4.47. Measured and simulated water level in Group 8 wells.

Group 9 Wells

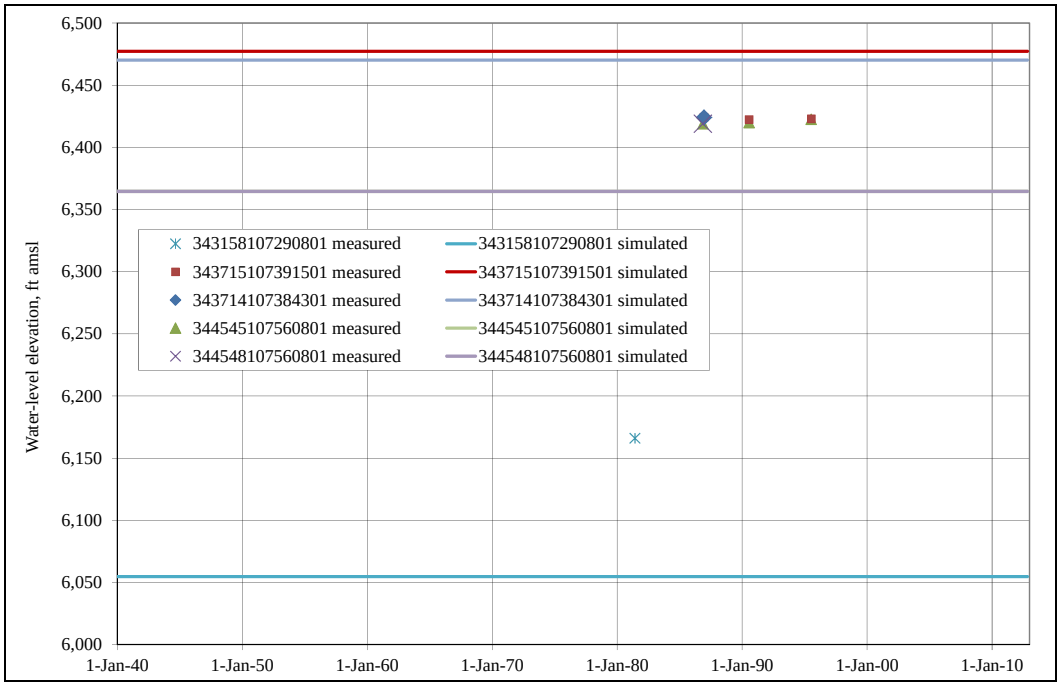

Figure 4.48. Measured and simulated water level in Group 9 wells.

Group 10 Wells

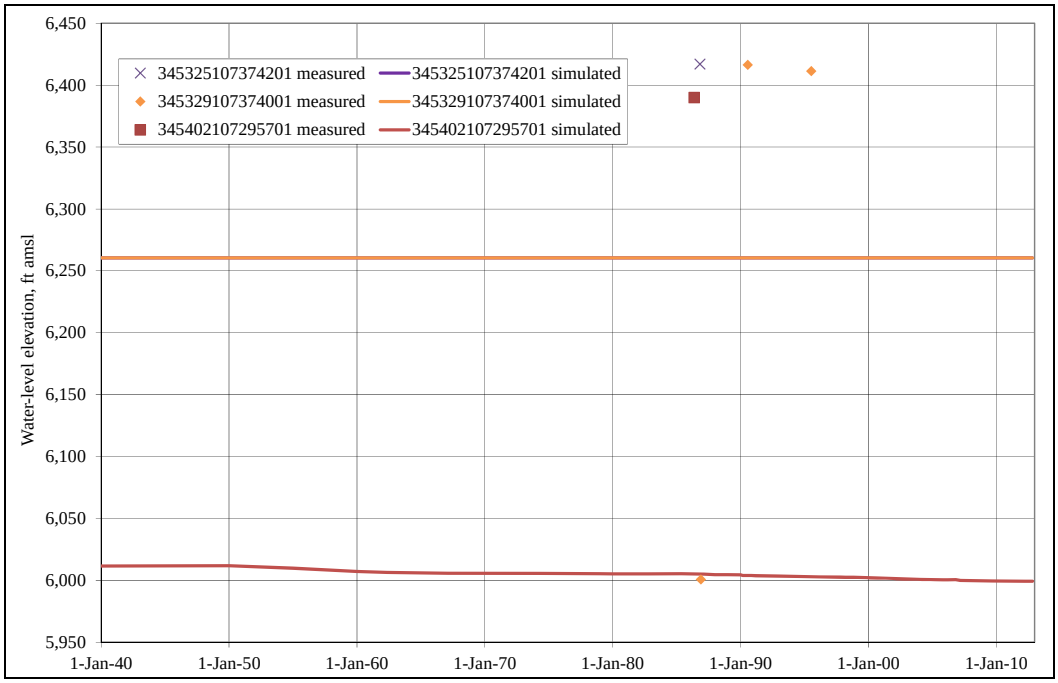

Figure 4.49. Measured and simulated water levels in Group 10 wells.

Group 11 Wells

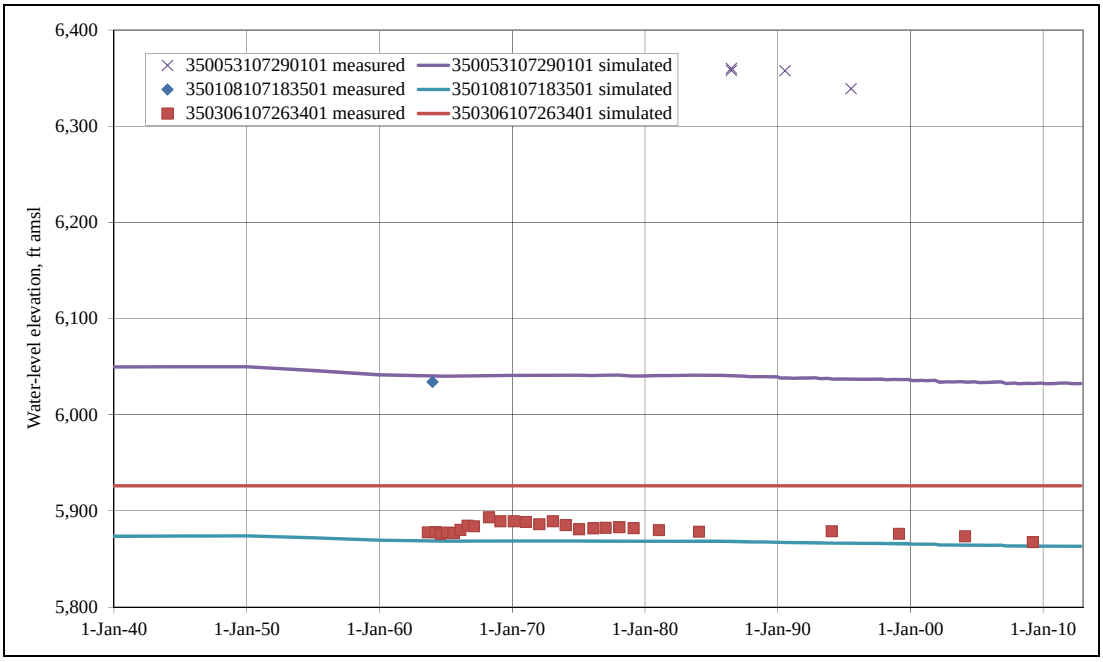

Figure 4.50. Measured and simulated water level in Group 11 wells.

Group 12 Wells

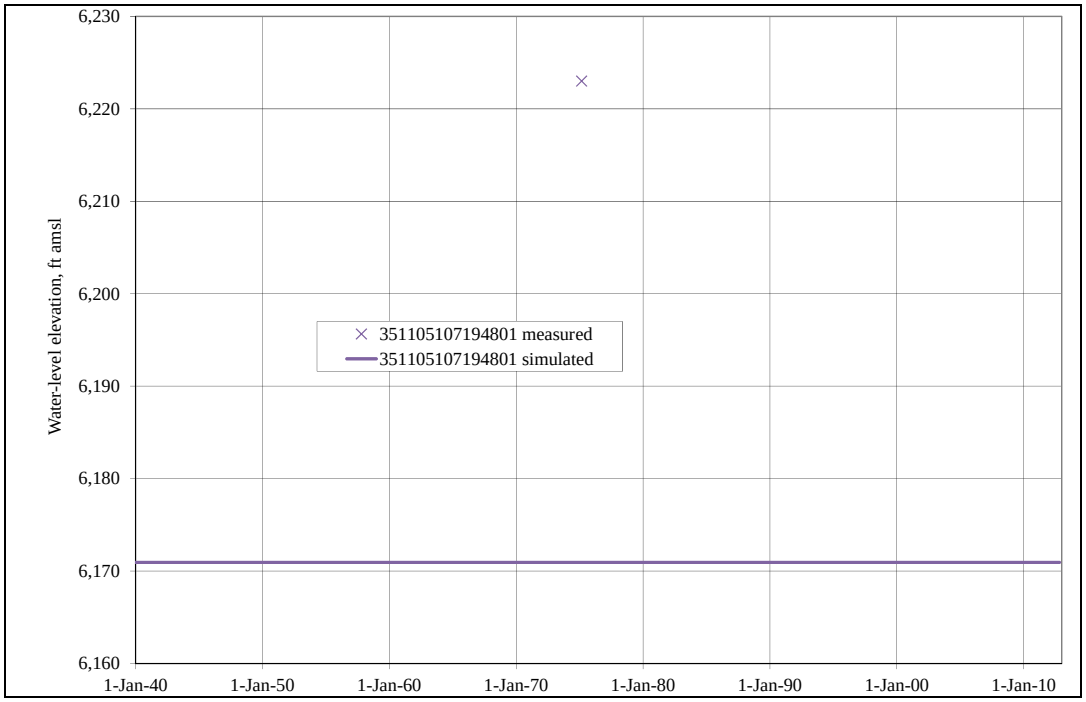

Figure 4.51. Measured and simulated water level in Group 12 wells.

Group 13 Wells

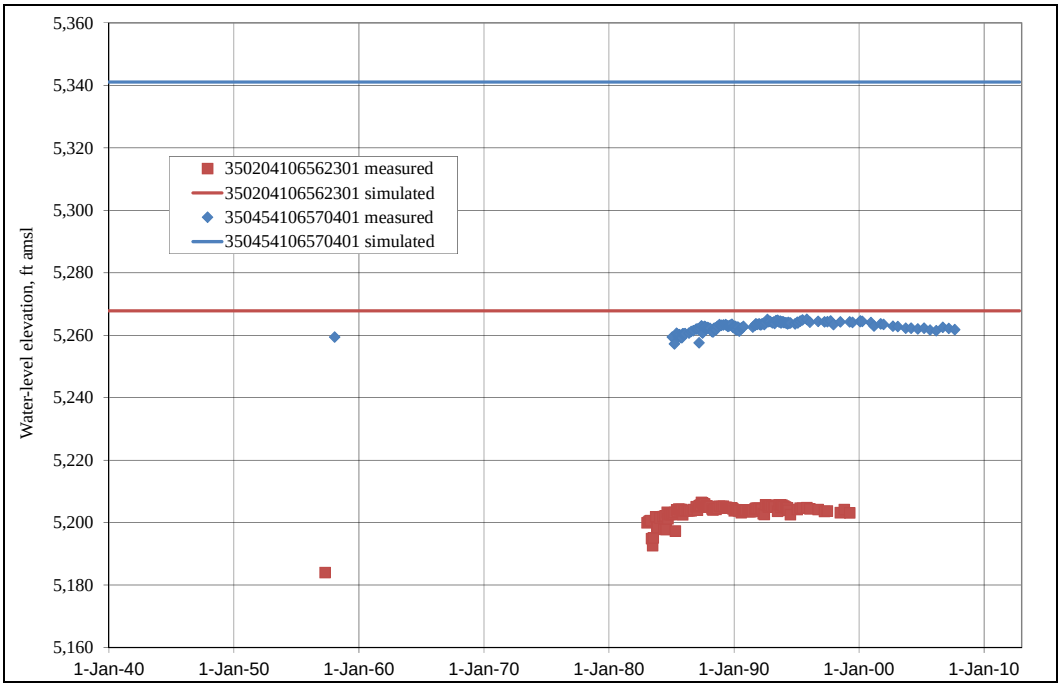

Figure 4.52. Measured and simulated water level in Group 13 wells.

Group 14 Wells

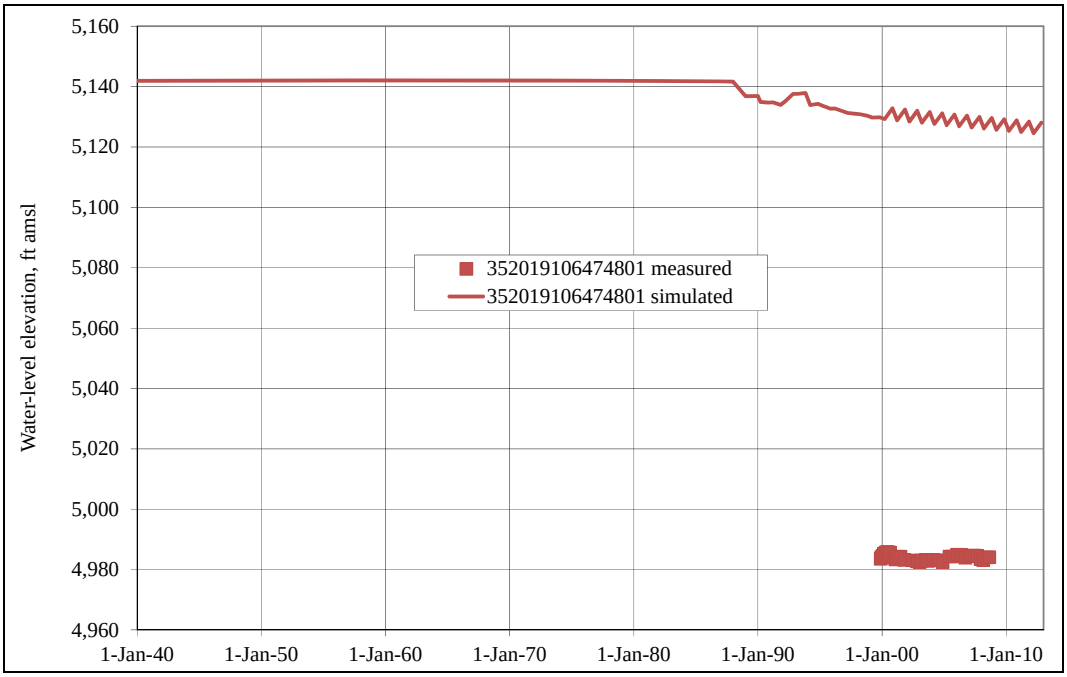

Figure 4.53. Measured and simulated water level in Group 14 wells.

4.6.3 Aquifer Test

Measured and simulated aquifer test drawdown in the pumping well and observation well during the test of the Sandoval County wells are presented on Figure 4.54 and Figure 4.55, respectively. The agreement is good, recognizing the apparent later pumping of the observation well (Fig. 4.15) that was not reported (INTERA, 2008) and not simulated.

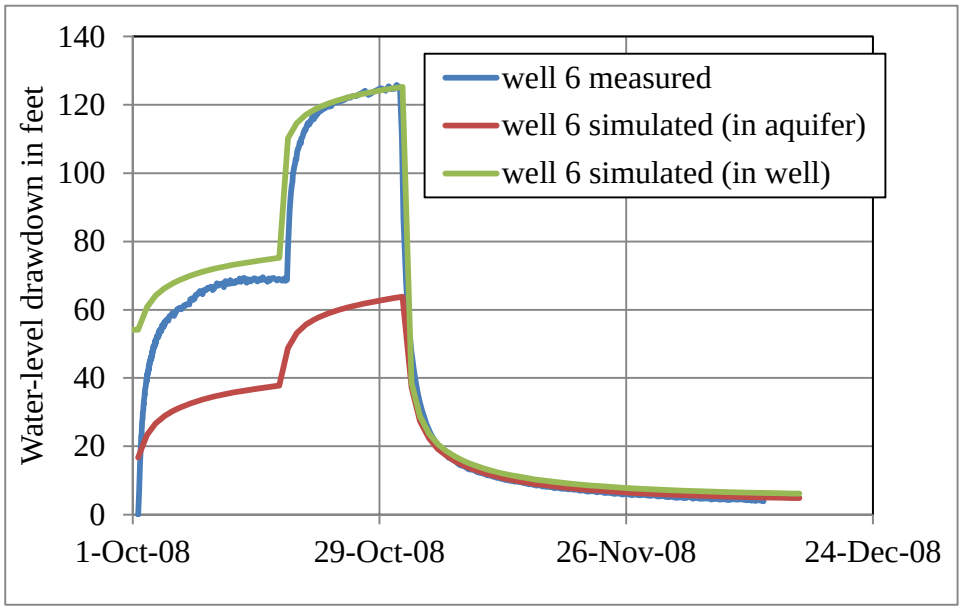

Figure 4.54. Measured and simulated water-level drawdown in pumping well (Well 6).

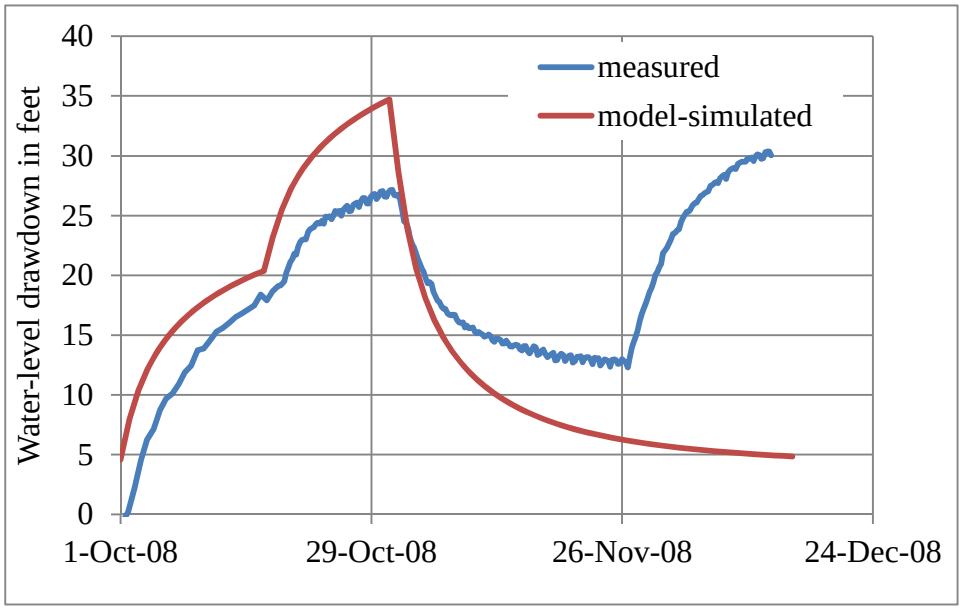

Figure 4.55. Measured and simulated water-level drawdown in observation well (Well 5).

5.0 PREDICTED DRAWDOWN AND SURFACE DISCHARGE EFFECTS

The calibrated groundwater-flow model was used to project the effects of proposed deep aquifer development. Scenarios were selected involving pumping from three potential deep well development areas, shown on Figure 5.1:

- Rio Puerco fault zone, in the San Andres–Glorietta aquifer
- Llano de Albuquerque, in the San Andres–Glorietta aquifer
- South of Interstate 40, in the Dakota-Morrison aquifer

Three scenarios, representing low, intermediate, and high levels of development in each area, were examined. Initial conditions for the projections were taken from the end of the historical simulation.

A maximum pumping rate of 1,000 gallons per minute (1,600 ac-ft/yr) per well was assumed. Pumping rates were further constrained to permit a maximum depth-to-water of 3,000 ft, or a minimum of 30 percent remaining saturated aquifer thickness, whichever is the higher water-level elevation. MODFLOW module LAK2 (Jones, 2011) was used to simulate in-well water levels. Well efficiency similar to that of Sandoval County pumping Well 6 (Fig. 4.54) was assumed.

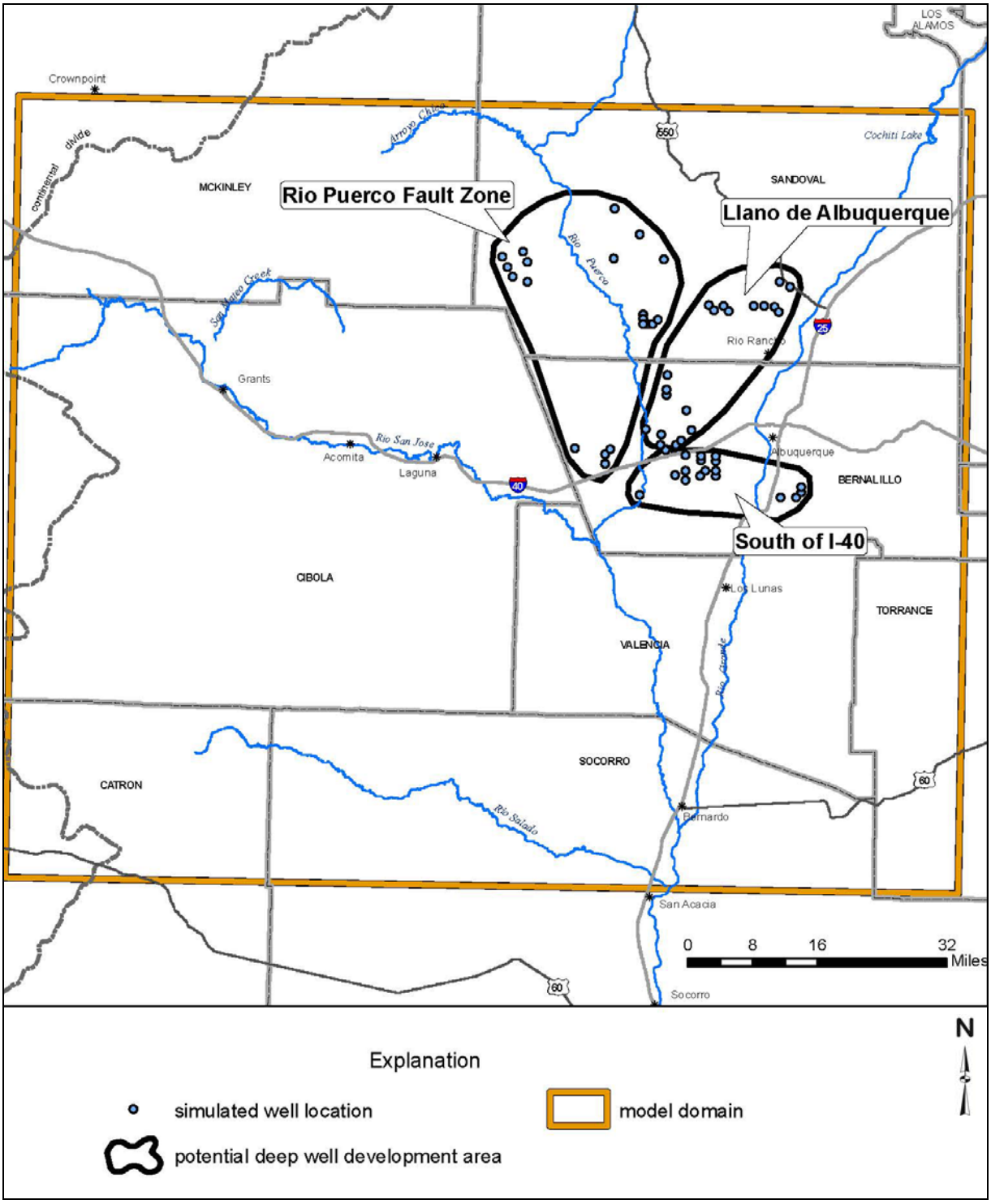

Figure 5.1. Location of simulated deep-aquifer pumping wells.

5.1 Low-level Development

The pumping of six wells, two in each area, was simulated. Total pumping for the simulation, initially at 9,600 ac-ft/yr, was at about 8,400 ac-ft/yr for most of the 40-year simulation.

Projected surface-discharge effects on the MRGB system and on the Rio Puerco / Rio San Jose system are shown on Figure 5.2. Reduced discharge directly to the MRGB system after 40 years is about 600 ac-ft/yr, or about 7.1 percent of the pumping rate. Reduction of discharge to the Rio Puerco / Rio San Jose system is about 800 ac-ft/yr, or 9.5 percent of pumping rate.

Projected water-level drawdown after 40 years of pumping is shown on Figure 5.3. Projected pumping lift after 1 year ranges from 443 to 2,109 ft, with lift after 40 years between 661 and 2,466 ft.

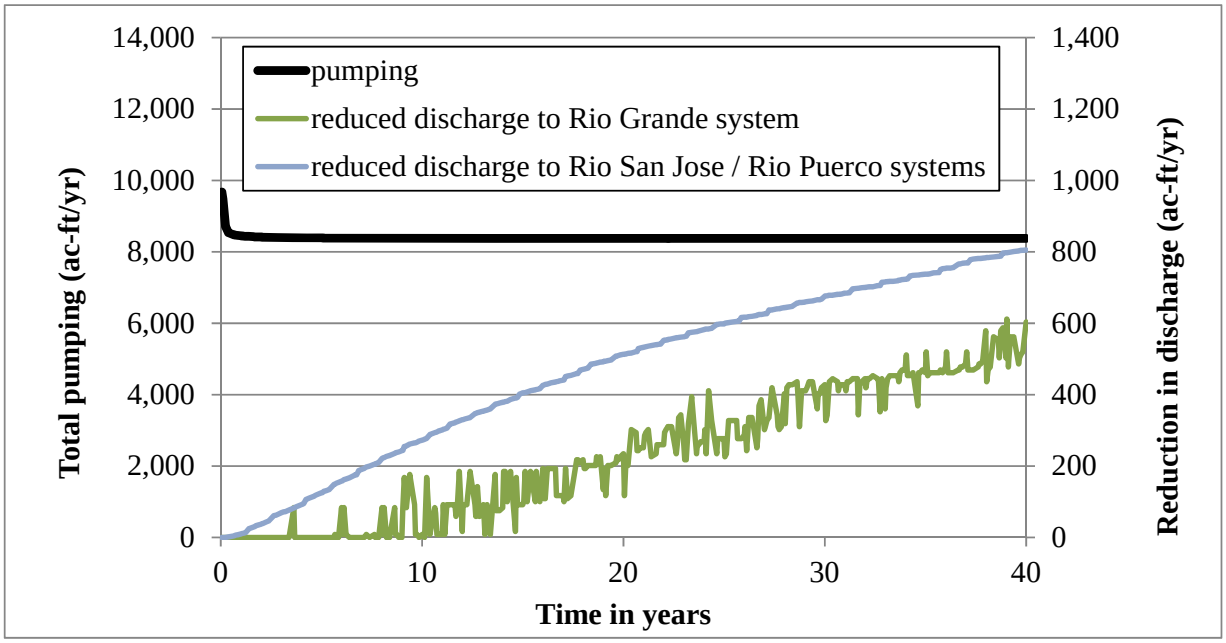

Figure 5.2. Projected surface discharge changes, low-development scenario.

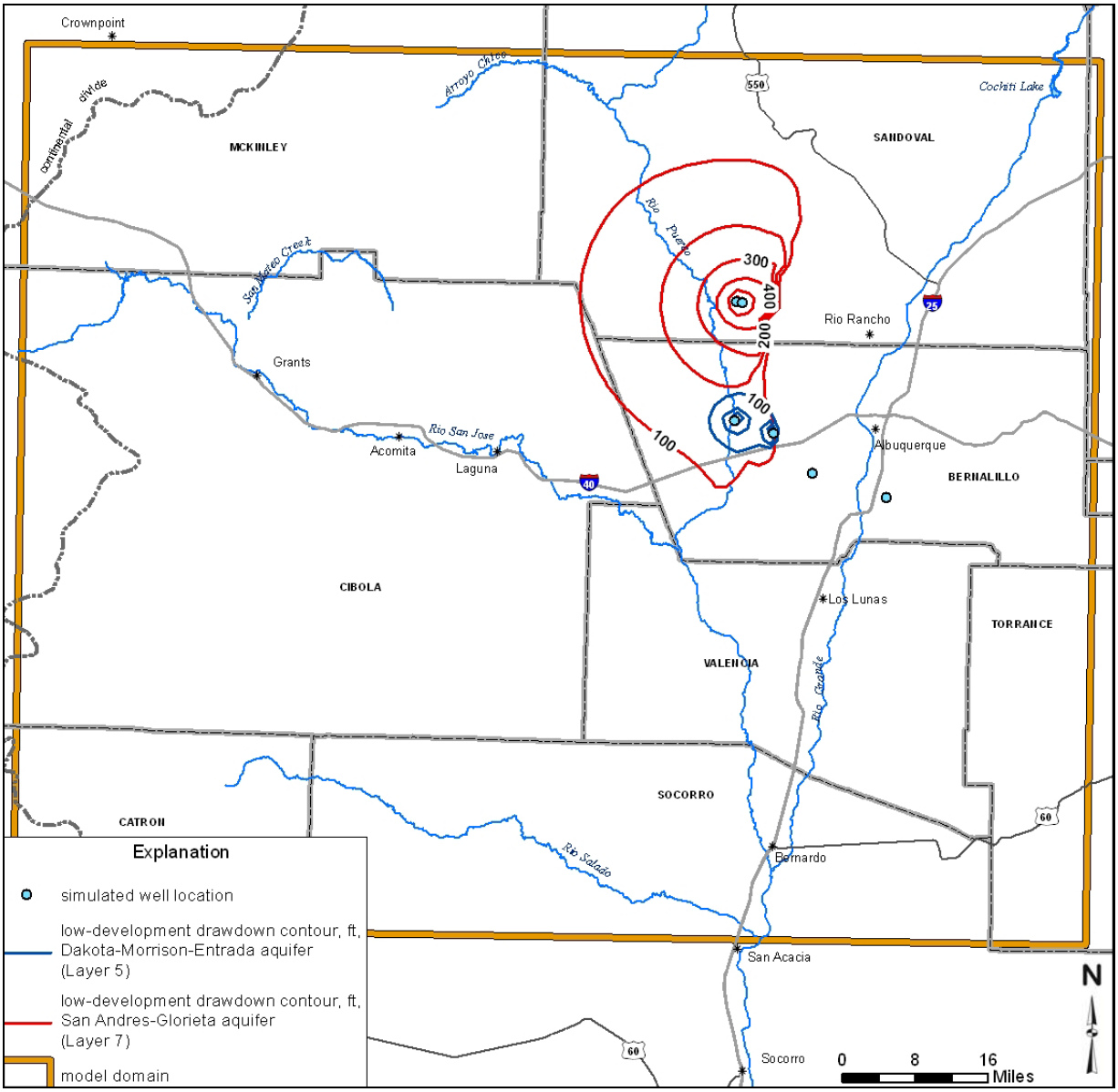

Figure 5.3. Projected groundwater-level drawdown, low-development scenario.

5.2 Intermediate-level Development

The pumping of thirty wells, ten in each area, was simulated. Total pumping for the simulation was initially 48,000 ac-ft/yr, declining to 37,300 ac-ft/yr after 40 years.

Projected surface-discharge effects on the MRGB system and on the Rio Puerco / Rio San Jose system are shown on Figure 5.4. Reduced discharge directly to the MRGB system after 40 years is about 3,200 ac-ft/yr, or about 6.7 percent of the pumping rate. Reduction to the Rio Puerco / Rio San Jose system is about 2,500 ac-ft/yr, or 8.6 percent of pumping rate.

Projected water level drawdown after 40 years of pumping is shown on Figure 5.5. Projected pumping lift after 1 year ranges from 449 to 3,000 ft, with lift after 40 years between 807 and 3,000 ft.

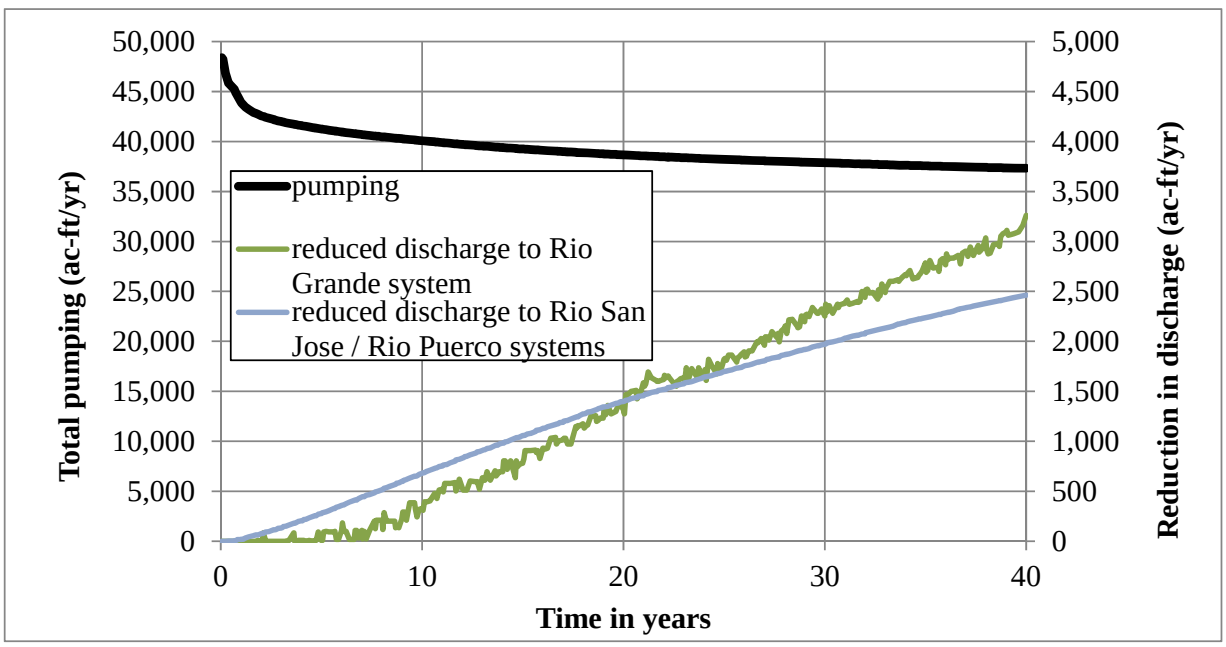

Figure 5.4. Projected surface discharge changes, intermediate-development scenario.

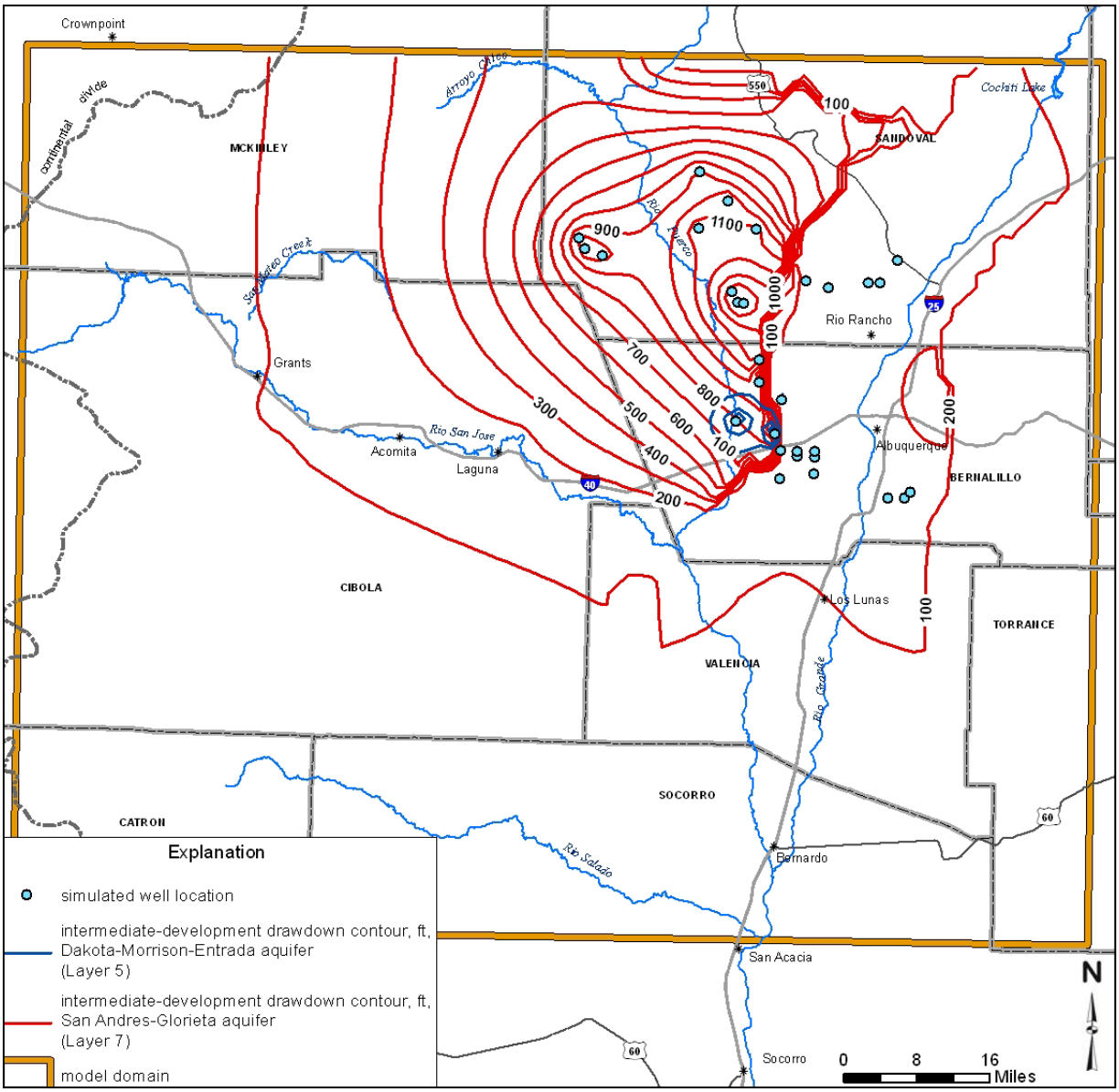

Figure 5.5. Projected groundwater-level drawdown, intermediate-development scenario.

5.3 High-level Development

The pumping of 60 wells, 20 from each area, was simulated. Total pumping for the simulation was initially 96,000 ac-ft/yr, declining to 64,000 ac-ft/yr after 40 years.

Projected surface-discharge effects on the MRGB system and on the Rio Puerco / Rio San Jose system are shown on Figure 5.6. Reduced discharge directly to the MRGB system and to the Rio San Jose system after 40 years is about 4,400 ac-ft/yr each, or 4.6 percent of pumping rate from each system.

Projected water level drawdown after 40 years of pumping is shown on Figure 5.7. Projected pumping lift after 1 year ranges from 579 to 3,000 ft, with lift after 40 years between 874 and 3,000 ft.

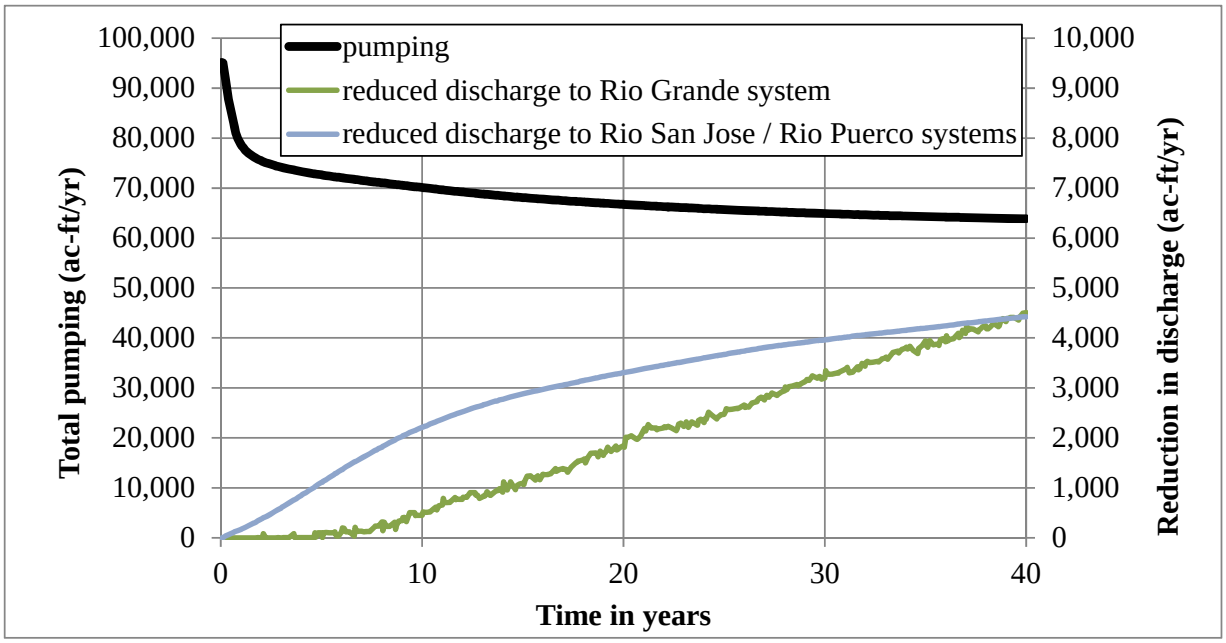

Figure 5.6. Projected surface discharge changes, high-development scenario.

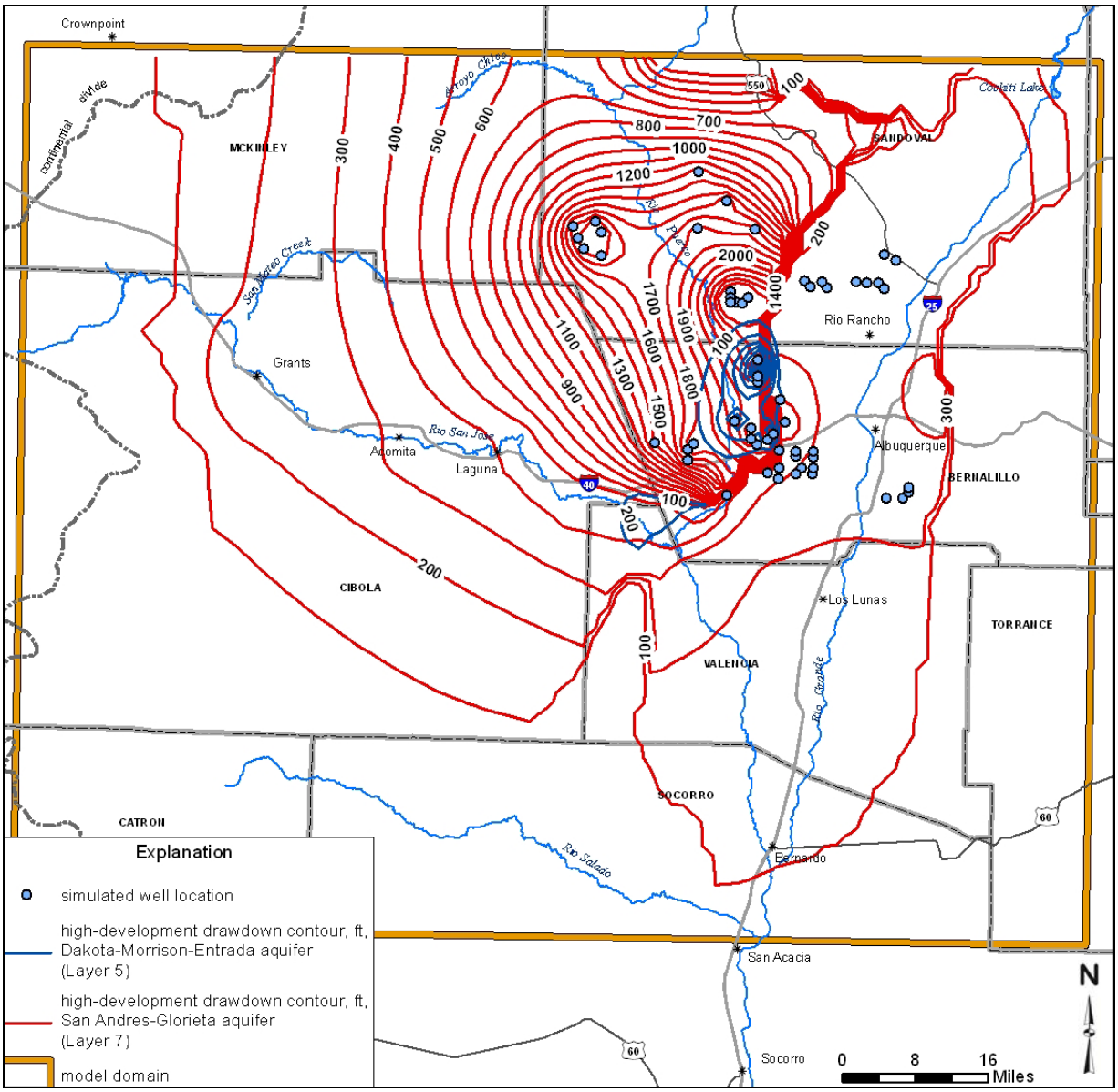

Figure 5.7. Projected groundwater-level drawdown, high-development scenario.

6.0 REFERENCES

Anderholm, S.K., 2001, Mountain-front recharge along the eastern side of the Middle Rio Grande Basin, central New Mexico: U.S. Geological Survey Water-Resources Investigations Report 00-4010, 36 p.

Baars, D.L., 1962, Permian systems of Colorado Plateau: American Association of Petroleum Geologists Bulletin, v. 46, n. 2, pp. 149-218.

Baldwin, J.A., and Anderholm, S.K., 1992, Hydrogeology and ground-water chemistry of the San Andres-Glorieta aquifer in the Acoma Embayment and Eastern Zuni Uplift, West-Central New Mexico: U.S. Geological Survey Water-Resources Investigations Report 91-4033, 304 p. and 2 plates.

[BGW] Balleau Groundwater, Inc., 2013, Documentation of preliminary Bluewater Basin Water-Use Compilation: Balleau Groundwater, Inc., consultant's letter report to New Mexico Office of the State Engineer, June 29, 2012; includes MS Excel spreadsheet.

Barroll, P., 2001, Documentation of the administrative groundwater model for the Middle Rio Grande Basin: New Mexico Office of the State Engineer Hydrology Bureau Report 99-3, 22 p. plus figures and appendices.

Beaumont, E.C., 1961, Petroleum exploration in a part of north-central New Mexico: New Mexico Geological Society Guidebook for the 12th Field Conference, pp. 175-185.

Brown, C.L., Karlstrom, K.E., Heizler, M., and Unruh, D., 1999, Paleoproterozoic deformation, metamorphism, and Ar/Ar thermal history of the 1.65-Ga Manzanita pluton, Manzanita Mountains, New Mexico: New Mexico Geological Society Guidebook for the 50th Field Conference, pp. 255-268.

Bryan, K., 1938, The Ceja del Rio Puerco: A border feature in the basin and range province of New Mexico, Part II, Stratigraphy and Structure: Journal of Geology, V. 46, pp. 1-16.

Carpenter, C.L., and Shomaker, J.W., 1998, Drawdown effects associated with pumping at the Mt. Taylor Uranium Mine, New Mexico: John Shomaker & Associates, Inc. consultant's report for the City of Gallup, 24 p., plus figures.

Connell, S.D., 2011, Preliminary study of the geologic framework of the southeastern Colorado Plateau-northwestern Albuquerque Basin transition, New Mexico: New Mexico Bureau of Geology and Mineral Resources Open-File Report 539.

Cooper, J.B., and John, E.C., 1968, Geology and ground-water occurrence in Southeastern McKinley County, New Mexico: New Mexico State Engineer Technical Report 35, 108 p. and several plates.

Craigg, S.D., Dam, W.L., Kernodle, J.M., Thorn, C.R., and Levings, G.W., 1989, Hydrogeology of the Dakota Sandstone in the San Juan structural basin, New Mexico, Colorado, Arizona, and Utah: U.S. Geological Survey Hydrologic Investigations Atlas HA-720-I, 2 sheets.

Dam, W.L., Kernodle, J.M., Levings, G.W., and Craigg, S.D., 1990, Hydrogeology of the Morrison Formation in the San Juan structural basin, New Mexico, Colorado, Arizona, and Utah: U.S. Geological Survey Hydrologic Investigations Atlas HA-720-J, 2 sheets.

Eldridge, D.B., Crossey, L.J., Karlstrom, K.E., Fischer, T, Geissman, J.W., Mills, S., Phillips, F., and Asmeron, Y., 2003, Salt Springs and Quaternary Travertine Deposits in the Rio Grande rift: A Connection between past and present Hydrologic Systems: Geological Society of America Abstracts with Programs, v. 35, n. 5, p. 37.

Fitzsimmons, J.P., 1959, The structure and geomorphology of west-central New Mexico: New Mexico Geological Society Guidebook for the 10th Field Conference, pp. 112-116.

Foster, R.W., 1957, Stratigraphy of west-central New Mexico *in* Geology of the Southwestern San Juan Basin: Four Corners Geological Society Second Field Conference, p. 62–72.

Frenzel, P.F., 1992, Simulation of ground-water flow in the San Andres-Glorieta Aquifer in the Acoma Embayment and Eastern Zuni Uplift, West-Central New Mexico: U.S. Geological Survey Water-Resources Investigations Report 91-4099, 381 p.

Frenzel, P.F., and Lyford, F.P., 1982, Estimates of vertical hydraulic conductivity and regional ground-water flow rates in rocks of Jurassic and Cretaceous age, San Juan Basin, New Mexico and Colorado: U.S. Geological Survey Water-Resources Investigations Report 82-4015, 59 p.

Gordon, E.D., 1961, Geology and ground-water resources of the Grants-Bluewater Area, Valencia County, New Mexico: New Mexico Office of the State Engineer Technical Report 20, 109 p.

Grauch, V.J.S., and Connell, S.D., 2013, New perspectives on the geometry of the Albuquerque Basin, Rio Grande rift, New Mexico: Insights from Geophysical Models of rift-fill Thickness, *in* Hudson, M.R., and Grauch, V.J.S., eds., New perspectives on the Rio Grande rift: from Tectonics to Groundwater: Geological Society of America Special Publication 494, 500 p.

Guyton, W.F., and Associates, 1978, Production of water from Westwater Canyon aquifer near Crownpoint, New Mexico, by Phillips Uranium Corporation for uranium mining: consultant's report to Phillips Uranium Corp. (NMOSE files, File No. SJ-109).

Hallett, R.B., Kyle, P.R., and McIntosh, W.C., 1997, Paleomagnetic and $^{40}Ar/^{39}Ar$ age constraints on the chronologic evolution of the Rio Puerco volcanic necks and Mesa Prieta west-central New Mexico: Implications for transition zone magmatism: Geological Society of America Bulletin, v. 109, n. 1, pp. 95-106.

Harbaugh, A.W., Banta, E.R., Hill, M.C., and McDonald, M.G., 2000, MODFLOW-2000, The U.S. Geological Survey modular ground-water model – User guide to modularization concepts and the ground-water flow process: U.S. Geological Survey Open-File Report 00-92, 121 p.

Hawley, J.W., and Haase, C.S., 1992, Hydrogeologic framework of the northern Albuquerque Basin, New Mexico: New Mexico Bureau of Geology and Mineral Resources Open-file Report 387, text and 7 plates.

Hearne, G.A., 1977, Evaluation of a potential well field near Church Rock as a water supply for Gallup, New Mexico: U.S. Geological Survey Water Resources Investigations Report 77-98, 21 p.

Hogan, J.F., Phillips, F.M., Mills, S.K., Hendrickx, J.M.H., Ruiz, J., Chesley, J.T., and Asmerom, Y., 2007, Geologic origins of salinization in a semi-arid river: The role of sedimentary basins brines: Geology, v. 35, n. 12, pp. 1063-1066.

INTERA, 2008, Draft Sandoval County Rio Puerco basin water development project, aquifer test and analysis report: INTERA consultant's report for Sandoval County, 46 p., plus appendices.

Jones, M.A., 2011, Lak2: A computer program to simulate the presence of lakes and other open water bodies within a groundwater flow system using the MODFLOW Groundwater Flow Model: Conference Proceedings of the MODFLOW and more 2011: Integrated Hydrologic Modeling, pp. 125-129.

[JSAI] John Shomaker & Associates, Inc., 2010, Interpretation of 73-day multi-well pumping tests, New Mexico Interstate Stream Commission Seven Rivers Well Field: John Shomaker & Associates, Inc. consultant's report, 39 p. plus illustrations and appendices.

[JSAI] John Shomaker & Associates, Inc., 2011, Evaluation of the Effects of Pumping from Deep Bedrock Aquifers in and near the Rio Puerco Valley, Bernalillo and Sandoval Counties, New Mexico: John Shomaker & Associates, Inc. consultant's report, 38 p. plus illustrations and appendices.

Kelley, V.C., and Clinton, N.J., 1960, Fracture systems and tectonic elements of the Colorado Plateau: University of New Mexico Publications in Geology Number 6, 104 p.

Kelley, V.C., and Northrop, S.A., 1975, Geology of Sandia Mountains and vicinity, New Mexico: New Mexico Bureau of Mines and Mineral Resources Memoir 29, 136 p.

Kernodle, J.M., 1996, Hydrogeology and steady state simulation of ground-water flow in the San Juan Basin, New Mexico, Colorado, Arizona, and Utah: USGS Water-Resources Investigations Report 95-4187, 117 p.

Kernodle, J. M., McAda, D. P., and Thorn, C. R., 1995, Simulation of ground-water flow in the Albuquerque Basin, central New Mexico, 1901-1994, with projections to 2020: U.S. Geological Survey Water-Resources Investigations Report 94-4251, 114 p.

Kernodle, J.M., and Scott, W.B., 1986, Three-dimensional model simulation of steady-state ground-water flow in the Albuquerque-Belen Basin, New Mexico: U.S. Geological Survey Water-Resources Investigations Report 84-4353, 58 p.

Levings, G.W., Kernodle, J.M., and Thorn, C.R., 1996, Summary of the San Juan structural basin regional aquifer-system analysis, New Mexico, Colorado, Arizona, and Utah: U.S. Geological Survey Water-Resources Investigations Report 95-4188, 55 p.

Lyford, F.P., 1979, Modeled effects of uranium-mine dewatering on water resources in northwestern New Mexico: U.S. Department of the Interior, San Juan Basin Regional Uranium Study, Working Paper 37, 46 p.

Lyford, F.P., and Frenzel, P.F., 1979 rev., Ground water in the San Juan Basin, New Mexico and Colorado—the existing environment: U.S. Department of the Interior, San Juan Basin Regional Uranium Study, Working Paper 23, 22 p.

Lyford, F.P., Frenzel, P.F., and Stone, W.J., 1980, Preliminary estimates of effects of uranium-mine dewatering on water levels, San Juan Basin: New Mexico Bureau of Mines & Mineral Resources, Memoir 38, pp. 320-333.

Maldonado, F., Slate, J.L., Love, D.W., Connell, S.D., Cole, J.C., and Karlstrom, K.E., 2007, Geologic map of the Pueblo of Isleta Tribal lands and vicinity, Bernalillo, Torrance, and Valencia Counties, Central New Mexico: U.S. Geological Survey Scientific Investigations, Map 2913, 1 sheet.

McAda, D.P., and Barroll, P., 2002, Simulation of ground-water flow in the Middle Rio Grande Basin between Cochiti and San Acacia, New Mexico: U.S. Geological Survey Water-Resources Investigations Report 02-4200, 81 p.

McDonald, M.G., and Harbaugh, A.W., 1988, A modular three-dimensional finite-difference ground-water flow model: U.S. Geological Survey Techniques of Water Resources Investigations, Book 6, Chapter A1, 586 p.

McLaughlin, D.B., 1984, A comparative analysis of groundwater model formulation—the San Andres-Glorieta case study: U.S. Army Corps of Engineers, Hydrologic Engineering Center, Research Document RD-22, 86 p.

Melis, E.A., 2008, Geologic interpretation of deep wells west of the Rio Grande in Bernalillo and Sandoval Counties, New Mexico: John Shomaker & Assoc., Inc. technical memorandum to New Mexico Interstate Stream Commission, 10 p. and appendices.

Melis, E.A., 2009, Interim report of regional groundwater-flow model to evaluate the effects of deep bedrock groundwater withdrawals on the Middle Rio Grande Basin Aquifer System: John Shomaker & Assoc., Inc., consultant's report to NM Interstate Stream Commission, 56 p. and appendices.

Melis, E.A., and McCoy, A.M., 2010, Preliminary hydrogeologic evaluation of the Colorado Plateau-Middle Rio Grande Basin transition, New Mexico: John Shomaker & Assoc., Inc., consultant's report to New Mexico Interstate Stream Commission, 30 p. and appendices.

Miller, R.S., 1988, User's guide for RIV2—a package for routing and accounting of river discharge for a modular, three-dimensional, finite-difference, ground-water flow model: U.S. Geological Survey Open-File Report 88-345, 33 p.

Molenaar, C.M., 1977, San Juan Basin time-stratigraphic nomenclature chart: New Mexico Geological Society, Guidebook, 28th Field Conference, pp. 251-258.

Moore, S.J., and Anderholm, S.K., 2002, Spatial and temporal variations in streamflow, dissolved solids, nutrients, and suspended sediments in the Rio Grande Valley Study Unit, Colorado, New Mexico, and Texas, 1993-1995: U.S. Geological Survey Water-Resources investigations Report 02-4224, 58 p.

Newell, D.L., Crossey, L.J., Karlstrom, K.E., Fischer, T.P., Hilton, and D.R., 2005, Continental-scale links between the mantle and groundwater systems of the western United States: Evidence from travertine springs and regional He isotope data: GSA Today, v. 15, n. 12, pp. 4-10.

Plummer, L.N., Bexfield, L.M., Anderholm, S.K., Sanford, W.E., and Busenberg, E., 2004a, Geochemical characteristics of ground-water flow in the Santa Fe Group Aquifer System, Middle Rio Grande Basin, New Mexico: U.S. Geological Survey Water-Resources Investigations Report 03-4131, 395 p. with tables and CD-ROM.

Plummer, N.L., Bexfield, L.M., Anderholm, S.K., Sanford, W.E., and Busenberg, E., 2004b, Hydrochemical tracers in the middle Rio Grande Basin, U.S.A.: 1. Conceptualization of groundwater flow: Hydrogeology Journal, v. 12, n. 4, pp. 359-388.

Risser, D.W., and Lyford, F.P., 1983, Water resources on the Pueblo of Laguna, West-Central New Mexico: U.S. Geological Survey Water-Resources Investigations Report 83-4038, 308 p. and several plates.

Roy, M., 2005, A Summary of ideas on the timing and distribution of rock and surface uplift across the Colorado Plateau: Geological Society of America Abstracts with Programs, v. 37, n. 7, p. 109.

Sanford, W.E., Plummer, N.L., McAda, D.P., Bexfield, L.M., and Anderholm, S.K., 2004, Hydrochemical tracers in the middle Rio Grande Basin, U.S.A.: 2. Calibration of a groundwater-flow model: Hydrogeology Journal, v. 12, n. 4, pp. 389-407.

Sengebush, R.M., 2008, Structural and Stratigraphic Controls of Deep Brackish Water Exploration, Rio Puerco Basin, New Mexico: Proceedings Volume of the 2008 Spring Meeting of the New Mexico Geological Society, Socorro, New Mexico, 47 p.

Shomaker, J.W., 1995, A study of the sources of water withdrawn from wells in a sequence of confined aquifers, Gallup Basin, New Mexico: Ph.D. dissertation, University of Birmingham (England), 166 p. plus appendices.

Shomaker, J.W., 2008, Evaluation of RG-88934 pumping test results and pumping test report (INTERA, 2008): John Shomaker & Associates, Inc. consultant's letter report to Sandoval County and the New Mexico Interstate Stream Commission.

Shomaker, J.W., Beaumont, E.C., and Kottlowski, F.E., 1971, Strippable low-sulfur coal resources of the San Juan Basin in New Mexico and Colorado: New Mexico Bureau of Mines and Mineral Resources Memoir 25, 189 p.

Slack, P.B., 1975, Tectonic development of the northeast part of the Rio Puerco Fault Zone, New Mexico: Geology, v. 3, n. 11, pp. 425-434.

Slack, P.B., and Campbell, J.A., 1976, Structural geology of the Rio Puerco fault zone and its relationship to central New Mexico tectonics: New Mexico Geological Society Special Publication 6, pp. 46-52.

Stone, W.J., Lyford, F.P., Frenzel, P.F., Mizell, N.H., and Padgett, E.T., 1983, Hydrogeology and water resources of San Juan Basin, New Mexico: New Mexico Bureau of Mines and Mineral Resources Hydrogeologic Report 6, 70 p. and several plates.

Strickland, D., Heizler, M.T., Selverstone, J., and Karlstrom, K.E., 2003, Proterozoic Evolution of the Zuni Mountains, western New Mexico: relationship to the Jemez Lineament and Implications for a Complex Cooling History: *in* N.M. Geological Society Guidebook, 54th Field Conference, Geology of the Zuni Plateau, pp. 109-117.

Taylor, D.J., and Huffman, A.C., 1998, Map showing inferred and mapped basement faults, San Juan Basin and vicinity, New Mexico and Colorado: U.S. Geological Survey Geologic Investigations Series I-2461, scale 1:500,000.

Thaden, R.E., and Zech, R.S., 1986, Structure contour map of the San Juan Basin and vicinity: *in* Turner-Peterson, C.E., Santos, E.S., and Fishman, N.S., (editors), A Basin Analysis Case Study: The Morrison Formation Grants Uranium Region New Mexico: American Association of Petroleum Geologists Studies in Geology, v. 22, p. 35-45.

Thorn, C.R., McAda, D.P., and Kernodle, J.M., 1993, Geohydrologic framework and hydrologic conditions in the Albuquerque Basin, Central New Mexico: U.S. Geological Survey Water-Resources Investigations Report 93-4149, 106 p. and two plates.

Tiedeman, C.R., Kernodle, J.R., and McAda, D.P., 1998, Application of Nonlinear-Regression Methods to a ground-water flow model of the Albuquerque Basin, New Mexico: U.S. Geological Survey Water-Resources Investigations Report 98-4172, 90 p.

[USGS] U.S. Geological Survey National Water Inventory System (NWIS): http://waterdata.usgs.gov/nwis

White, W. D., and Kues, G. E., 1992, Inventory of springs in the State of New Mexico: U.S. Geological Survey Open-File Report 92-118, 253 p.

Wright, H.E., 1946, Tertiary and quaternary geology of the Lower Rio Puerco area, New Mexico: Bulletin of the Geological Society of America, V. 57, pp. 383-456, 10 pls., 12 figs.